

# Photon-resolved Floquet theory approach to spectroscopic quantum sensing

Georg Engelhardt,<sup>1,2,3,\*</sup> Konstantin Dorfman,<sup>4,5,†</sup> and Zhedong Zhang<sup>6,7,‡</sup>

<sup>1</sup>International Quantum Academy, Shenzhen 518048, China

<sup>2</sup>Shenzhen Institute for Quantum Science and Engineering,

Southern University of Science and Technology, Shenzhen 518055, China

<sup>3</sup>Guangdong Provincial Key Laboratory of Quantum Science and Engineering,  
Southern University of Science and Technology, Shenzhen, 518055, China

<sup>4</sup>Center for Theoretical Physics and School of Physics and Optoelectronic Engineering,  
Hainan University, Haikou, China, 570228, China

<sup>5</sup>Himalayan Institute for Advanced Study, Unit of Gopinath Seva Foundation,  
MIG 38, Avas Vikas, Rishikesh, Uttarakhand 249201, India

<sup>6</sup>Department of Physics, City University of Hong Kong, Kowloon, Hong Kong SAR

<sup>7</sup>Shenzhen Research Institute, City University of Hong Kong, Shenzhen, Guangdong 518057, China

(Dated: June 11, 2025)

Spectroscopic methods play a vital role in quantum sensing, which uses the quantized nature of atoms or molecules to reach astonishing precision for sensing of, e.g., electric or magnetic fields. In the theoretical treatment, one typically invokes semiclassical methods to describe the light-matter interaction between quantum emitters, e.g., atoms or molecules, and a strong coherent laser field. However, these semiclassical approaches struggle to predict the stochastic measurement fluctuations beyond the mean value, necessary to predict the sensitivity of spectroscopic quantum sensing protocols. Here, we develop a theoretical framework based on the recently developed Photon-resolved Floquet theory (PRFT) which is capable to predict the measurement statistics describing higher order statistics of coherent quantum states of light. The PRFT constructs flow equations for the cumulants of the photonic measurement statistics utilizing only the semiclassical dynamics of the matter system. We apply the PRFT to spectroscopic quantum sensing using dissipative two-level and four-level systems (describing electric field sensing with Rydberg atoms), and demonstrate how to calculate the Fisher information of the measurement statistics with respect to various system parameters. In doing so, we demonstrate that the PRFT is a flexible tool allowing to improve the sensitivity of spectroscopic quantum sensing devices by several orders of magnitudes.

## I. INTRODUCTION

It is hard to overstate the importance of spectroscopy in science and technology, reaching from medicine, environmental monitoring, pharmaceutical research, material science to public safety, to mention but a few. The advent of the laser enabled experimentalists to generate light sources with outstanding properties, e.g., pulses featuring a duration of few Femto seconds, an extreme narrow bandwidth below 1 Hz, or peak intensities exceeding  $10^{20}$  W/cm<sup>2</sup>. These technological advances have allowed researchers to study atomic and molecular processes, such as isomerization [1], photo dissociation [2], conical intersections [3], polariton dynamics [4, 5], as well as free-space superradiance [6–8] with astonishing precision.

Moreover, spectroscopic methods find vital applications in quantum sensing, which deploys either coherence, entanglement or the quantized structure of matter to improve the measurement precision beyond classical means [9–11]. Experiments using the coherence of cold-atom matter-wave interferometers are currently being developed for precision measurement of the gravitational

field, requiring spectroscopic methods for state preparation and readout [12–14]. Squeezed light assists in the detection of gravitation waves at LIGO [15]. Protocols deploying entangled photons have the potential to improve spectroscopic precision measurements [16] as they can circumvent the time-frequency uncertainty relation [17–19]. The quantized nature of atoms is the basis for the already ultra-precise but ever-improving definition of the time-standard using atomic and optical clocks [20, 21].

Likewise, optical magnetometry, which measures the rotation of linearly polarized light due to the Faraday effect induced by the interaction with the quantized-level structure of alkali atoms, is a highly-precise spectroscopic quantum sensing method for the measurement of magnetic fields [22–27]. In combination with noble atoms, optical magnetometry is presently employed in the search for the elusive dark matter [28–30]. Moreover, the huge polarizability of highly-excited states of alkali atoms makes these so-called Rydberg atoms extremely susceptible to electromagnetic fields in the microwave and radio wavelength regimes [31]. The resulting change in the optical absorption of an optical probe laser can then be measured using electromagnetically-induced transparency protocols [32–40]. This approach finds also application in the search of dark matter [41]. Such spectroscopic quantum sensing protocols using coherent laser light have a very simple experimental setup, as sketched in Fig. 1. A laser emits coherent light which

\* georg-engelhardt-research@outlook.com

† dorfmank@hainanu.edu.cn

‡ zzhan26@cityu.edu.hk

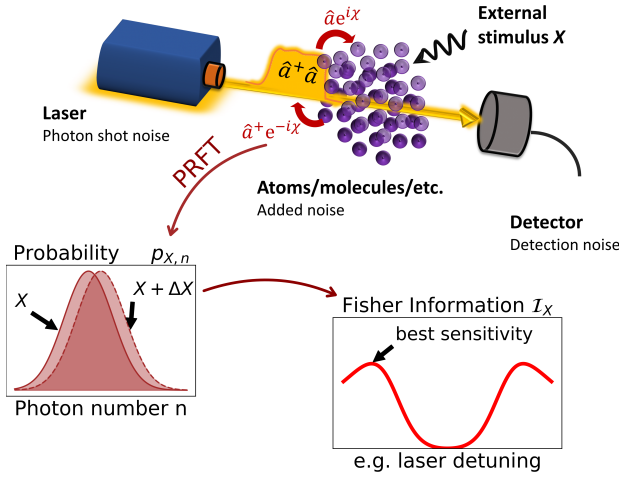


FIG. 1. Sketch of the spectroscopic setup, in which laser light interacts with an atomic ensemble, before it is finally measured by a detector. The PRFT includes counting fields  $\chi$  into the semiclassical dynamics allowing to predict the measured photonic probability distribution. The presence of an external stimulus  $X$  changes the measurement statistics from which one can estimate the strength of  $X$ . The Fisher information predicted by the PRFT assists in finding experimental parameters (e.g., the laser detuning) which optimize the measurement sensitivity.

interacts with an ensemble of atoms or other quantum emitters before its intensity, phase or polarization rotation is being measured by a photon detector setup. The presence of an external stimulus (denoted by  $X$  in Fig. 1) changes the optical properties of the atoms, resulting in a modified measurement statistics at the photon detector, from which one can statistically infer the strength of that stimulus.

To theoretically predict the mean values of spectroscopic signals, a series of powerful methods for nonlinear spectroscopy have been devised. For instance, diagrammatic techniques have proven useful to match each order of the measured intensity to a term in the perturbative expansion [42]. In the high-intensity regime, one usually resorts to semiclassical approaches like the quantum master equation [43] in combination with the Maxwell-Bloch theory [44]. Even though these established semiclassical methods reliably predict the mean value of the measured spectroscopic signal, they do not directly provide information about the fluctuations of the experimental measurements.

Typically, there are three distinct sources of noise in a spectroscopic setup as sketched in Fig. 1: (a) the photon-shot noise of the laser-light source; (b) the noise occurring during the light-matter interaction, which might have a thermal origin; (c) the detection noise appearing due to an imperfect measurement process. While the estimation of the photon-shot noise and the detection noise is straightforward, the prediction of the noise

added by the light-matter interaction is nontrivial, and bears fundamental limitations on the measurement sensitivity. To predict the measurement statistics beyond the mean value, more advanced methods such as phase-space methods [43], quantum trajectories [45], and the input-output theory [46] can be employed. While general, these methods become difficult to evaluate in practice: Phase space methods require to solve complex partial differential equations. Input-output theory will lead to multi-time correlation functions of the polarization operator, which are nontrivial to evaluate even within a semiclassical approximation [47].

In this paper, we develop an alternative method to predict the measurement statistic in spectroscopic experiments based on a full-counting statistics approach [48]. The derivation of this method takes advantage of the recently developed Photon-resolved Floquet theory (PRFT), which is a semiclassical method of light-matter interaction, not only capable of predicting the state of the driven matter system, but also the detailed photon statistics of the driving field [49–51]. It thus constitutes a suitable tool to calculate the noise added by the light-matter interaction as sketched in Fig. 1. Using the PRFT, it is then possible to project the measurement sensitivity  $\langle \Delta X^2 \rangle$  of a spectroscopic quantum sensing protocol via the celebrated Cramer-Rao bound [52, 53]

$$\langle \Delta X^2 \rangle \geq \frac{1}{I_X}, \quad (1)$$

where the Fisher information

$$I_X = \sum_n p_{X,n} (\partial_X \ln p_{X,n})^2, \quad (2)$$

is a function of the  $X$ -dependent photonic probabilities predicted by the PRFT. Using the Fisher information, it is then possible to optimize the measurement precision by finding experimental parameters, e.g., the laser detuning, maximizing the Fisher information as illustrated in Fig. 1.

The PRFT takes advantage of the rich methodologies of full-counting statistics of electron transport through mesoscopic structures in electronic systems [54–67], where a spatially confined quantum system, such as quantum dots or single-electron transistors, is coupled to two or more electronic leads. A thermodynamic bias between the leads drives an electron current through the quantum system, whose statistics can be traced by implementing so-called counting fields into the equations of motion of the reduced density matrix of the confined quantum system. More recently, full-counting statistics has been also applied in the study of heat transport through quantum systems [68–71].

Similarly, the PRFT includes counting fields into the semiclassical equations of motion of the quantum emitters, which trace the photon exchange between several coherent driving fields. In its original form, the PRFT has been a generic theoretical framework which has not

been applied to realistic physical systems so far [49–51]. Moreover, the semiclassical approximation invoked in the establishment of the PRFT, does not take into account the photon number dependence of the creation and annihilation operators. These two major issues will be addressed in this work.

The theoretical framework developed here, which applies the PRFT to spectroscopic measurements, relies only on semiclassical methods, in which light and matter are, respectively, described quantum mechanically and classically, and is nevertheless capable to predict the measurement statistics of prominent spectroscopic observables, namely, the intensity, polarization direction and phase shifts of the probe light in a coherent quantum state. We concentrate thereby on the calculation of the corresponding mean values and the covariance matrix, as they typically dominate the measurement statistic for a large number of non-interacting quantum emitters. We further derive flow equations for low-order cumulants, which are reminiscent of the Maxwell-Bloch equation for the mean value of the electric field. These flow equations can be easily integrated numerically, and in some special cases can be solved analytically.

We apply the framework to an ensemble of two-level systems which are subject to a laser field, whose measurement statistics in spectroscopic quantum sensing is to be determined. In a full quantum description, this system can be represented as a dissipative Tavis-Cummings model [72], which cannot be solved exactly (neither analytically nor numerically) because of the large number of photons in the driving field. However, using the PRFT approach, it is possible to analytically study the stochastic properties of the system. Using these findings, we derive analytical expressions for the Fisher information of the atomic density and the probe field detuning, which allows to determine an experimental configuration optimizing the measurement sensitivity. To demonstrate the broad applicability of our method, we carry out a similar analysis for an atomic four-level system, which is presently employed for spectroscopic quantum sensing using Rydberg atoms [34, 35]. The PRFT thereby predicts that the measurement precision can be improved by several order of magnitudes by invoking a phase measurement instead of the commonly used intensity measurements.

The rest of this article is organized as follows: In Sec. II, we introduce the generic system under investigation and the theoretical framework. In Sec. III, we explain how to utilize the framework to calculate the measurement statistic of important spectroscopic observables, namely, the intensity, the polarization direction and phase shift of a coherent light field, from which one can calculate the Fisher information of spectroscopic sensing protocols. In Sec. IV, we apply the framework to analyze the spectroscopic properties of an ensemble of dissipative two-level systems. In Sec. V, we evaluate the measurement sensitivity of an ensemble of four-level atoms. In Sec. VI we conclude and discuss our findings.

Details and derivations are given in the Appendices.

## II. FRAMEWORK

In this section, we introduce the generic light-matter system for which we develop methods to predict the measurement statistics in spectroscopic measurements with coherent light. Thereby, we apply the PRFT by introducing counting-fields into the semiclassical equation of motions, which predict the major characteristics of the photonic probability distribution required to calculate the Fisher information.

### A. System

The spectroscopic setup investigated in this work is sketched in Fig. 1, in which strong laser light propagates through an ensemble of quantum emitters (e.g., atoms or molecules), to which we will refer as the matter system in the following. For concreteness, we specify the discussion to atoms but remark that the framework has broader applicability. In a microscopic quantum optical description, the Hamiltonian is given by

$$\hat{H} = \sum_{m=1}^N \hat{H}_m + \sum_{k=1}^D \omega_k \hat{a}_k^\dagger \hat{a}_k + \sum_{m,k} g_{m,k} \hat{V}_m (\hat{a}_k^\dagger + \hat{a}_k), \quad (3)$$

where  $\hat{H}_m$  describes the quantum emitter  $m$  in the absence of the laser fields, and  $\hat{V}_m$  denotes the corresponding polarization operator. The photonic creation and annihilation operators  $\hat{a}_k^\dagger, \hat{a}_k$  quantize the light emitted by lasers with frequencies  $\omega_k$ . The light-matter interaction strength is parameterized by the couplings  $g_{m,k}$ . After transversing the atomic ensemble, the transmitted light is measured by a detector setup.

More precisely, we assume that the laser light consists of a sequence of pulses with duration  $t_P$  within the total measurement time  $t_M$ . A specific pulse is quantized by a set of photonic operators  $\hat{a}_k^\dagger, \hat{a}_k$  whose statistics is measured afterwards in the detection setup. These photonic operators might quantize, e.g., different frequencies of the laser light, the polarization direction of linearly polarized light, or some other quantized photonic observables. We envision that the laser pulses interact with a particular atom  $m$ , during which photons can be either absorbed by the atom, or redistributed between the photonic modes. This interaction process can be parameterized by the time-dependent coupling function  $g_{m,k}(t)$ , whose time dependence is determined by the amplitude and shape of the pulse. A microscopic motivation of the Hamiltonian in Eq. (3) is given in Appendix A.

Prior to the interaction of a pulse with the ensemble of atoms, the joint system is assumed to be in the product

state

$$\rho_{\text{tot}}(t=0) = \rho_{\text{M}}(0) \otimes |\alpha\rangle \langle \alpha|, \quad (4)$$

in which the matter state

$$\rho_{\text{M}}(t=0) = \bigotimes_{j=1}^N \rho_{\text{M},j}(0) \quad (5)$$

is a tensor product of the density matrices of the individual atoms. The initial state of the photonic modes is assumed to be a pure state, which is parameterized by

$$|\alpha\rangle = \sum_{\mathbf{n}} a_{\mathbf{n}} |\mathbf{n}\rangle, \quad a_{\mathbf{n}} = \frac{1}{(2\pi)^{\frac{D}{4}} \sqrt{\det \Sigma}} e^{-\frac{1}{4}(\mathbf{n}-\bar{\mathbf{n}})\Sigma^{-2}(\mathbf{n}-\bar{\mathbf{n}})^T} e^{i\bar{\boldsymbol{\varphi}} \cdot \mathbf{n}}, \quad (6)$$

where we have introduced the vector notation  $\mathbf{n} = (n_1, \dots, n_D)$  for the photon numbers  $n_k$ , which label the Fock states  $|\mathbf{n}\rangle = \bigotimes_{k=1}^D |n_k\rangle$ . The photonic state is assumed to have well-defined mean photon numbers  $\bar{\mathbf{n}}$  and mean phases  $\bar{\boldsymbol{\varphi}} = (\bar{\varphi}_1, \dots, \bar{\varphi}_D)$ . The covariance matrix  $\Sigma^2$  parameterize the photon-shot noise and mutual correlations between the photonic modes.

In the following, we investigate the light-matter interaction in the semiclassical regime, which can be defined by a diverging covariance matrix  $\Sigma^2$ . To make this limit precise, we assume that  $\Sigma^2 = \sigma \tilde{\Sigma}^2$ , where the matrix  $\tilde{\Sigma}^2$  shall be constant. The semiclassical limit can then be controlled by assuming the limit  $\sigma \rightarrow \infty$ .

In the semiclassical limit, the photonic creation and annihilation in Eq. (3) can be approximated by their values at the mean-photon numbers  $\bar{\mathbf{n}}$ . More precisely, after a transformation of the Hamiltonian in Eq. (3) into a rotating frame defined by  $U^{(\text{free})} = \exp\left(-i \sum_k \omega_k \hat{a}_k^\dagger \hat{a}_k t\right)$ , we replace the photonic operators in the Hamiltonian with complex-valued numbers, i.e.,

$$\hat{a}_k \rightarrow \sqrt{\bar{n}_k} e^{i\varphi_k - i\omega_k t}. \quad (7)$$

The corresponding Hamiltonian in the semiclassical limit is given by

$$\hat{\mathcal{H}}_{\boldsymbol{\varphi}}(t) = \sum_{m=1}^N \hat{\mathcal{H}}_{m,\boldsymbol{\varphi}}(t), \quad \hat{\mathcal{H}}_{m,\boldsymbol{\varphi}}(t) = \hat{H}_m + \sum_k \Omega_{m,k}(t) \hat{V}_m \cos(\omega_k t - \varphi_k), \quad (8)$$

which acts only on the matter system. Thereby, we have introduced the time-dependent Rabi frequencies  $\Omega_{m,k}(t) = 2g_{m,k}(t)\sqrt{\bar{n}_k}$ . As we assume noninteracting quantum emitters, the Hamiltonian can be expressed as a sum over the quantum emitter index  $m$ . For each semiclassical quantum-emitter Hamiltonian  $\hat{\mathcal{H}}_{m,\boldsymbol{\varphi}}(t)$ , the

time-evolution operator given by

$$\hat{\mathcal{U}}_{\bar{\mathbf{n}},m,\boldsymbol{\varphi}}(t) = \hat{\mathcal{T}} e^{-i \int_0^t \hat{\mathcal{H}}_{m,\boldsymbol{\varphi}}(t') dt'} \quad (9)$$

describes the time-evolution of the matter system in the semiclassical regime. As we assume identical quantum emitters in this paper, we will neglect the index  $m$  hereafter. For later purpose, we have added the mean-photon number vector  $\bar{\mathbf{n}}$  as an index to the time-evolution operator. Despite the absence of the photonic operators in Eq. (8), the PRFT can predict the detailed information about the photonic state solely based on the semiclassical time-evolution operator Eq. (9) as we will show in the remaining part of this paper.

## B. Full-counting statistics

Before introducing the PRFT, we first explain the concepts of full-counting statistics, on which the PRFT relies on. The cumulant-generating function  $K_{\boldsymbol{\chi}}(t)$  of the photonic probability distribution is defined by

$$K_{\boldsymbol{\chi}}(t) = \log \left\langle e^{-i \sum_k \chi_k \hat{a}_k^\dagger \hat{a}_k} \right\rangle, \quad (10)$$

where  $\langle \bullet \rangle$  denotes the expectation value with regard to an arbitrary quantum state. For instance, for the Gaussian state in Eq. (6), the cumulant-generating function is given by

$$K_{\boldsymbol{\chi}} = e^{-i\bar{\mathbf{n}} \cdot \boldsymbol{\chi} - \boldsymbol{\chi} \Sigma^2 \boldsymbol{\chi}}. \quad (11)$$

For brevity, we have represented the counting fields using a vector notation  $\boldsymbol{\chi} = (\bar{\chi}_1, \dots, \bar{\chi}_D)$ .

The cumulants of the photonic probability distribution are defined as the derivatives of the cumulant-generating function with respect to the counting fields

$$\kappa_{l_1 \dots l_D} \equiv i^{l_1 + \dots + l_D} \frac{d^{l_1}}{d\chi_1^{l_1}} \dots \frac{d^{l_D}}{d\chi_D^{l_D}} K_{\boldsymbol{\chi}=\mathbf{0}}, \quad (12)$$

where the  $l_k$  are positive integer-valued numbers.

The cumulants allow for a geometric interpretation of the characteristic features of the probability distribution, and have convenient mathematical properties. For example, the first and second cumulants, which explicitly read

$$\begin{aligned} \bar{n}_k &= \kappa_{0 \dots l_k=1 \dots 0} \\ &= \sum_{\mathbf{n}} n_k p_{\mathbf{n}}, \\ \sigma_{k_1 k_2}^2 &= \kappa_{0 \dots l_{k_1}=1 \dots l_{k_2}=1 \dots 0} \\ &= \sum_{\mathbf{n}} [n_{k_1} - \bar{n}_{k_1}] [n_{k_2} - \bar{n}_{k_2}(t)] p_{\mathbf{n}}(t). \end{aligned} \quad (13)$$

are the means and the covariances of the probability distribution. For a notational reason, we combine the  $\sigma_{k_1 k_2}^2(t)$  into the covariance matrix  $(\Sigma^2)_{k_1, k_2} = \sigma_{k_1 k_2}^2$ ,

whose diagonal elements represents the variances of the probability distribution.

### C. Photon-resolved Floquet theory

Floquet theory is a theoretical method to analyze periodically-driven quantum systems, where the Hamiltonian

$$\hat{H}(t) = \hat{H}(t + \tau) \quad (14)$$

is time periodic with period  $\tau$  [73]. Floquet theory finds important applications in the control of non-equilibrium quantum-phase transition [74–77], in the classification of topological phases of matter [78–81], and in the analysis of quantum-time crystals [82–84], to mention but a few. Floquet theory can be regarded as a semiclassical method of light-matter interaction, which treats the matter as quantum and the coherent light field driving the dynamics as classical. Considering a mono-chromatic driving field with frequency  $\omega = 2\pi/\tau$  and defining the energy-flow operator as

$$\hat{\mathcal{J}}(t) = \frac{d}{dt} \hat{H}(t), \quad (15)$$

we can define the operator counting the number of photons which the matter systems has interchanged with the coherent driving field of frequency  $\omega$  as

$$\Delta \hat{n} = \frac{1}{\omega} \int_0^t \hat{\mathcal{J}}(t') dt' \quad (16)$$

during the interaction time  $t$ . Using this operator, one can calculate the cumulants of the photonic probability distribution. The generalization to polychromatic driving is straightforward [85, 86]. However, the evaluation of higher-order cumulants is numerically cumbersome, as it requires high-dimensional integration of multi-time correlation functions for  $\hat{\mathcal{J}}(t)$ .

To circumvent this obstacle, the PRFT has been developed recently [51]. Like the Floquet theory, the PRFT relies only on the semiclassical time evolution of the matter system given by the Hamiltonian in Eq. (8), but is still capable to predict the measurement statistics of the coherent photonic field by introducing counting-fields into the semiclassical Hamiltonian. This is possible as we consider coherent quantum states of light, which feature relatively small fluctuations around the mean-photon numbers and the mean phases. The aim of the PRFT is to express the photonic measurement statistics in terms of the cumulant-generating function in Eq. (10). For the interaction with a single-quantum emitter in Eq. (8), the PRFT shows that the cumulant-generating function in Eq. (10) can be expressed as

$$K_{\chi}(t) = K_{\bar{n},\chi}(t) K_{\chi}(0), \quad (17)$$

where  $K_{\chi}(0)$  denotes the initial cumulant-generating function given in Eq. (11). The information about the light-matter interaction is contained in the dynamical-moment-generating function

$$K_{\bar{n},\chi}(t) = \log \left\langle \hat{\mathcal{U}}_{\bar{n},\bar{\varphi}-\frac{\chi}{2}}^{\dagger}(t) \hat{\mathcal{U}}_{\bar{n},\bar{\varphi}+\frac{\chi}{2}}(t) \right\rangle_0, \quad (18)$$

where the semiclassical time-evolution operator is given in Eq. (9). Thus, the PRFT introduces for each coherent photonic driving field  $k$ , a corresponding counting field  $\chi_k$ , which allows to obtain the photon statistics of the light-matter interaction dependent on the driving frequency  $\omega_k$  or any other photonic quantum number encoded by  $k$ .

Importantly, the PRFT becomes exact in Sambe space in the semiclassical limit  $\sigma \rightarrow \infty$  [51]. The Sambe space is equivalent to replacing  $\hat{a}_k^{\dagger} \hat{a}_k \rightarrow \sum_{n_k} n_k |n_k\rangle \langle n_k|$  and  $\hat{a}_k \rightarrow \sum_{n_k} \sqrt{n_k} |n_k\rangle \langle n_k + 1|$  [87]. Intriguingly, the PRFT predicts a macroscopic light-matter entanglement effect, in which both subsystems become entangled in the Floquet basis.

To apply the PRFT to spectroscopy, in which the light-field interacts with a macroscopic number of quantum emitters, we derive a flow equation that describes the cumulant-generating function as a function of the propagation distance  $z$  of the pulses through the quantum emitter ensemble. This basic concept is sketched in Fig. 2(a). As shown in Appendix B, this flow equation for the cumulant-generating function is given by

$$\frac{d}{dz} K_{\bar{n},\chi}(z) = \rho_A \mathcal{A} K_{\text{aux},\bar{n},\chi}(z), \quad (19)$$

where  $\rho_A$  denotes the density of the quantum emitters and  $\mathcal{A}$  is the (effective) cross section of the laser. The initial condition is given by the Gaussian cumulant-generating function in Eq. (11). The function  $K_{\text{aux},\bar{n},\chi}$  will be denoted as the auxiliary-generating function and is defined as

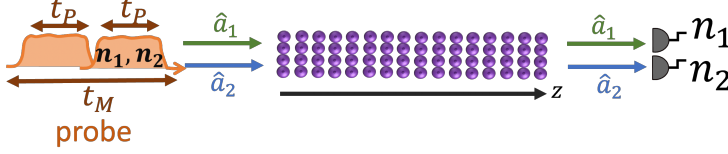
$$K_{\text{aux},\bar{n},\chi}(z) = \sum_{r=0}^{\infty} \sum_{\iota_1 + \dots + \iota_D = r} \left\{ \frac{\partial_{\bar{n}_1}^{\iota_1} \dots \partial_{\bar{n}_D}^{\iota_D}}{\iota_1! \dots \iota_D!} K_{\bar{n},\chi}(z) \right\} \times \prod_{k=1}^D [\partial_{-i\chi_k} K_{\bar{n},\chi}(z) - \bar{n}_k]^{\iota_k}. \quad (20)$$

In the following, we explain the elements in the auxiliary-generating function in more detail:

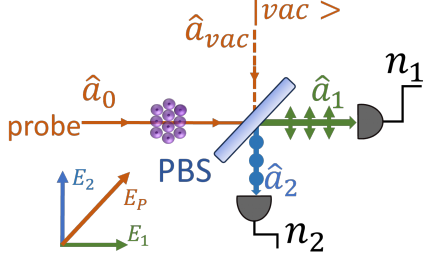
The central building block appearing in the auxiliary-generating function is the dynamical cumulant-generating function in Eq. (18) evaluated at the measurement time  $t = t_M$ . In Eq. (20), we express the dynamical cumulant-generating function as a function of the propagation distance  $z$  to highlight a possible position dependence.

The auxiliary-generating function in Eq. (20) contains a summation over  $r$ , which appears due to a Taylor expansion of the dynamical cumulant generating function

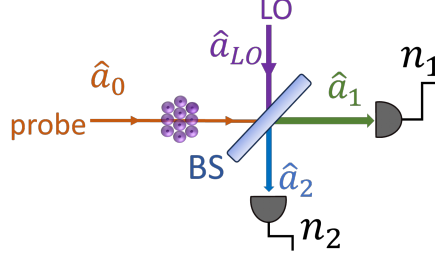
a) Flow equations



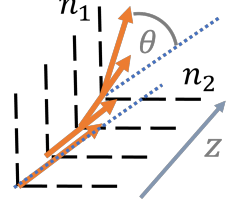
b) Polarization measurement



c) Phase measurement



d) laboratory frame



e) rotated frame

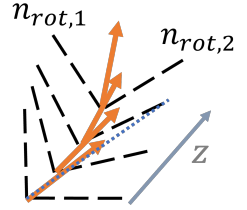


FIG. 2. (a) Sketch of the general setup: A probe field, which can be quantized in terms of the operators  $\hat{a}_k$  for  $k = 1, 2$  propagates through a cloud of atoms (or any other kind of quantum emitters). This generic setup can, e.g., represent a polarization direction measurement as sketched in (b), or a phase measurement as sketched in (c). (d) Illustration of the fixed laboratory frame used to measure linearly polarized light. The polarization direction rotates by an angle of  $\theta$ . (e) Rotated measurement basis, in which the polarization direction always encloses an angle of  $\pi/4$  with both measurement directions.

in Eq. (18). The subscript of the second summation ( $\iota_1 + \dots + \iota_D = r$ ) means that we have to sum over all combinations  $\iota_1, \dots, \iota_D$  whose index sum equals  $r$ . In this context, the symbols  $\partial \bar{n}_k^{\iota_k}$  denote the  $\iota_k$ -th derivatives of the dynamical cumulant-generation function with respect to the mean photon number  $\bar{n}_k$ .

The  $r = 0$  term just equals the auxiliary generator in Eq. (18). This term describes the photon statistics correctly if one would replace the photonic operators in the Hamiltonian in Eq. (3) by their counterparts in Sambe space. The higher-order terms  $r > 0$  in Eq. (20) appear because of the photon-number dependence of the photonic creation and annihilation operators  $\langle n_k - 1 | \hat{a}_k | n_k \rangle = \langle n_k | \hat{a}_k^\dagger | n_k - 1 \rangle = \sqrt{n_k}$ . As these terms are related to the deformation of the photonic state in phase space, we will refer to them as phase-space terms in the following. Its interpretation will be discussed in more detail in Sec. II D.

Moreover, the symbol  $\partial_{-\chi_k}$  denotes the derivative with respect to the counting field  $\chi_k$ , which act on the cumulant-generating function at position  $z$ . Because of this term, the flow equation in Eq. (19) becomes a non-linear partial differential equation, which cannot be solved, neither numerically nor analytically. The usage of Eq. (19) will be discussed in the next section.

#### D. Mean and variance

In general, the flow equation for the cumulant-generating function in Eq. (19) cannot be integrated. However, it can be considered as an *equation-generating equation*, as we will demonstrate here. More precisely,

by deriving Eq. (19) with respect to the counting fields, we can generate flow equations for low-order cumulants. We will demonstrate this for the first two cumulants, and comment on the construction of higher-order flow equations.

(i) Deriving Eq. (19) with respect to each counting field  $\chi_k$ , we obtain the flow equation for the mean photon numbers

$$\frac{d}{dz} \bar{\mathbf{n}} = \mathbf{I}_{\bar{\mathbf{n}}}, \quad (21)$$

where the coefficient on the right-hand side is explicitly given by

$$[\mathbf{I}_{\bar{\mathbf{n}}}]_k = \rho_A \mathcal{A} \partial_{\chi_k} \mathcal{K}_{\bar{\mathbf{n}}, \chi=0}(z). \quad (22)$$

Importantly, this flow equation is a nonlinear differential equation, as  $\mathbf{I}_{\bar{\mathbf{n}}}$  depends on the mean photon numbers in a nonlinear fashion. Thus, we have to continuously update  $\bar{\mathbf{n}} = \bar{\mathbf{n}}(z)$  when (numerically) solving Eq. (21).

(ii) Deriving Eq. (19) two times with respect to the counting fields  $\chi_k$ , we obtain the flow equation for the covariance matrix

$$\frac{d}{dz} \Sigma^2 = \mathbf{D}_{\bar{\mathbf{n}}} + \mathbf{C}_{\bar{\mathbf{n}}} \Sigma^2 + \Sigma^2 \mathbf{C}_{\bar{\mathbf{n}}}, \quad (23)$$

where

$$\begin{aligned} [\mathbf{D}_{\bar{\mathbf{n}}}]_{k_1, k_2} &= \rho_A \mathcal{A} \partial_{\chi_{k_1}} \partial_{\chi_{k_2}} \mathcal{K}_{\bar{\mathbf{n}}, \chi=0}(z), \\ [\mathbf{C}_{\bar{\mathbf{n}}}]_{k_1, k_2} &= \rho_A \mathcal{A} \partial_{\bar{n}_{k_1}} \partial_{\chi_{k_2}} \mathcal{K}_{\bar{\mathbf{n}}, \chi=0}(z). \end{aligned} \quad (24)$$

This equation has to be solved with  $\Sigma^2$  of the photonic

state in Eq. (6) as initial condition. Noteworthy, the coefficient matrices  $\mathbf{D}_{\bar{n}}$  and  $\mathbf{C}_{\bar{n}}$  depend on the mean photon numbers.

The matrix  $\mathbf{D}_{\bar{n}}$  is obtained by a twofold derivation of the dynamical cumulant-generating function with respect to the counting fields. Using similar methods as in Ref. [50], it is possible to show that  $[\mathbf{D}_{\bar{n}}]_{k_1, k_2} \geq 0$ , i.e., its contribution enhances the variance. For this reason, we denote this term as the diffusion matrix in the following.

The other coefficient matrix  $\mathbf{C}_{\bar{n}}$  incorporates the photon number dependence of the creation and annihilation operators into the dynamical equation, and describes the resulting deformation of the photonic probability distribution. We will denote it as the phase-space matrix in the following.

(iii) In a similar fashion, one can derive the flow equations for higher-order cumulants. Inspection of Eq. (19) shows that the flow equation for a cumulant of order  $l = l_1 + \dots + l_D$  involves the Taylor expansion up to order  $r = l - 1$  of the dynamical cumulant-generating function in Eq. (20). Consequently, a cumulant of order  $l$  cannot depend on a higher-order cumulant  $l' > l$ . In the derivation of the Eq. (19) it has been assumed that the laser pulses interact with an ensemble of non-interacting quantum emitters. For this reason, the probability distribution will approach (stay) a Gaussian function for long enough propagation distances  $z$ . Consequently, the knowledge of the first two cumulant orders is enough to describe realistic measurement statistics.

### III. SPECTROSCOPIC QUANTUM SENSING

In Sec. II, we have established a theoretical framework which is capable of predicting the photon exchange between pulses of light and an ensemble of quantum emitters without further specifying the physical meaning of the photonic operators. In this section, we now link the photonic operators in the Hamiltonian in Eq. (3) to relevant observables in spectroscopic quantum sensing, namely the intensity of a laser, the polarization direction of linearly polarized light and the phase shift of the laser-light imposed by the light-matter interaction. In doing so, we provide practical guidelines on how to best integrate the flow equations in Eqs. (21) and (23), and explain how this can be utilized to evaluate the Fisher information in Eq. (2).

#### A. Intensity

A vital observable in spectroscopic experiments is the optical intensity of the laser field, which is defined as the radiation energy traversing a unit area  $\mathcal{A}$  within a unit time. In contrast, the PRFT counts the number of photons contained in a laser pulse. The laser intensity of a pulse with frequency  $\omega$ , duration  $t_P$  and cross section

$\mathcal{A}$  can be estimated by

$$I_L = \frac{\hbar\omega}{t_P \mathcal{A}} n. \quad (25)$$

where  $n$  is the measured photon number. Thus, from the statistics of the photon number  $n$  (as predicted by the PRFT), we can obtain the intensity.

To improve the signal to noise ratio of the intensity measurement, one can invoke longer measurement times  $t_M$  by recording the measurement outcomes for the continuous train of pulses. Quantizing the pulses with the photonic operators  $\hat{a}_k$ , we denote the measured photon number by  $n_k$ . Crucially, the  $n_k$  can not be regarded as independent random variables. Rather, the photon numbers are highly correlated because of memory effects of the atoms, which the pulses interact with. For example, the correlation time of the atomic dynamics can be determined by relaxation processes with rate  $\gamma$  such that  $t_P \ll 1/\gamma$ .

To estimate the mean intensity of this pulse train, we employ the cumulative photon number  $\sum_k n_k$  as a random variable. Comparing with the definition of the cumulant-generating function in Eq. (10), we see that we can simply obtain the statistics of the cumulative photon number by setting all counting-fields equally  $\chi_k = \chi$ . We then evaluate the flow equations in Sec. II C for  $\chi$  and  $t = t_M$  in Eq. (18). The intensity of the radiation field can be then estimated as

$$I_L = \frac{\hbar\omega}{t_M \mathcal{A}} \sum_{k=1}^D n_k, \quad (26)$$

where the statistics of the cumulative photon number  $\sum_{k=1}^D n_k$  can be obtained using the dynamical cumulant-generator function in Eq. (18) with integration time  $t_M$ . Noteworthy, in principle it is possible to construct more precise estimators for the intensity based on the joint photonic measurement probabilities  $p_{n_1 \dots n_D}$  using, e.g., a Markov-chain approach. However, this would exceed the scope of this work and will be considered elsewhere.

#### B. Polarization direction

In this section, we assume that the laser pulse is initially polarized in the direction

$$\mathbf{E}_{\text{in}}(\mathbf{r}, t) \propto \mathbf{e}_x + \mathbf{e}_y, \quad (27)$$

where  $\mathbf{e}_x$  and  $\mathbf{e}_y$  denote the unit vectors in x and y directions as shown in the inset of Fig. 2(b). Accordingly, we introduce the operators  $\hat{a}_1$  and  $\hat{a}_2$  which quantize the electromagnetic field of the laser pulse in x and y directions, respectively. Thus, initially, both occupation number operators  $\hat{n}_\alpha = \hat{a}_\alpha^\dagger \hat{a}_\alpha$  with  $\alpha = 1, 2$  have the

same mean value,

$$\langle \hat{n}_1 \rangle_{\text{in}} = \langle \hat{n}_2 \rangle_{\text{in}} = \frac{\bar{n}_+^{(\text{in})}}{2}, \quad (28)$$

where  $\bar{n}_+^{(\text{in})}$  is the initial total number of photons in the pulse, which is a function of its shape, duration and frequency. The choice of the basis direction in Eq. (27) is in principle arbitrary as long as the photonic field in both directions is macroscopically occupied. Yet, the initial symmetric occupation in both measurement direction is advantageous for the evaluation of the flow equations.

When the light pulse is propagating through an ensemble of quantum emitters, the polarization direction can be changed, e.g., because of the Faraday effect. The change in the polarization direction manifests itself in an imbalance in the photonic occupations of  $\hat{n}_1$  and  $\hat{n}_2$ . The photon numbers can be measured using a polarization beam splitter and two photon detectors as sketched in Fig. 2(b), from which we can infer the mean value of the polarization rotation  $\bar{\theta}$  via

$$\sin \bar{\theta} = \frac{\sqrt{\bar{n}_2} - \sqrt{\bar{n}_1}}{\sqrt{2\bar{n}_+}}, \quad (29)$$

where  $\bar{n}_\alpha$  is the mean photon number at detector  $\alpha = 1, 2$ , and  $\bar{n}_+ = \bar{n}_1 + \bar{n}_2$ .

### C. Phase

Even though the PRFT is a framework which counts the number of photons, it is also capable to predict the statistics of phase measurements. This assertion becomes clear when recalling that it is only possible to measure intensities in optical experiments. A phase measurement is typically carried out by superposing the probe field (whose phase is to be measured) with a local oscillator, and then inferring the phase information from the intensity change of the resulting light field.

The corresponding experimental setup is depicted in Fig. 2(c), where the probe field is quantized by  $\hat{a}_0$  and the local oscillator is quantized by  $\hat{a}_{\text{LO}}$ . Using a beam-splitter, we create the two superposition output fields  $\hat{a}_1, \hat{a}_2$ , which are related to the input fields  $\hat{a}_0, \hat{a}_{\text{LO}}$  via

$$\begin{aligned} \hat{a}_1 &= \frac{1}{\sqrt{2}} (\hat{a}_{\text{LO}} + i\hat{a}_0), \\ \hat{a}_2 &= \frac{1}{\sqrt{2}} (\hat{a}_{\text{LO}} - i\hat{a}_0). \end{aligned} \quad (30)$$

For illustration, let us assume that the probe pulse is in a coherent state with complex amplitude  $\sqrt{\bar{n}_0}e^{i\bar{\varphi}_0}$ , where  $\bar{n}_0$  is the mean photon number and  $\bar{\varphi}_0$  is the phase to be measured. Likewise, the local oscillator is in a coherent state with complex amplitude  $\sqrt{\bar{n}_{\text{LO}}}e^{i\bar{\varphi}_{\text{LO}}}$ . Denoting the mean occupations of the operators by  $\bar{n}_\alpha = \langle \hat{a}_\alpha^\dagger \hat{a}_\alpha \rangle$  for  $\alpha = 1, 2$ , we find relations for the sum and difference of

the mean photon numbers

$$\begin{aligned} \bar{n}_1 + \bar{n}_2 &= \bar{n}_0 + \bar{n}_{\text{LO}}, \\ \bar{n}_1 - \bar{n}_2 &= 2\sqrt{\bar{n}_0\bar{n}_{\text{LO}}} \sin(\bar{\varphi}_0 - \bar{\varphi}_{\text{LO}}), \end{aligned} \quad (31)$$

from which we can infer the phase of the probe field via

$$\sin(\bar{\varphi}_0 - \bar{\varphi}_{\text{LO}}) = \frac{\bar{n}_1 - \bar{n}_2}{2\sqrt{\bar{n}_0\bar{n}_{\text{LO}}}}. \quad (32)$$

Thus, we obtain the phase information via a photon number measurement, which is closely related to the intensity.

Based on these considerations, we can now establish a connection to the PRFT. To this end, we assume that originally the quantum emitters interact with the probe field via the operator  $\hat{a}_0$  in the Hamiltonian. Now we invert Eq. (30), i.e.,

$$\hat{a}_0 = \frac{1}{\sqrt{2}i} (\hat{a}_1 - \hat{a}_2) \quad (33)$$

and insert this into the Hamiltonian. As a consequence, the quantum emitters interact now with the two modes  $\hat{a}_1, \hat{a}_2$ , for which we can use the formalism in Sec. II to calculate the projected measurement statistics. The replacement in Eq. (33) is a unitary transformation into the basis of measurement. Thus, we express the Hamiltonian in exactly the basis, in which we will finally measure the photon statistics.

### D. Relation between polarization and phase measurements

It is worth noting that the polarization direction measurement in Sec. IIIB and the phase-shift measurement in Sec. IIIC are intimately related. The mutual connection becomes clear when recalling that linearly polarized light can be considered as a superposition of two circularly polarized light modes, where the modes have an orthogonal polarization. Using simple geometric considerations, one finds that a phase shift of one circularly polarized mode  $\Delta\bar{\varphi}$  leads to a rotation of the resulting linearly polarized light  $\Delta\bar{\theta}$ , and both angles are related by

$$\Delta\bar{\varphi} = 2\Delta\bar{\theta}. \quad (34)$$

This is the origin of the celebrated Faraday effect, in which each circular polarization mode of the light field is subject to a different susceptibility for matter in an external magnetic field.

We can discover this effect also when comparing Eqs. (29) and (32). To this end, we assume that both modes are initially equally occupied according to Eq. (28). Deriving Eq. (29) with respect to the position

$z$ , we find

$$\frac{d}{dz}\bar{\theta} = \frac{\frac{d}{dz}\bar{n}_1 - \frac{d}{dz}\bar{n}_2}{2\bar{n}_+}, \quad (35)$$

which is the differential change of the rotation axis induced by the light-matter interaction. Likewise, for the phase shift in Eq. (32), we assume that originally  $\bar{n} = \bar{n}_{\text{LO}}$  and  $\bar{\varphi} = \bar{\varphi}_{\text{LO}}$ . Deriving then Eq. (32) with respect to  $z$ , we find

$$\frac{d}{dz}\bar{\varphi} = \frac{\frac{d}{dz}\bar{n}_1 - \frac{d}{dz}\bar{n}_2}{\bar{n}_+}, \quad (36)$$

which describes the differential change of the measured phase due to the light-matter interaction.

Comparing Eq. (35) with Eq. (36), we readily find

$$\frac{d\bar{\varphi}}{dz} = 2\frac{d\bar{\theta}}{dz}, \quad (37)$$

which is simply the differential form of Eq. (34). This relation implies that we can formally map a phase-shift measurement to a polarization-direction measurement. The later interpretation might be more appealing, as the measured photonic operators already appear in the original Hamiltonian. This more intuitive approach helps us to represent the phase measurement in a form, which is more convenient for the numerical and analytical integration, as will be explained in the next section.

### E. Rotating measurement frame

For the following explanations, we consider a polarization measurement as introduced in Sec. IIIB. The flow equations in Eqs. (21) and (23) predict the measured photonic probabilities in a basis which is fixed in the laboratory frame. While this setup is intuitive, there are two advantages to consider a measurement basis, which rotates along with the polarization direction of the light pulse:

- (i) The PRFT is only valid if the photonic driving fields are highly occupied. For particular rotation angles, the occupation of one of the modes might vanish, which makes the integration of the flow equations invalid within the PRFT.
- (ii) The matrices  $C_{\bar{n}}$  in Eq. (23) often dominate the time evolution of the covariance matrix. In a rotating measurement frame, these matrices will be rendered small, which enables a stable numerical integration and a theoretical analysis.

The two different measurement basis setups are sketched in Fig. 2(d) and Fig. 2(e), showing the fixed and rotated measurement directions for various positions  $z$ , respectively. In the rotated basis, the instantaneous direction of the electric field polarization is depicted by the red

arrow, and encloses a  $\pi/4$  angle with both rotated basis directions for all positions  $z$ .

To parameterize the rotation, we utilize the position dependent mean polarization angel  $\bar{\theta} = \bar{\theta}(z)$  defined in Eq. (29). In terms of  $\bar{\theta}$ , the rotated photonic operators are defined by

$$\begin{aligned} \hat{a}_{\text{rot},1} &= \cos\bar{\theta}\hat{a}_1 - \sin\bar{\theta}\hat{a}_2, \\ \hat{a}_{\text{rot},2} &= \sin\bar{\theta}\hat{a}_1 + \cos\bar{\theta}\hat{a}_2. \end{aligned} \quad (38)$$

The angel  $\bar{\theta}$  is chosen such that for all positions  $z$  the mean occupations of the photonic modes  $\hat{n}_{\text{rot},\alpha} = \hat{a}_{\text{rot},\alpha}^\dagger \hat{a}_{\text{rot},\alpha}$  with  $\alpha = 1, 2$  are equal, i.e.,

$$\langle \hat{n}_{\text{rot},1} \rangle = \langle \hat{n}_{\text{rot},2} \rangle \equiv \frac{\bar{n}_+(z)}{2}, \quad (39)$$

where  $\bar{n}_+(z)$  denotes the total number of photons in both modes.

As shown in Appendix C1, the rotation angle and the total number of photons can be calculated using the following differential relations

$$\begin{aligned} \frac{d\bar{\theta}}{dz} &= \frac{\partial_z \bar{n}_{\text{rot},2} - \partial_z \bar{n}_{\text{rot},1}}{2\bar{n}_+}, \\ \frac{d\bar{n}_+}{dz} &= \partial_z \bar{n}_{\text{rot},2} + \partial_z \bar{n}_{\text{rot},1}. \end{aligned} \quad (40)$$

Thereby,  $\partial_z \bar{n}_{\text{rot},\alpha}$  refers to the derivatives of the mean photon number  $\bar{n}_{\text{rot},\alpha}$  in the fixed measurement basis and can be evaluated via

$$\partial_z \bar{n}_{\text{rot},\alpha} = [\mathbf{I}_{\bar{n}_{\text{rot}}}]_\alpha, \quad (41)$$

where  $\mathbf{I}_{\bar{n}_{\text{rot}}}$  is the photon flux vector in Eq. (22) for the semiclassical Hamiltonian, in which the photonic mode occupations satisfy the rotation condition in Eq. (39).

The differential equation for the correlation matrix, as it will be measured in the rotated measurement basis, is given by

$$\begin{aligned} \frac{d}{dz}\Sigma_{\text{rot}}^2 &= D_{\bar{n}_{\text{rot}}} + \tilde{C}_{\bar{n}_{\text{rot}}}\Sigma_{\text{rot}}^2 + \Sigma_{\text{rot}}^2\tilde{C}_{\bar{n}_{\text{rot}}}, \\ \tilde{C}_{\bar{n}_{\text{rot}}} &= C_{\bar{n}_{\text{rot}}} - \frac{d\bar{\theta}}{dz}\hat{\Xi}, \end{aligned} \quad (42)$$

where we have introduced  $\hat{\Xi} = i\hat{\sigma}_y + \hat{\sigma}_z$  ( $\hat{\sigma}_\alpha$  with  $\alpha = x, y, z$  denoting the common Pauli matrices). Thereby,  $D_{\bar{n}_{\text{rot}}}$  and  $C_{\bar{n}_{\text{rot}}}$  refer to the diffusion and phase-space matrices as defined in Eq. (24), but evaluated under the rotation condition in Eq. (39). Typically, the entries of  $\tilde{C}_{\bar{n}_{\text{rot}}}$  are significantly smaller than the ones of  $C_{\bar{n}_{\text{rot}}}$ , enabling a more efficient numerical and analytical treatment.

Conversely, in terms of the observables  $\bar{n}_+$  and  $\bar{\theta}$ , it is also straightforward to retrieve the means and covariances for the measurement in the original measurement

basis in the lab frame by evaluating

$$\begin{pmatrix} \bar{n}_1 \\ \bar{n}_2 \end{pmatrix} = \bar{n}_+ \begin{pmatrix} \cos^2(\frac{\pi}{4} + \bar{\theta}) \\ \sin^2(\frac{\pi}{4} + \bar{\theta}) \end{pmatrix}, \quad (43)$$

and

$$\Sigma_{\alpha,\beta}^2 = \frac{2\sqrt{\bar{n}_\alpha}\sqrt{\bar{n}_\beta}}{\bar{n}_+} \left( e^{i\bar{\theta}\hat{\sigma}_y} \Sigma_{\text{rot}}^2 e^{-i\bar{\theta}\hat{\sigma}_y} \right)_{\alpha,\beta}, \quad (44)$$

for  $\alpha, \beta = 1, 2$ . The detailed derivation is given in Appendix C 1.

Using the relation between rotation and phase measurements in Sec. III D, one can also transform a phase measurement into an adjusted measurement setup, which simplifies the flow equation. Physically, instead of rotating the measurement basis, we adjust the amplitude and phase of the local oscillator such that Eq. (39) is fulfilled. This implies that  $\bar{n} = \bar{n}_{\text{LO}}$  and  $\bar{\varphi} = \bar{\varphi}_{\text{LO}}$ . Using the correspondence in Eq. (34), we can interpret the phase measurement as a *virtual* polarization measurement. After calculating the virtual polarization change, we can then use Eq. (34) to obtain the mean phase value. Moreover, the measurement statistics of the covariance matrix is the same in the phase and the polarization estimations.

#### F. Fisher information

According to the Cramer-Rao bound in Eq. (1), the measurement precision is bounded by the inverse Fisher information. Under the assumption of a Gaussian probability distribution, the leading-order term of the Fisher information is given by

$$\mathcal{I}_X = (\partial_X \bar{\mathbf{n}}_X) \Sigma_X^{-2} (\partial_X \bar{\mathbf{n}}_X)^T, \quad (45)$$

as shown in Appendix D. Thus, it can be expressed in terms of the mean values and covariance matrix of the probability distribution of  $\mathbf{n}$ . As the photonic probability distribution approaches a Gaussian distribution when interacting with a macroscopic number of independent quantum emitters, we will use Eq. (45) in the following calculations.

When working in the rotated measurement basis introduced in Sec. III E, the measurement statistics and the Fisher information can be conveniently expressed in terms of

$$\begin{aligned} n_+ &= n_1 + n_2, \\ n_- &= n_1 - n_2. \end{aligned} \quad (46)$$

The total photon number  $n_+$  carries information about the total intensity of a laser pulse, while the photon number difference  $n_-$  is related to the phase shift  $\bar{\theta}$  via Eq. (32). We recall that, by definition, the mean value  $\bar{n}_- = 0$  in the rotated measurement basis, such that the information about the polarization rotation is expressed by  $\bar{\theta}$ . In the rotated measurement picture,  $\partial_X \bar{\mathbf{n}}_X$  can be

simply evaluated via

$$\partial_X \bar{\mathbf{n}}_X = \bar{n}_+ \frac{d\bar{\theta}}{dX} \begin{pmatrix} 1 \\ -1 \end{pmatrix} + \frac{d\bar{n}_+}{dX} \begin{pmatrix} 1 \\ 1 \end{pmatrix}, \quad (47)$$

as can be shown using Eq. (43) for  $\bar{\theta} = 0$ .

#### IV. TAVIS-CUMMINGS MODEL

To demonstrate the theoretical concepts in Sec. II and Sec. III for a concrete example, we consider here a dissipative version of the celebrated Tavis-Cummings model, whose Hamiltonian reads

$$\hat{H} = \hat{H}_{\text{TC}} + \hat{H}_{\text{Bath}}. \quad (48)$$

Thereby, the closed Tavis-Cummings model is given by

$$\begin{aligned} \hat{H}_{\text{TC}} &= \omega \hat{a}_0^\dagger \hat{a}_0 + \sum_m \frac{\epsilon}{2} \hat{\sigma}_{m,z} \\ &+ \sum_m g_m(t) \left( \hat{\sigma}_{m,-} \hat{a}_0^\dagger + \hat{\sigma}_{m,+} \hat{a}_0 \right), \end{aligned} \quad (49)$$

where the photonic operators  $\hat{a}_0, \hat{a}_0^\dagger$  quantizes a laser pulse with frequency  $\omega$ ,  $\hat{\sigma}_{m,z}$  describes the two levels of atom  $m$ , which has level splitting  $\epsilon$ . The coupling operators of the quantum emitters are given by the Pauli operators  $\hat{\sigma}_{m,-}, \hat{\sigma}_{m,+}$ , whose time-dependent coupling to the photonic field is parameterized by  $g_m(t)$ . We recall that the time-dependence of  $g_m(t)$  is determined by the pulse shape and quantum emitter location.

Moreover, each quantum emitter is coupled to its own bath which gives rise to dissipation. The bath and the coupling operators are described by

$$\hat{H}_{\text{Bath}} = \sum_{m,q} \omega_q \hat{b}_{m,q}^\dagger \hat{b}_{m,q} + \sum_{m,q} v_q \left( \hat{\sigma}_{m,-} \hat{b}_{m,q}^\dagger + \text{h.c.} \right), \quad (50)$$

where the bosonic bath modes  $\hat{b}_{m,q}$  with frequency  $\omega_q$  are coupled to the quantum emitters with strength  $v_q$ . We assume that the baths are in a thermal state with temperature  $k_B T \ll \hbar\omega$ .

In the rest of this section, we will use the PRFT to estimate the counting statistics for the phase-shift measurement of the probe pulse quantized by  $\hat{a}_0$ . A sketch of the corresponding experimental setup and the dissipative two-level systems can be found in Fig. 3(a) and Fig. 3(b), respectively.

##### A. Cumulant-generating function

The first step in the framework is to get an expression for the dynamical cumulant-generating function defined in Eq. (18). Using Eq. (33) we represent the Hamiltonian

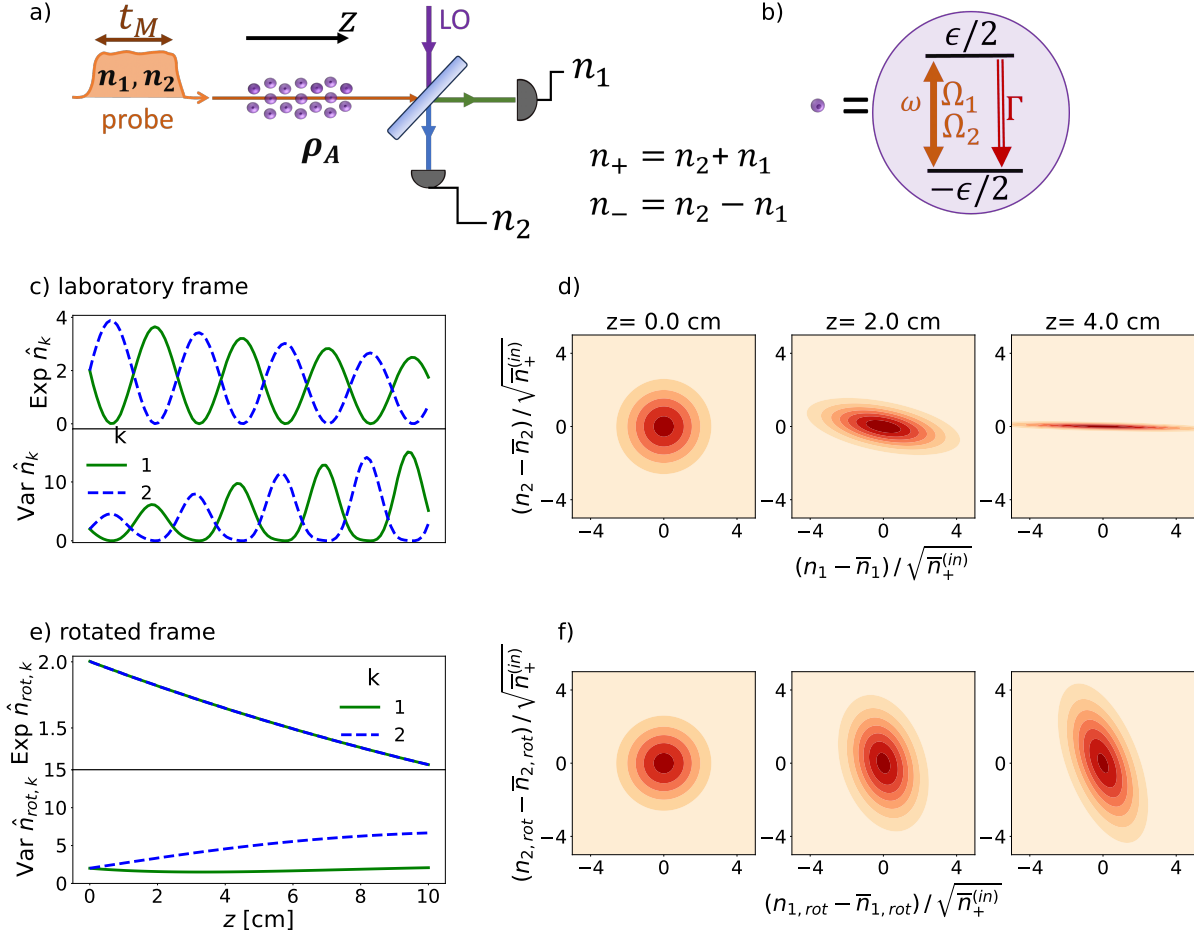


FIG. 3. (a) Experimental setup designed for a phase measurement. (b) Dissipative two-level system. (c) Mean photon number and the variance as a function of propagation distance  $z$  for the mode  $k = 1, 2$  in the laboratory measurement frame. (d) Probability distribution for three selected distances. (e) and (f) depict the same as (c) and (d) but in the rotated measurement basis. The dynamics in the rotated frame is obtained by integrating the flow equations in Eqs. (40) and (42) using the coefficients in Eqs. (63), (64) and (65). The values in the laboratory frame can be obtained using Eqs. (43) and (44). Parameters are  $\gamma = 1$  Mhz,  $z_{\max} = 10$  cm,  $P = 100$  mW,  $\mathcal{A} = 1$  cm<sup>2</sup>,  $\rho_A = 10^{14}$  m<sup>-3</sup>,  $t_M = 1$  s and atomic dipole moment  $d = 5ea_0$ . This gives rise to an overall Rabi frequency of  $\Omega = 60$  MHz.

in the measurement basis, which reads

$$\begin{aligned} \hat{H}_{\text{TC}} = & \sum_{k=1,2} \omega \hat{a}_k^\dagger \hat{a}_k + \sum_m \frac{\epsilon}{2} \hat{\sigma}_{m,z} \\ & + \sum_{m,k=1,2} \left[ \frac{g_m(t)}{\sqrt{2}} i \hat{\sigma}_{m,-} \hat{a}_k^\dagger + \text{h.c.} \right]. \end{aligned} \quad (51)$$

Next, we consider the Hamiltonian in the semiclassical limit by replacing  $\hat{a}_k \rightarrow \sqrt{\bar{n}_k} e^{i\varphi_k}$ , such that

$$\hat{\mathcal{H}}(t) = \sum_m \hat{\mathcal{H}}_{m,\varphi}(t) + \hat{H}_{\text{Bath}}, \quad (52)$$

where the semiclassical light-matter interaction of two-level system  $m$  is described by

$$\hat{\mathcal{H}}_{m,\varphi}(t) = \frac{\epsilon}{2} \hat{\sigma}_{m,z} + \sum_{k=1,2} \left[ \frac{\Omega_{m,k}(t)}{2} e^{i(\omega t - \varphi_k)} \hat{\sigma}_{m,-} + \text{h.c.} \right], \quad (53)$$

in which the effective Rabi frequencies are given by  $\Omega_{m,k}(t) = \sqrt{2\bar{n}_k} g_{m,k}(t)$ . In the following, we will omit the index  $m$ , as the quantum emitters are formally decoupled in the semiclassical Hamiltonian and assumed to be identical. Of note, the Tavis-Cummings model describes the light-matter interaction within a rotating-wave approximation, which allows us to derive analytical expression of the measurement statistics. Yet, we emphasize that the methods developed in this work are also applica-

ble for models beyond the rotating-wave approximation.

As each quantum emitter is coupled to a continuum of bath modes, we cannot exactly construct the semi-classical time-evolution operator in Eq. (9). Instead, we use an open quantum system approach of the PRFT to construct the dynamical moment-generating function in Eq. (18). To this end, we deploy a generalized quantum master equation, which describes the system-bath coupling in second-order perturbation theory as introduced in Ref. [50]. To obtain the dynamical moment-generating function, we first have to integrate the generalized master equation

$$\frac{d}{dt}\rho_{\chi} = \mathcal{L}_{\bar{n},\chi}\rho_{\chi}, \quad (54)$$

and then use the generalized density matrix of the quantum-emitter system  $\rho_{\chi}$  to construct the dynamical moment-generating function via

$$\mathcal{K}_{\bar{n},\chi}(z) = \log \text{tr} [\rho_{\chi}(t_M)] \rightarrow \lambda_{\bar{n},\chi} t_M. \quad (55)$$

The information about the laser pulse properties (i.e., the occupations of the photonic modes) is expressed by the subscript  $\bar{n}$  of the generalized Liouvillian. For long enough measurement times  $t_M$ , the generating function becomes proportional to the dominating eigenvalue of the Liouvillian, i.e., the eigenvalue which is  $\lambda_{\bar{n},\chi} \rightarrow 0$  for  $\chi \rightarrow 0$  [50], which leads to the simple expression for the generating function in Eq. (55).

For the Hamiltonian in Eq. (53) under the influence of the dissipative bath modes, the generalized Liouvillian is time-independent and given by

$$\begin{aligned} \mathcal{L}_{\bar{n},\chi}\rho = & -i \left[ \hat{\mathcal{H}}_{\varphi+\frac{\chi}{2}}\rho - \rho\hat{\mathcal{H}}_{\varphi-\frac{\chi}{2}} \right] \\ & + \gamma \left[ \hat{\sigma}_-\rho\hat{\sigma}_+ - \frac{1}{2} \{\rho, \hat{\sigma}_+\hat{\sigma}_-\} \right], \end{aligned} \quad (56)$$

where  $\gamma$  parameterizes the coupling strength of the atoms to the bath modes, and the Hamiltonian acting on the quantum emitters reads as

$$\hat{\mathcal{H}}_{\varphi} = \frac{\epsilon_{\Delta}}{2} \hat{\sigma}_z + \sum_{k=1,2} \left[ \frac{\Omega_k}{2} e^{i\varphi_k} \hat{\sigma}_- + \text{h.c.} \right], \quad (57)$$

where  $\epsilon_{\Delta} = \epsilon - \omega$  denotes the laser detuning. For simplicity, we consider a Rabi frequency which is constant during the pulse duration  $t_M$ .

## B. Flow equations

We are now in position to construct the flow equations for the mean and the covariance matrix in Eqs. (21) and (23), respectively, using the generating function in Eq. (55). The analytical calculation of the low-order derivatives with respect to the counting fields is demonstrated in Appendix F 1. The following formulas are represented in a vector notation in the basis  $(n_1, n_2)$ .

The photon flux coefficients defined in Eq. (22) read

$$\begin{aligned} \mathbf{I}_{\bar{n}} = & \frac{t_M \rho_A \mathcal{A}}{4\epsilon_{\Delta}^2 + 2\Omega_{\tilde{\varphi}}^2 + \gamma} \left[ \Omega_1 \Omega_2 \epsilon_{\Delta} \sin(\tilde{\varphi}) \begin{pmatrix} 1 \\ -1 \end{pmatrix} \right. \\ & \left. - \gamma \begin{pmatrix} \Omega_1^2 \\ \Omega_2^2 \end{pmatrix} - \gamma \Omega_1 \Omega_2 \cos(\tilde{\varphi}) \begin{pmatrix} 1 \\ 1 \end{pmatrix} \right], \end{aligned} \quad (58)$$

where we have introduced

$$\Omega_{\tilde{\varphi}}^2 = \Omega_1^2 + 2\Omega_1 \Omega_2 \cos(\tilde{\varphi}) + \Omega_2^2. \quad (59)$$

This is the effective Rabi frequency which the two-level experiences due to the driving of the two modes. Moreover, we have defined  $\tilde{\varphi} = \bar{\varphi}_1 - \bar{\varphi}_2$ . The term proportional to  $\epsilon_{\Delta}$  gives rise to a mean-photon number imbalance between modes  $k = 1$  and  $k = 2$ , which can be associated with a phase shift according to the explanations in Eq. (32). The terms proportional to  $\gamma$  describe absorption of photons by the dissipative two-level systems.

The diffusive matrix defined in Eq. (24) can be represented as

$$\mathbf{D}_{\bar{n}} \approx \rho_A \mathcal{A} t_M \frac{32\Omega_1^2 \Omega_2^2 \Omega_{\tilde{\varphi}}^4 \sin^2(\tilde{\varphi})}{\gamma [4\epsilon_{\Delta}^2 + 2\Omega_{\tilde{\varphi}}^2]^3} \begin{pmatrix} 1 & -1 \\ -1 & 1 \end{pmatrix} + \mathcal{O}(\gamma^0), \quad (60)$$

which we have expanded for small dissipation  $\gamma$ . The full expression can be found in Eq. (F4). Interestingly, the lowest order contribution scales with  $\gamma^{-1}$ . The matrix has two eigenvectors. The first one is  $(1, 1)$  and has a vanishing eigenvalue, and thus does not contribute to the diffusive dynamics. The second one is  $(1, -1)$  and has a finite eigenvalue and thus contributes to the diffusion. As the eigenvector  $(1, -1)$  is proportional to the first line in Eq. (58), and the leading order of the diffusion matrix is proportional to  $\sin^2(\tilde{\varphi})$  we conclude that the leading order of  $\mathbf{D}_{\bar{n}}$  describes phase diffusion.

Finally, the phase-space matrix defined in Eq. (24) can be calculated by deriving the photon fluxes with respect to the mean photon numbers  $\bar{n}_1, \bar{n}_2$ . In doing so, we obtain

$$\begin{aligned} \mathbf{C}_{\bar{n}} = & \frac{\rho_A \mathcal{A} t_M}{4\epsilon_{\Delta}^2 + 2\Omega_{\tilde{\varphi}}^2 + \gamma} \left[ \frac{\Omega_1 \Omega_2 \epsilon_{\Delta}}{2} \sin(\tilde{\varphi}) \begin{pmatrix} \frac{1}{\bar{n}_1} & \frac{1}{\bar{n}_2} \\ -\frac{1}{\bar{n}_1} & -\frac{1}{\bar{n}_2} \end{pmatrix} \right. \\ & - \gamma \begin{pmatrix} \frac{\Omega_1^2}{\bar{n}_1} & 0 \\ 0 & \frac{\Omega_2^2}{\bar{n}_2} \end{pmatrix} - \frac{\Omega_1 \Omega_2 \gamma}{2} \cos(\tilde{\varphi}) \begin{pmatrix} \frac{1}{\bar{n}_1} & \frac{1}{\bar{n}_2} \\ \frac{1}{\bar{n}_1} & \frac{1}{\bar{n}_2} \end{pmatrix} \\ & \left. - \frac{\mathbf{I}_{\bar{n}}}{\rho_A \mathcal{A} t_M} \otimes \left( \frac{d\Omega_{\tilde{\varphi}}^2}{d\bar{n}_1}, \frac{d\Omega_{\tilde{\varphi}}^2}{d\bar{n}_2} \right) \right]. \end{aligned} \quad (61)$$

where  $\otimes$  denotes the tensor product of two vectors producing a matrix. The first three terms in the rectangular bracket are the derivatives of the first three terms in the rectangular bracket in Eq. (58). The fourth term in the bracket is generated by the prefactor in Eq. (58), and has

not been explicitly written down for brevity.

The mean-photon numbers and the corresponding variances as a function of position  $z$  are depicted in Fig. 3(c). For small distances  $z$ , we observe that the mean value of  $\hat{n}_1$  decreases while the mean value of  $\hat{n}_2$  increases. This means that the polarization direction rotates towards the  $y$  direction. Likewise, the variance of  $\hat{n}_1$  decreases while the variance of  $\hat{n}_2$  increases. This is a consequence of the phase space terms  $C_{\bar{n}}$  in Eq. (61) which describe the deformation of the probability distribution due the photon-number dependence of the creation and annihilation operators. The effect of the diffusion matrix  $D_{\bar{n}}$  leads to an overall increase of the variance for larger  $z$ .

In Fig. 3(d), we depict the probability distribution for three propagation distances. For  $z = 2$  cm, the distribution is noticeably deformed due to the action of the phase space terms  $C_{\bar{n}}$ . This deformation is even clearer for  $z = 4$  cm for which the  $\text{Var } \hat{n}_2$  almost vanishes. At this point,  $\bar{n}_2 \approx 0$ , meaning that the measurement direction is almost orthogonal to the polarization of the laser field such that the corresponding photon mode is close to its vacuum state.

### C. Rotating frame

For the reasons explained in Sec. III E, it is beneficial to integrate the flow equations in a rotating frame, in which  $\Omega_1 = \Omega_2 \equiv \Omega/\sqrt{2}$  and  $\bar{\varphi} = \pi/2$ . In doing so, the coefficients in Sec. (IV B) and the equations of motion simplify drastically, enabling a theoretical analysis in limiting cases.

The photon-flux coefficients in Eq. (58) read

$$\mathbf{I}_{\bar{n}_{\text{rot}}} = \frac{\rho_A \mathcal{A} t_M}{4\epsilon_\Delta^2 + 2\Omega^2 + \gamma^2} \left[ \epsilon_\Delta \Omega^2 \begin{pmatrix} 1 \\ -1 \end{pmatrix} - \gamma \Omega^2 \begin{pmatrix} 1 \\ 1 \end{pmatrix} \right], \quad (62)$$

which allows us to express the equations for the phase shift and the total number of photons according to Sec. (III E) as

$$\begin{aligned} \frac{d\bar{\varphi}}{dz} &= \frac{\rho_A \mathcal{A} t_M}{\bar{n}_+} \frac{\epsilon_\Delta \Omega^2}{4\epsilon_\Delta^2 + 2\Omega^2 + \gamma^2}, \\ \frac{d\bar{n}_+}{dz} &= -\rho_A \mathcal{A} t_M \frac{\gamma \Omega^2}{4\epsilon_\Delta^2 + 2\Omega^2 + \gamma^2}. \end{aligned} \quad (63)$$

Notably, the integration of the phase shift equation is trivial for a vanishing  $\gamma$ , for which  $\bar{n}_+$  becomes constant: Noting that in the rotated basis  $\Omega = g\sqrt{\bar{n}_+}$ , we see that the right-hand side of the phase equation becomes independent of  $z$ .

Likewise, the diffusion matrix simplifies and now reads

$$D_{\bar{n}_{\text{rot}}} \approx \frac{8\rho_A \mathcal{A} t_M \Omega^8}{\gamma [4\epsilon_\Delta^2 + 2\Omega^2]^3} \begin{pmatrix} 1 & -1 \\ -1 & 1 \end{pmatrix} + \mathcal{O}(\gamma^0). \quad (64)$$

As for the phase-shift equation (63), the diffusion matrix becomes independent of position for a small dissipation  $\gamma$ , allowing for an analytical integration of the variance equation.

A drastic simplification appears for the phase-space matrix, which in the rotated frame becomes

$$\tilde{C}_{\bar{n}_{\text{rot}}} = \frac{t_M \rho_A \mathcal{A}}{\bar{n}_+} \frac{\Omega^2}{4\epsilon_\Delta^2 + 2\Omega^2 + \gamma^2} \times \left[ -4\gamma \begin{pmatrix} 1 & 0 \\ 0 & 1 \end{pmatrix} - \frac{\mathbf{I}_{\bar{n}_{\text{rot}}}}{\rho_A \mathcal{A} t_M} \otimes \begin{pmatrix} 1 \\ 1 \end{pmatrix} \right], \quad (65)$$

i.e., the first and the third terms in Eq. (61) disappear. The first term in the bracket corresponds to the dissipative dynamics, which results in a contraction of the covariance matrix. The second term describes the photon-number dependence of the Rabi frequency.

In Fig. 3(c), we depict the means and variances of the photonic modes  $k = 1, 2$  in the rotated measurement frame. By definition,  $\bar{n}_{\text{rot},1} = \bar{n}_{\text{rot},2} = \bar{n}_+/2$  for all positions. The total mean photon number is declining because of the absorption by the atoms. The rapid oscillations of the variance, which are visible in the laboratory frame, disappear in the rotated measurement frame.

Interestingly, we find that the variances of both modes are not equal. While the variance of mode  $k = 1$  decreases, the variance of mode  $k = 2$  significantly increases. This asymmetry is a consequence of a distortion of the probability distribution as depicted for selected values of  $z$  in Fig. 3(d). The distortion is driven by the second term of the phase-space coefficient in Eq. (65): The vector  $(1, 1)$  acts on  $\Sigma$  in the direction of  $\bar{n}_+$ , and distorts the covariance matrix controlled by  $\mathbf{I}_{\bar{n}}$ .

We interpret this distortion as a result of the dependence of the energy level splitting in the two-level on the photon number (i.e., the laser intensity): The larger the light intensity, the larger the level splitting. This relation leads to a reduced photon transfer between the atoms and the photonic modes for larger photon numbers. As the variance of the photonic probability distribution is on the order  $\sqrt{\bar{n}_k}$ , and the level splitting is a function of the Rabi frequencies  $\Omega_k \propto \sqrt{\bar{n}_k}$ , i.e., the variance and Rabi frequencies both change on the same order of magnitude, the level splitting dependence thus results in a significant distortion of the probability distribution.

### D. Mean and variance

Using the coefficients in Sec. IV C, we can integrate Eq. (42) and analyze the measurement statistics after the laser pulses have propagated through the atomic cloud at  $z = z_{\text{max}}$ . The results are depicted in Fig. 4.

In Fig. 4(a), we depict the mean photon number  $\bar{n}_+$  and the phase shift  $\bar{\varphi}_0$  along with their corresponding variances as a function of the detuning  $\epsilon_\Delta$ . Note that the variance associated with the  $\bar{\varphi}_0$  measurement is given by

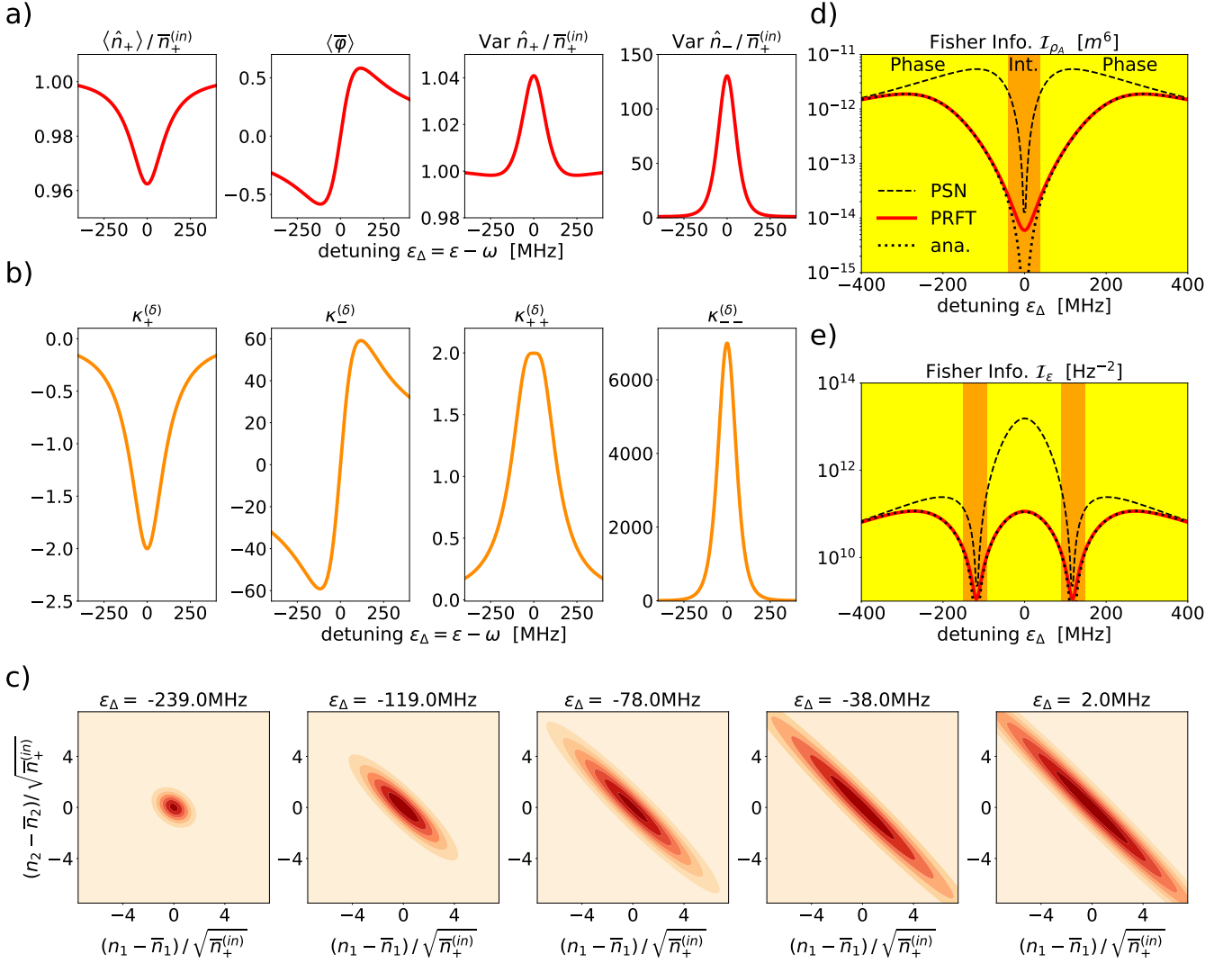


FIG. 4. Measurement statistics for the dissipative Tavis-Cummings model in Eq. (48). (a) Means and variances for the observed photon numbers  $n_+$  and  $n_-$  obtained by integrating the flow equations in Eqs. (40) and (42) using the coefficients in Eqs. (63), (64) and (65). (b) Corresponding cumulant aptitudes at  $z = 0$  given in Eq. (67). (c) Probability distributions for selected detunings. (d) Fisher information for the atom density as a function of detuning. The dashed line shows the Fisher information where the photonic variance has been estimated with the initial photon-shot noise (PSN). (e) is the same as (d), but for the Fisher information for the detuning. Overall parameters are the same as in Fig. 3.

the variance of  $n_-$ . The mean total photon number  $\bar{n}_+$  exhibits the common absorption dip at resonance  $\epsilon_\Delta = 0$ , while the mean phase shift  $\bar{\varphi}_0$  resembles the well-known dispersion-relation curve. The variance of  $n_+$  and  $n_-$  both exhibit a single peak at resonance. While the variance of  $n_+$  hardly overcomes the photon-shot-noise, the variance of  $n_-$  exceeds the photon-shot noise by more than two orders of magnitude.

To analyze this effect theoretically, we first note that the photon number statistics of  $n_+$  and  $n_-$  can be obtained by expressing the cumulant-generating function in Eq. (10) in terms of the new counting fields  $\chi_+ =$

$(\chi_1 + \chi_2)/2$  and  $\chi_- = (\chi_1 - \chi_2)/2$ . For a theoretical purpose, we introduce the coefficients

$$\begin{aligned} \kappa_\alpha^{(\delta)} &= \frac{i}{t_M} \partial_{\chi_\alpha} \mathcal{K}_{\bar{n}_{\text{rot}}, \chi=0}, \\ \kappa_{\alpha\beta}^{(\delta)} &= -\frac{1}{t_M} \partial_{\chi_\alpha} \partial_{\chi_\beta} \mathcal{K}_{\bar{n}_{\text{rot}}, \chi=0}, \end{aligned} \quad (66)$$

with  $\alpha, \beta = +, -$ , which we denote as cumulant aptitudes in the following. They describe the intrinsic ability of a single atom to modify the photonic statistics of their driving fields. The dynamical cumulant-generating function

is thereby evaluated in the rotating frame (as expressed by  $\bar{n}_{\text{rot}}$ ) for which  $\bar{n}_{\text{rot},-} = 0$ .

Analytically, the evaluation of the cumulant aptitudes is closely related to the calculation of the flow equation coefficient matrices in the rotated measurement basis in Sec. IV C, and we obtain

$$\begin{aligned}\kappa_+^{(\delta)} &= \frac{\gamma\Omega^2}{4\epsilon_\Delta^2 + 2\Omega^2 + \gamma}, \\ \kappa_-^{(\delta)} &= \frac{2\epsilon_\Delta\Omega^2}{4\epsilon_\Delta^2 + 2\Omega^2 + \gamma}, \\ \kappa_{++}^{(\delta)} &= \frac{\gamma\Omega^2}{4\epsilon_\Delta^2 + 2\Omega^2 + \gamma^2} + \frac{\Omega^4\gamma(8\epsilon_\Delta^2 - 6\gamma^2)}{(4\epsilon_\Delta^2 + 2\Omega^2 + \gamma^2)^3}, \\ \kappa_{--}^{(\delta)} &= \frac{2\Omega^4 + \gamma^2\Omega^2}{\gamma(4\epsilon_\Delta^2 + 2\Omega^2 + \gamma^2)} - \frac{8\epsilon_\Delta^2\Omega^4(4\Omega^2 + 4\epsilon_\Delta^2 + 5\gamma^2)}{\gamma(4\epsilon_\Delta^2 + 2\Omega^2 + \gamma^2)^3},\end{aligned}\quad (67)$$

as shown in Appendix F 2. The cumulant aptitudes are depicted in Fig. 4(b) below the corresponding measured cumulants. We see that the aptitudes closely resemble the corresponding cumulants, which shows the basic importance of the aptitudes to describe the response of the matter system to an external driving field. In particular, from Eq. (67) we learn that the phase variance aptitude  $\kappa_{--}^{(\delta)}$  is proportional to  $1/\gamma$ , which is the essential driver of the phase fluctuations. As investigated in Ref. [50] and also explained in Appendix G, the  $1/\gamma$  dependency originates from incoherent jumps between the two eigenstates of the two-level system, each of which featuring distinct optical properties, leading to diverging fluctuations.

To further illustrate the large fluctuations of  $n_-$ , we depict the photonic probability distribution shown in Fig. 4(c) as a function of the photon numbers  $n_1$  and  $n_2$  for various detunings. The closer the detuning is to the resonance  $\epsilon_\Delta = 0$ , the more the probability ellipsoid extends across the diagonal, which is in agreement with the variances in Fig. 4(a) and the cumulant aptitude  $\kappa_{--}^{(\delta)}$  in Fig. 4(b). This effect describes the tremendous fluctuations which can appear in phase measurements.

### E. Fisher information

We continue to discuss the spectroscopic setup sketched in Fig. 3(a) for its potential in spectroscopic quantum sensing. In the following, we will focus on the estimation of two quantities, namely the atomic density  $\rho_A$ , and the level splitting  $\epsilon$ , which could be a function of an unknown external stimulus.

Using Eq. (45), which we evaluate using the mean values and covariance matrix obtained by the numerical integration of the flow equations, we can conveniently estimate the Fisher information for vast parameter regimes. In Fig. 4(d) and Fig. 4(e) we depict the Fisher information  $\mathcal{I}_X$  for the estimation of the density  $X = \rho_A$  and the

energy splitting  $X = \epsilon$  as a function of the detuning by a red solid line. Both Fisher informations exhibit a non-trivial dependence on the detuning. Thus, the methods introduced in this work constitute a flexible methodology to quickly find experimental parameters which optimize the sensitivity of the measurement apparatus.

To emphasize the importance of taking the added fluctuation predicted by the variance flow equation in Eq. (42) into account, we depict also a simplistic variance estimate by a dashed black line, which approximates the noise by the photon-shot noise of the incoming laser pulse. As we observe in Fig. 4(d) and Fig. 4(e), this oversimplified estimate drastically fails to accurately predict the actual Fisher information by several orders of magnitudes. Only far away from resonance, where the variance aptitude is strongly suppressed [see Fig. 4(d)], and very close to the resonance condition, where the Fisher information is mainly carried by the total photon-number change, the shot-noise estimate succeeds to be a reliable measure.

### F. Small dissipation

To better understand the functional dependence of the Fisher information on the experimental parameters, we investigate the Fisher information in the small dissipation regime  $\gamma \ll \Omega$ . In this limit, it is safe to assume that  $\bar{n}_+$  is constant, for which the integration of the flow equations in the rotating measurement frame becomes trivial. Integrating Eq. (63), the total phase shift becomes

$$\bar{\varphi}_0 = \frac{t_M \rho_A \mathcal{A} z_{\text{max}}}{\bar{n}_+} \frac{2\epsilon_\Delta \Omega^2}{4\epsilon_\Delta^2 + 2\Omega^2} + \mathcal{O}(\gamma^0), \quad (68)$$

where we have neglected terms of order  $\gamma^0$ . Noteworthy, if  $\Omega \ll \epsilon_\Delta$ , we find that  $\bar{\varphi}$  is independent of  $\bar{n}_+$  as  $\Omega^2 \propto \bar{n}_+$ . In the opposite regime  $\Omega \gg \epsilon_\Delta$ , the phase shift is suppressed by a factor  $\bar{n}_+^{-1}$ .

Integrating Eq. (42) using Eq. (64) to obtain the covariance matrix in the weak dissipation regime, we find

$$\begin{aligned}\Sigma^2 &= \begin{pmatrix} \frac{\bar{n}_+}{2} & 0 \\ 0 & \frac{\bar{n}_+}{2} \end{pmatrix} \\ &+ 8t_M \rho_A \mathcal{A} z_{\text{max}} \frac{\Omega^8}{\gamma(4\epsilon_\Delta^2 + 2\Omega^2)^3} \begin{pmatrix} 1 & -1 \\ -1 & 1 \end{pmatrix} \\ &+ \mathcal{O}(\gamma^0, \bar{n}_+^0),\end{aligned}\quad (69)$$

where we have neglected terms scaling with  $\gamma^0$  and  $\bar{n}_+^0$ . The first term is the photon-shot noise, while the second terms describes the noise added by the light-matter interaction. According to the explanations in Sec. IV D, it describes the fluctuations appearing in the phase measurement. The product  $N_A = \rho_A \mathcal{A} z_{\text{max}}$  is the total number of two-level systems interacting with the laser pulse.

Using now Eq. (45) to calculate the Fisher information

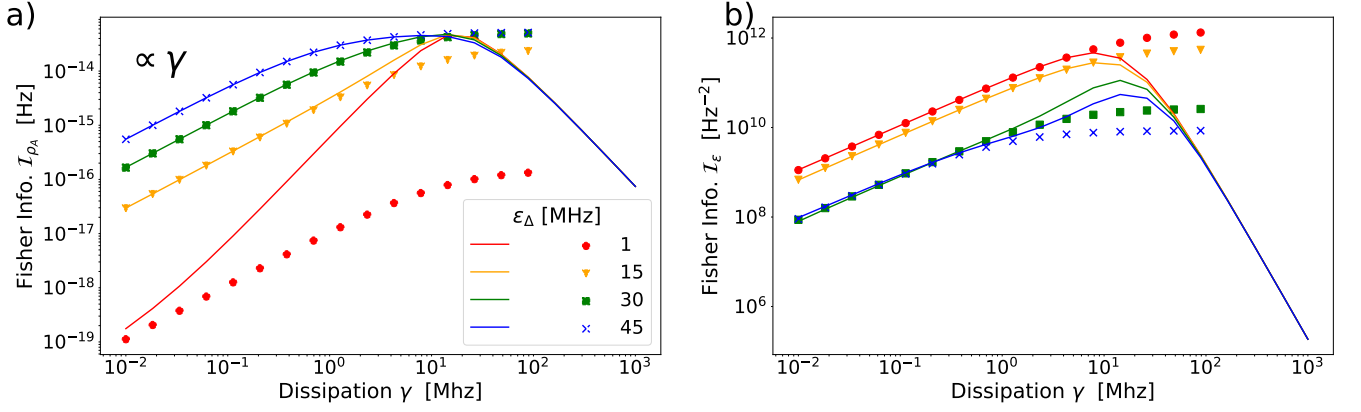


FIG. 5. Fisher information of the atom density  $\mathcal{I}_{\rho_A}$  and the detuning  $\mathcal{I}_\epsilon$  for the Tavis-Cummings model as function of dissipation rate  $\gamma$  depicted in panels (a) and (b), respectively. The solid lines show the numerical results obtained by integrating the flow equations using the coefficients in Eqs. (62), (64), and (65). The symbols show the analytical calculations in Eq. (70) and (71). The overall parameters are the same as in Fig. 3.

for the atom density, we obtain

$$\mathcal{I}_{\rho_A} \approx \frac{\left(t_M \mathcal{A} z_{\max} \frac{2\epsilon_\Delta \Omega^2}{4\epsilon_\Delta^2 + 2\Omega^2}\right)^2}{\bar{n}_+ + 8t_M N_A \frac{\Omega^8}{\gamma(4\epsilon_\Delta^2 + 2\Omega^2)^3}}, \quad (70)$$

which is valid in the weak dissipation limit. Likewise, we find that the Fisher information for the energy splitting is given by

$$\mathcal{I}_\epsilon \approx \frac{\left[t_M N_A \frac{\Omega^2(4\epsilon_\Delta^2 - 2\Omega^2)}{(4\epsilon_\Delta^2 + 2\Omega^2)^2}\right]^2}{\bar{n}_+ + 8t_M N_A \frac{\Omega^8}{\gamma(4\epsilon_\Delta^2 + 2\Omega^2)^3}}. \quad (71)$$

For comparison, these analytical expressions are depicted in Fig. 4(d) and Fig. 4(e), respectively, with dotted lines, which agree with the actual Fisher information for vast parameter regimes. For the detunings for which we observe deviations, the total photon number measurement  $n_+$  contributes significantly to the Fisher information. Overall, we observe that the Fisher information contained in the phase shift is considerably larger than the one in the total photon number (i.e., intensity). For this reason, it is sufficient to optimize the Fisher information related to the phase information, that is approximately given by Eqs. (70) and (71).

In Fig. 4(d) we observe that the Fisher information has a minimum at  $\epsilon_\Delta = 0$ , which is a consequence of the vanishing derivative of  $\bar{\varphi}_0$  in Eq. (68) with respect to  $\rho_A$ . Similarly, we find a Fisher information minimum in Fig. 4(e), which is caused by the vanishing derivative of  $\bar{\varphi}_0$  with respect to  $\epsilon$ . Away from the resonance, the Fisher information  $\mathcal{I}_{\rho_A}$  increases and finally exhibits a turnover: For large detunings  $\epsilon_\Delta$ , the added noise [second term in the denominator of Eq. (70)] vanishes and only the photon-shot noise remains. In this parameter regime, the predictions of the PRFT and the naive photon-shot-

noise approximation agree with each other. The decreasing derivative of  $\bar{\varphi}_0$  in Eq. (68) for large detunings is eventually reflected in a decreasing Fisher information  $\mathcal{I}_{\rho_A}$ . A similar explanation holds for  $\mathcal{I}_\epsilon$ .

### G. Dissipation dependence

In Fig. 5, we investigate the dependence of the Fisher information on the dissipation rate  $\gamma$ . Intriguingly, we observe that both  $\mathcal{I}_{\rho_A}$  and  $\mathcal{I}_\epsilon$  exhibit a turnover as a function of  $\gamma$ , i.e., they increase for small  $\gamma$  and decrease for large  $\gamma$ .

In the small  $\gamma$  regime, we can readily explain the enhancement of the Fisher information using Eqs. (70) and (71). If  $\gamma \rightarrow 0$ , we can neglect the photon-shot-noise term in the denominator, such that  $\mathcal{I}_{\rho_A} \propto \gamma$  and  $\mathcal{I}_\epsilon \propto \gamma$ . From this consideration we conclude that the increase of the Fisher information is driven by a decrease of the phase fluctuation in the measurement, while the differential change of the mean phase remains almost unchanged.

In the opposite regime of strong dissipation, we learn from Eq. (62) that the mean photon flux becomes increasingly suppressed for larger  $\gamma$ . This is consequently reflected in a decreasing Fisher information. In the large dissipation regime,  $\gamma$  dominates the atomic dynamics, such that all curves in Fig. 5 collapse on each other.

Worthwhile, similar turnovers as a function of system-bath coupling are well known from exciton and energy transport in molecular systems [88] and polariton systems [89]. Thereby, the transport efficiency is optimized by an interplay of coherent and incoherent dynamics. Surprisingly, here we observe a similar turnover, yet, in a genuine quantity of information science. Similar to transport in molecular systems, the optimal Fisher information requires a fine tuned coherent dynamics, which can be controlled by an appropriately adjusted dissipation rate  $\gamma$ .

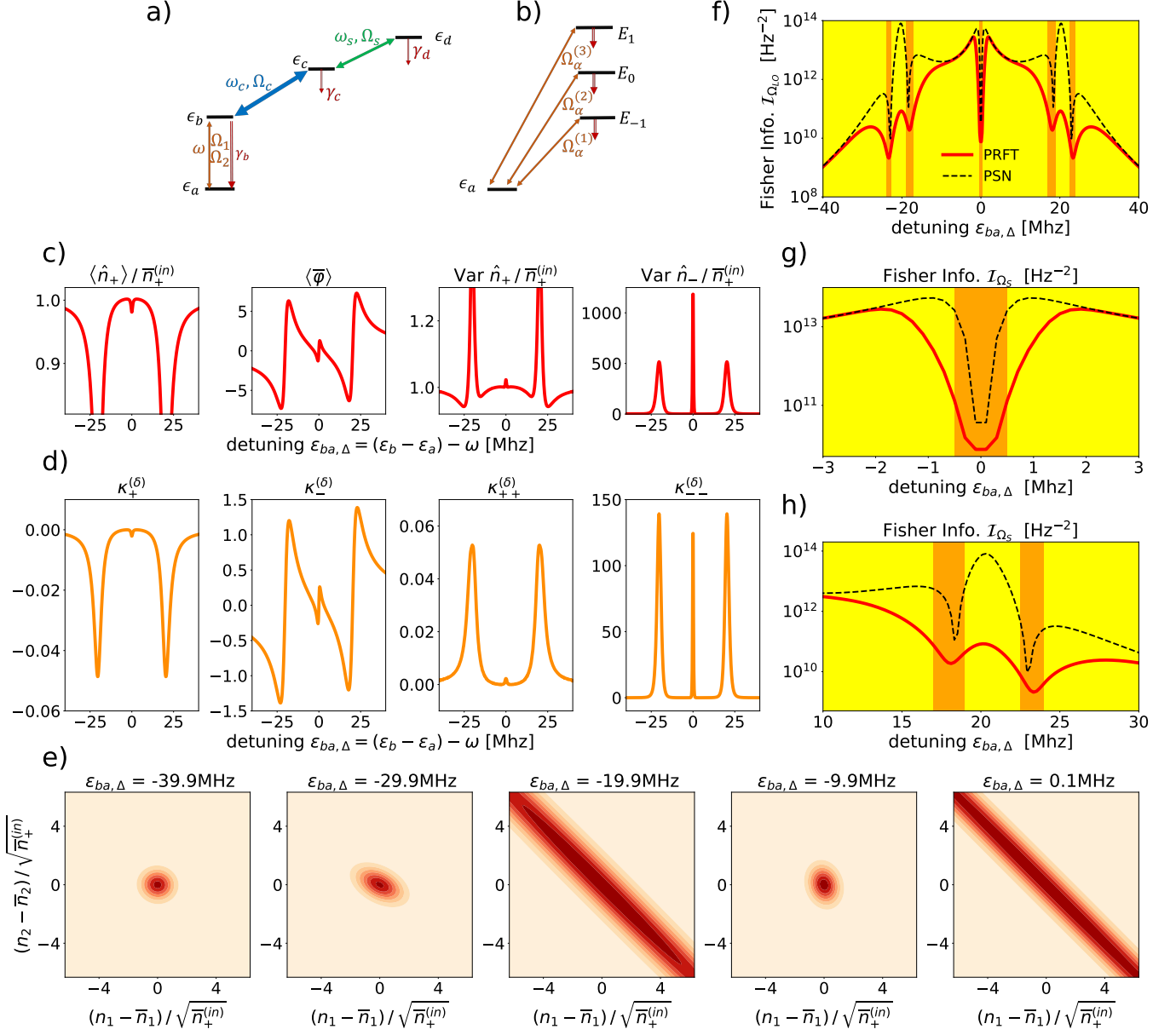


FIG. 6. Analysis of the measurement statistics for the four-level system in Eq. (72) which is sketched in the local basis in (a), and in the partially diagonalized basis in (b). (c) Mean values and variances of the photon measurement statistics, which are calculated in the same way as for Fig. 4. (d) Corresponding cumulant amplitudes at  $z = 0$ . (e) Photonic probability distribution for selected detunings. (f)-(h) Fisher information  $\mathcal{I}_{\Omega_S}$ . Parameters of the probe field are  $P = 0.1$  mW,  $\mathcal{A} = 1$  cm $^2$ ,  $t_P = 1$  s,  $\lambda = 500$  nm, and atomic dipole moment  $d = 5ea_0$ , which gives rise to an Rabi frequency of  $\Omega_P = 1.9$  MHz. Other parameters are  $\Omega_C = 20$  MHz,  $\Omega_S = 3$  MHz  $\gamma_b = 0.1$  MHz,  $\gamma_c = 0.01$  MHz  $= \gamma_d = 0.01$  MHz,  $z_{\max} = 10$  cm,  $\rho_A = 5 \cdot 10^{13}$  m $^{-3}$ , and  $t_M = 1$  s.

## V. FOUR-LEVEL SYSTEM

As a more sophisticated application, we consider an ensemble of four-level systems (i.e., atoms), whose level structure is sketched in Fig. 6(a). Thereby, the four energy levels  $j = a, b, c, d$  are coupled by three laser fields, namely, the probe, coupling, and signal lasers. The

Hamiltonian of a single atom coupled to the light field is given by

$$\begin{aligned} \hat{H}(t) = & \sum_{j=a,b,c,d} \epsilon_j |j\rangle \langle j| + \sum_{k=P,C,S} \omega_k \hat{a}_k^\dagger \hat{a}_k \\ & + [g_P \hat{a}_P |b\rangle \langle a| + g_C \hat{a}_C |c\rangle \langle b| + g_S \hat{a}_S |d\rangle \langle c| + \text{h.c.}], \end{aligned} \quad (72)$$

where  $\epsilon_j$  and  $|j\rangle$  denote the energies and the eigenstates of the atom. The probe, coupling, and signal fields are quantized by  $\hat{a}_P$ ,  $\hat{a}_C$ , and  $\hat{a}_S$ . The corresponding frequencies and light-matter coupling strengths are denoted by  $\omega_k$  and  $g_k$ , respectively.

This and similar protocols find application in the detection of electric fields in the radiofrequency regime using Rydberg states [32–40], and has been suggestion for the detection of axion dark matter in the galactic halo [90]. The signal to be estimated is proportional to the Rabi frequency  $\Omega_S = g_S \langle \hat{a}_S \rangle$  and typically in the range  $\omega_S < 20$  GHz, which couples two Rydberg states  $c$  and  $d$ . Here, we carry out a theoretical investigation of its sensitivity by estimating the Fisher information  $\mathcal{I}_X$  for  $X = \Omega_S$  utilizing the methods developed in this work.

### A. Semiclassical equations of motion

To estimate the measurement statistics for the four-level system, we follow the same steps introduced in Sec. IV for the two-level systems. We first express the probe field in the basis to be measured

$$\hat{a}_P = \frac{1}{\sqrt{2}i} (\hat{a}_1 - \hat{a}_2) \quad (73)$$

according to Eq. (33). Next, we transform the Hamiltonian into an interaction frame to remove the second term of the Hamiltonian in Eq. (72). The corresponding semiclassical Hamiltonian thus becomes

$$\begin{aligned} \hat{\mathcal{H}}_\varphi = & \sum_{j=a,b,c,d} \epsilon_{j,\Delta} |j\rangle \langle j| \\ & + \left[ \frac{\Omega_{P,\varphi}}{2} |b\rangle \langle a| + \frac{\Omega_C}{2} |c\rangle \langle b| + \frac{\Omega_S}{2} |d\rangle \langle c| + \text{h.c.} \right], \end{aligned} \quad (74)$$

where  $\epsilon_{a,\Delta} = \epsilon_a$ ,  $\epsilon_{b,\Delta} = \epsilon_b - \omega_P$ ,  $\epsilon_{c,\Delta} = \epsilon_c - \omega_P - \omega_C$  and  $\epsilon_{d,\Delta} = \epsilon_d - \omega_P - \omega_C - \omega_S$ . The Rabi frequencies of the coupling and signal fields are denoted by  $\Omega_C$  and  $\Omega_S$ . We choose the corresponding driving phases to be zero. We express the Rabi frequency of the probe field in terms of the Rabi frequencies of the measured fields  $\Omega_1$  and  $\Omega_2$  as

$$\Omega_{P,\varphi} = \frac{\sqrt{2}}{i} (\Omega_1 e^{i\varphi_1} - \Omega_2 e^{i\varphi_2}), \quad (75)$$

where  $\varphi_1$  and  $\varphi_2$  are the respective phases.

To construct the dynamical cumulant-generating function, we follow the same procedure as for the two-level system in Sec. IV A. To model dissipative effects, we solve the generalized Liouvillian equation

$$\frac{d}{dt} \rho_X = -i \left[ \hat{\mathcal{H}}_{\varphi+\frac{\pi}{2}} \rho_X - \rho_X \hat{\mathcal{H}}_{\varphi-\frac{\pi}{2}} \right] + \sum_{j=b,c,d} \gamma_j D_{|a\rangle\langle j|} \rho_X, \quad (76)$$

where  $\rho_X(t)$  denotes the reduced density matrix of a sin-

gle atom. The dynamical cumulant-generating function is then equal to the trace of  $\rho_X(t)$ . In Eq. (76), we have phenomenologically added the decay from the excited states to the ground states with dissipation rate  $\gamma_j$ , where the dissipator is defined by

$$D_{\hat{O}} \rho = \hat{O} \rho \hat{O}^\dagger - \frac{1}{2} \left( \hat{O}^\dagger \hat{O} \rho + \rho \hat{O}^\dagger \hat{O} \right). \quad (77)$$

The corresponding decay rates are denoted by  $\gamma_j$ .

### B. Findings

The numerically evaluated findings for the mean and variances of the measurement statistics of the total photon number and the phase estimation are depicted in Fig. 6(c). In contrast to the findings in Fig. 4(a), the four-level system exhibit three resonances, two of which feature broad absorption dips for  $\bar{n}_+$  around  $\epsilon_{ba,\Delta} \approx \pm 20$  MHz, and one narrow dip for  $\epsilon_{ba,\Delta} = 0$ . Accordingly, the dispersion of  $\bar{\varphi}$  consists of three characteristics phase steps. The variance of  $\hat{n}_+$  hardly deviates from the initial photon-shot noise. In contrast the variance of  $\hat{n}_-$  exceeds the initial photon-shot noise by several orders of magnitude for all three resonances. This is thus reminiscent to the findings in Fig. 4(a), where the variance of  $\hat{n}_-$  is significantly more pronounced than that of  $\hat{n}_+$ .

The corresponding cumulant aptitudes are depicted in Fig. 6(d), which exhibit a close resemblance with the means and the variances in Fig. 6(c). We conclude that the main information about the measured photon statistics is directly determined by these quantities. In Fig. 6(e), we depict the probability distribution for selected detunings, which illustrates the dominance of the  $\hat{n}_-$  noise over the  $\hat{n}_+$  noise for parameters close to the resonance.

In Fig. 6(f), we depict the estimate for the Fisher information  $\mathcal{I}_{\Omega_S}$ . As the system is more sophisticated than the two-level system in Sec. IV, the overall dependence of all investigated quantities on the system parameters is more complicated. We compare the Fisher information predicted by the PRFT with the photon-shot-noise estimation as we did in Fig. 4. In doing so, we find that the shot-noise estimation would drastically overestimate the Fisher information by more than three orders of magnitude.

In Fig. 6(g), and Fig. 6(h) we depict the Fisher information in two special detuning intervals  $\epsilon_{ba,\Delta} \in [-3 \text{ MHz}, 3 \text{ MHz}]$  and  $\epsilon_{ba,\Delta} \in [10 \text{ MHz}, 30 \text{ MHz}]$ . Notably, Fig. 6(g) and Fig. 6(h) closely resemble Fig. 4(d) and Fig. 4(e), respectively, investigating the two-level system. This close resemblance will be explained in the next section.

### C. Analysis

The more advanced four-level system does not allow for a simple non-perturbative treatment as the two-level system in Sec. IV. Nevertheless, here we give some analytical arguments which explain why Fig. 4(d) and Fig. 4(e) closely resemble Fig. 6(g) and Fig. 6(h).

To this end, we assume that the probe-field Rabi frequency is significantly smaller than the Rabi frequencies of the coupling and the signal fields. In this regime, it is beneficial to represent the three excited states in their diagonal basis as sketched in Fig. 6(b). In this basis, the Hamiltonian reads

$$\hat{\mathcal{H}}_{\varphi} = \sum_{j=a,0,\pm 1} E_{j,\Delta} |j\rangle \langle j| + \sum_{j=0,\pm 1} \left[ \frac{\Omega_{j,\varphi}}{2} |j\rangle \langle 0| + \text{h.c.} \right], \quad (78)$$

where  $E_{a,\Delta} = \epsilon_a$ ,

$$\begin{aligned} E_{0,\Delta} &= \epsilon_b, \\ E_{\pm 1,\Delta} &= \epsilon_b \pm \frac{1}{2} \sqrt{\Omega_C^2 + \Omega_S^2}, \end{aligned} \quad (79)$$

denote the level energies, and

$$\begin{aligned} \Omega_{0,\varphi} &= \frac{\Omega_S}{2\sqrt{\Omega_C^2 + \Omega_S^2}} \Omega_{P,\varphi}, \\ \Omega_{\pm 1,\varphi} &= \pm \frac{\Omega_C}{\sqrt{\Omega_C^2 + \Omega_S^2}} \Omega_{P,\varphi} \end{aligned} \quad (80)$$

are the effective Rabi frequencies in the modified basis.

Based on this representation, we can interpret the ensemble of four-level systems as consisting of three ensembles of two-level systems with distinct physical properties. The respective excitation energies and Rabi frequencies of each two-level systems are given by Eqs. (79) and (80). Each ensemble of two-level systems contributes independently to the measurement properties in Fig. 6(c). For this reason, the means and variances of the total photon number measurement and the phase measurement appear to be a concatenation of three two-level-system measurements, each with a different excitation frequency.

We use this interpretation to explain the respective similarity of Fig. 4(d) and Fig. 4(e) with Fig. 6(g) and Fig. 6(h). The derivation of the mean photon numbers  $\bar{n}_k$  with respect to the signal Rabi frequency  $\Omega_S$  is closely related to the derivations of the Hamiltonian parameters in Eqs. (79) and (80) with respect to  $\Omega_S$ : From Eq. (79) we find that only  $E_{\pm 1,\Delta}$  have a functional dependence on  $\Omega_S$ , while from Eq. (80), we see that  $\Omega_{0,\varphi}$  depends more sensitively on  $\Omega_S$  than  $\Omega_{\pm 1,\varphi}$ . In other words, a variation of  $\Omega_S$  leads thus mainly to variations of  $\Omega_{0,\varphi}$  and  $E_{\pm 1,\Delta}$ .

A variation of  $\Omega_{0,\varphi}$  is closely related to a variation of the atomic density, as the probe field experiences an effectively modified impact of the atomic ensemble. As  $\Omega_{0,\varphi}$  is prevalent for detunings close to  $\epsilon_{ba,\Delta} = 0$ ,

the Fisher information in Fig. 4(d) for the density estimation resembles the Fisher information in Fig. 6(g). Likewise, a variation of  $E_{\pm 1,\Delta}$  corresponds to a variation of the level splitting in a two-level system. As the  $E_{\pm 1,\Delta}$  variation impact is prevalent for detunings close to  $\epsilon_{ba,\Delta} = \pm 20\text{MHz}$ , the Fisher information in Fig. 4(e) for  $\epsilon$  resembles the Fisher information in Fig. 6(h).

Our analysis in terms of the partially diagonalized Hamiltonian in Eq. (78) is thus capable to explain the overall structure of the Fisher information in Fig. 6(f) in the parameter regime investigated here. The investigation of arbitrary parameter regimes of this four-level model would require a more comprehensive numerical study and a more sophisticated analytical treatment, which exceeds the scope of the present work.

### VI. CONCLUSIONS

We have developed a comprehensive framework of light-matter interaction which is capable of predicting the spectroscopic measurement statistics by evaluating the semiclassical dynamics of quantum emitters, such as atoms and molecules. This allows us to predict the sensitivity of spectroscopic quantum sensing protocol in terms of the Fisher information. The framework constructs flow equations for the mean values and the covariance matrix of relevant spectroscopic observables. In this work, we have focused on the measurement statistics related to the intensity, the polarization direction and the phase shift. The application to dissipative two-level systems and four-level systems has demonstrated the flexibility of the developed framework.

We conjecture that the spectroscopic analysis deploying a full-counting-statistics approach has plenty of application potential. In particular, it can optimize the operational configuration of currently existing spectroscopic quantum sensing devices, which deploy complicated level structures or periodic driving protocols [30, 34, 35]. As our approach is non-perturbative, it allows us to predict and interpret the statistical features close to resonance conditions, for which both the signal and the noise are strongly enhanced. This might show advantageous when extending the current methods to investigate the dynamics of laser systems, which are naturally closely related to spectroscopy. Laser systems, which typically work close to resonance conditions to enhance the gain, often suffer from phase diffusion, which can be investigated with virtually the same methods as introduced here. Moreover, the simplicity of the semiclassical approach enables us to investigate the measurement statistics of interacting many-body system, and their potential in quantum sensing.

Furthermore, there are several relevant topics which have not been addressed in this work. In the cases studied in Secs. IV and V, we have focused on the stationary state. When assuming short pulse durations  $t_P$ , one must integrate the Schrödinger equation (or Liou-

ville equation) to obtain the correct dynamical cumulant-generating function. This will be important for transient dynamics, for example, in the read-out of atomic interferometers. In addition, we have not considered some other effects, such as the Doppler shift or a broken rotational symmetry of the quantum emitters, for which the integration of the flow equations will become more elaborate.

Moreover, in our studies we have assumed that the measurement time is relatively long. Modern measurement devices allow to record spectroscopic signals with a high temporal resolution. As the PRFT counts the number of accumulated photons, it accounts for the time-averaged signal. A theoretical prediction of the precise joint probability distribution for the time-resolved measurement statistics will give a higher estimate for the Fisher information. As such, the Fisher information predicted by the PRFT can be interpreted as a lower bound for the Fisher information of the joint probability distribution. Given that the PRFT can also construct Kraus operators related to specific measurement outcomes [50], it is also possible to calculate the detailed joint probability distribution. These questions will be addressed in future work.

## ACKNOWLEDGMENTS

G.E. acknowledges the support by the National Natural Science Foundation of China (Grant No. W2432004). Z.Z. acknowledges the Excellent Young Scientists Fund by National Science Foundation of China (No. 9240172), the General Fund by National Science Foundation of China (No. 12474364), and the National Science Foundation of China/RGC Collaborative Research Scheme (No. 9054901).

## Appendix A: Light-matter Hamiltonian

### 1. Microscopic Hamiltonian

We consider a system consisting of an ensemble of  $N$  quantum emitters, e.g., atoms or molecules, which interacts with the light field. For concreteness, we will refer to atoms in the following. To describe the system in a microscopic fashion, we deploy the following light-matter Hamiltonian

$$\hat{H} = \hat{H}_M + \hat{H}_L + \hat{H}_{LM}, \quad (\text{A1})$$

where  $\hat{H}_M$  acts on the matter system. The free radiation Hamiltonian and the light-matter interaction Hamiltonians are given by

$$\hat{H}_L = \sum_{\mathbf{k}, \lambda} \omega_{\mathbf{k}} \hat{d}_{\mathbf{k}, \lambda}^\dagger \hat{d}_{\mathbf{k}, \lambda}, \quad (\text{A2})$$

$$\hat{H}_{LM} = \sum_{m=1}^N \int d\mathbf{r} \hat{\mathbf{E}}(\mathbf{r}) \cdot \hat{\mathbf{P}}_m(\mathbf{r}), \quad (\text{A3})$$

respectively.

In terms of the photonic creation and annihilation operators,  $\hat{d}_{\mathbf{k}, \lambda}^\dagger$  and  $\hat{d}_{\mathbf{k}, \lambda}$ , the radiation Hamiltonian is diagonal with photonic mode frequencies  $\omega_{\mathbf{k}}$ , which is given by the dispersion relation of the radiation field in the cloud of atoms. The electric field operator  $\hat{\mathbf{E}}(\mathbf{r})$  can be expressed as

$$\hat{\mathbf{E}}(\mathbf{r}) = \sum_{\mathbf{k}, \lambda} i\epsilon_{\mathbf{k}} \mathbf{e}_{\mathbf{k}, \lambda} \left( \hat{d}_{\mathbf{k}, \lambda}^\dagger e^{-i\mathbf{k} \cdot \mathbf{r}} - \hat{d}_{\mathbf{k}, \lambda} e^{i\mathbf{k} \cdot \mathbf{r}} \right), \quad (\text{A4})$$

where  $\mathbf{k}$  denotes the wavevector of the plain electromagnetic waves, and  $\lambda = 1, 2$  labels the polarization. The corresponding polarization vectors are given by  $\mathbf{e}_{\mathbf{k}, \lambda}$ . The polarization of atom  $m$  is denoted by  $\hat{\mathbf{P}}_m(\mathbf{r})$ .

### 2. Definition of the laser pulses

Before proceeding, we first define the spectroscopic observables of interest on a sound theoretical basis. In realistic experiments, it is not possible to measure the occupation of the photonic operators  $\hat{d}_{\mathbf{k}, \lambda}$  describing plain waves, as their mode function extends over the full space. Instead, in optical spectroscopy a laser pulse transverses a cloud of atoms and is then measured using a photon-multiplier. Alternatively, continuous wave lasers are being deployed, which can be likewise interpreted as a continuous train of laser pulses.

For this reason, we establish a theoretical definition of laser pulses in terms of the windowed Fourier transformation [91]. For simplicity, we reduce the three dimensional system to the single dimension of propagation of the laser field, i.e., we consider a (quasi) one-dimensional system extended in  $z$  direction. To this end, we first define the directed photonic field operators in position space by

$$\begin{aligned} \hat{d}_{\lambda}^{\rightarrow}(r) &= \sum_{k>0, \lambda} \hat{d}_{k, \lambda} e^{ikr}, \\ \hat{d}_{\lambda}^{\leftarrow}(r) &= \sum_{k<0, \lambda} \hat{d}_{k, \lambda} e^{ikr}. \end{aligned} \quad (\text{A5})$$

The commutation relations of these operators converge to the common photonic commutation relations if the quantization volume of the  $\hat{d}_{k, \lambda}$  approaches infinity. In terms of the directed operators, we now introduce the windowed Fourier transformation. Thereby, we distribute the one-dimensional space into intervals of length  $L$ , such that the  $j$ -th interval starts at  $r_j = jL$  and ends at  $r_{j+1} = (j+1)L$ . For each interval, we now define a set of Fourier transformed operators

$$\hat{a}_{\lambda, j, M}^{\rightarrow} \equiv \int_{r_j}^{r_{j+1}} \hat{d}_{\lambda}^{\rightarrow}(r) e^{-ik_M r} dr, \quad (\text{A6})$$

which can be regarded as the operators quantizing the laser pulses. Each index combination  $(\lambda, j, M)$  labels one specific photonic operator, which can be associated with a laser pulse. Thereby,  $\lambda = 1, 2$  denotes the polarization, the integer  $j$  refers to the spatial position, and the integer  $M$  corresponding to the (windowed) wave number  $k_M = \frac{2\pi}{L}M$ . The pulse length is given by  $L$ , while the bandwidth of the pulse, defined by  $\Delta k = k_{M+1} - k_M$ , is  $\Delta k = 2\pi/L$ . Conversely, the directed electric field operators can be expressed as

$$d_{\lambda}^{\rightarrow}(r) = \tilde{\theta}(r_j, r_{j+1}, r) \sum_M \hat{a}_{\lambda,j,M}^{\rightarrow} e^{ik_M r}, \quad (\text{A7})$$

where we have introduced a modified Heaviside function  $\tilde{\theta}(x, y, z)$

$$\tilde{\theta}(x, y, z) = \begin{cases} 1 & \text{if } x < z \leq y, \\ 0 & \text{else} \end{cases}. \quad (\text{A8})$$

to simplify the notation.

With evolving time, the directed field operators in Eq. (A5) and the pulse operators defined in Eq. (A6) propagate along the  $z$  direction. We describe this propagation in an interaction picture defined by

$$\hat{U}_{\text{prop}}(t) = \exp \left( -it \sum_{k,\lambda} \omega_k \hat{d}_{k,\lambda}^{\dagger} \hat{d}_{k,\lambda} \right), \quad (\text{A9})$$

where we recall that  $\omega_k$  denotes the dispersion relation of light within the cloud of atoms, and not the free dispersion relation. To proceed, we assume that the laser pulses have a small wavelength  $\lambda = 2\pi/k_{M_0}$  as compared to the pulse length  $\lambda \ll L$ . In this regime, we can approximate the time-evolved directed photonic operators as

$$\begin{aligned} \hat{d}_{\lambda}^{\rightarrow}(r, t) &\equiv \hat{U}_{\text{prop}}^{\dagger}(t) \hat{d}_{\lambda}^{\rightarrow}(r) \hat{U}_{\text{prop}}(t) \\ &= \sum_{k>0,\lambda} \hat{d}_{k,\lambda} e^{i(kr - \omega_k)t} \\ &\approx \sum_{k>0,\lambda} \hat{d}_{k,\lambda} e^{i \left[ kr - \omega_{k_M} t - \frac{d\omega_{k_M}}{dk} (k - k_M)t \right]} \\ &= \hat{d}_{\lambda}^{\rightarrow}(r - c_G t) e^{-i(\omega_{k_M} - c_G k_M)t}. \end{aligned} \quad (\text{A10})$$

In the third line, we have approximated the dispersion relation  $\omega_k$  by its Taylor expansion around  $k_M$ . To this end, we have introduced  $c_G = \frac{d\omega_{k_M}}{dk}$ , which can be interpreted as the group velocity of the laser pulse. In doing so, the time-evolved directed photonic operators are shifted in position, and additionally acquire a time-dependent phase  $(\omega_{k_M} - c_G k_M)t$ .

Alternatively, we express the time-evolved electric field

operators using Eq. (A7) as

$$\begin{aligned} d_{\lambda}^{\rightarrow}(r, t) &= \sum_j \tilde{\theta}(r_j, r_{j+1}, r - c_G t) \\ &\times \sum_M \hat{a}_{\lambda,j,M}^{\rightarrow}(0) e^{ik_M r} e^{-i\omega_{k_M} t}, \end{aligned} \quad (\text{A11})$$

where the  $\hat{a}_{\lambda,j,M}^{\rightarrow}(0)$  are the initial pulse operators. Using this expression, we find that the Hamiltonian in the interaction picture defined by Eq. (A1) becomes

$$\hat{H}(t) = \hat{H}_M + H_{\text{LM}}(t), \quad (\text{A12})$$

where  $\hat{H}_M$  acts on the matter system, and the light-matter Hamiltonian is given by

$$\begin{aligned} \hat{H}_{\text{LM}} &= \sum_{m=1}^N \sum_{\lambda,j,M} \int dr \hat{\mathbf{P}}_m(r) \cdot \mathbf{e}_{\lambda} \\ &\times \tilde{\theta}(r_j, r_{j+1}, r - c_G t) \hat{a}_{\lambda,j,M}^{\rightarrow} e^{ik_M r} e^{-i\omega_{k_M} t} + \text{h.c.} \end{aligned} \quad (\text{A13})$$

For a notational reason, we now introduce the short-cuts  $\hat{a}_k = \hat{a}_{\lambda,j,M}^{\rightarrow}$  and  $\omega_k = \omega_{k_M}$  for the photonic operators and frequencies. Likewise, we use

$$g_{m,k}(t) \hat{V}_m = \int dr \tilde{\theta}(r_j, r_{j+1}, r - c_G t) \hat{\mathbf{P}}_m(r) \cdot \mathbf{e}_{\lambda} e^{ikr} \quad (\text{A14})$$

to write the light-matter Hamiltonian in a more compact fashion, where  $g_{m,k}(t)$  is a scalar number and  $\hat{V}_m$  is an operator acting on atom  $m$ . In doing so, we eventually arrive at the time-dependent quantum-optical Hamiltonian

$$\hat{H}(t) = \sum_{j=1}^N \hat{H}_{M,m} + \sum_{m,k} g_{m,k}(t) \hat{V}_m \left( \hat{a}_k^{\dagger} e^{i\omega_k t} + \hat{a}_k e^{-i\omega_k t} \right), \quad (\text{A15})$$

which is the same as in Eq. (3) but in a frame rotating with the frequencies  $\omega_k$ .

## Appendix B: Derivation of the cumulant flow equation

### 1. Exact moment-generating function

Here, we derive an expression for the moment-generating function of the laser pulse operators  $\hat{a}_k$  appearing in the Hamiltonian in Eq. (3). For later purpose, we assume a more generic light-matter initial state than the one in Eq. (4), namely

$$\rho_{\text{tot}}(t=0) = \rho^{(\text{M})}(0) \otimes \rho^{(\text{L})}(0), \quad (\text{B1})$$

i.e., where the light field is described by a mixed state instead of a pure state. The moment-generating function

of the photonic probability distribution is defined by

$$M_{\mathbf{X}}(t) \equiv \text{tr} \left[ \hat{U}^{(N)\dagger}(t) e^{-i \sum_k \chi_k \hat{a}_k^\dagger \hat{a}_k} \hat{U}^{(N)}(t) \rho_{\text{tot}}(0) \right], \quad (\text{B2})$$

where  $\hat{U}^{(N)}(t)$  denotes the time-evolution operator corresponding to the Hamiltonian in Eq. (3). The index  $N$  refers thereby to the number of quantum emitters. In an interaction picture defined by  $U^{(\text{free})} = \exp(-iH_L t)$  with  $H_L = \sum_k \omega_k \hat{a}_k^\dagger \hat{a}_k$ , the time-evolution operators can be

written as

$$\hat{U}^{(N)}(t) = \hat{U}^{(\text{free})}(t) \hat{U}^{(N,\text{int})}(t), \quad (\text{B3})$$

where  $\hat{U}^{(N,\text{int})}(t)$  denotes the time-evolution operator in the interaction picture. Evaluating the time-evolution operator in the Fock basis, we find

$$\begin{aligned} \left[ \hat{U}^{(N)}(t) \right]_{\mathbf{n}, \mathbf{n}_1} &= \langle \mathbf{n} | \hat{U}^{(N)}(t) | \mathbf{n}_1 \rangle \\ &= e^{-i\boldsymbol{\omega} \cdot \mathbf{n}} \left[ \hat{U}^{(N,\text{int})}(t) \right]_{\mathbf{n}, \mathbf{n}_1}. \end{aligned} \quad (\text{B4})$$

We can now evaluate the moment-generating function of the photonic probability distribution

---


$$\begin{aligned} M_{\mathbf{X}}(t) &= \sum_{\mathbf{n}, \mathbf{n}_1, \mathbf{n}_2} \text{tr} \left\{ \left[ \hat{U}^{(N)\dagger}(t) \right]_{\mathbf{n}-\mathbf{n}_1, \mathbf{n}} e^{-i\mathbf{X} \cdot \mathbf{n}} \left[ \hat{U}^{(N)}(t) \right]_{\mathbf{n}, \mathbf{n}-\mathbf{n}_2} \rho^{(\text{M})}(0) \right\} \rho_{\mathbf{n}-\mathbf{n}_1, \mathbf{n}-\mathbf{n}_2}^{(\text{L})} \\ &= \sum_{\mathbf{n}, \mathbf{n}_1, \mathbf{n}_2} \left\langle \left[ \hat{U}^{(N,\text{int})\dagger}(t) \right]_{\mathbf{n}-\mathbf{n}_1, \mathbf{n}} e^{-i\mathbf{X} \cdot \mathbf{n}} \left[ \hat{U}^{(N,\text{int})}(t) \right]_{\mathbf{n}, \mathbf{n}-\mathbf{n}_2} \right\rangle_0 \rho_{\mathbf{n}-\mathbf{n}_1, \mathbf{n}-\mathbf{n}_2}^{(\text{L})} \\ &= \sum_{\mathbf{n}, \mathbf{n}_1, \mathbf{n}_2} \left\langle \left[ \hat{U}^{(N,\text{int})\dagger}(t) \right]_{\bar{\mathbf{n}}+\mathbf{n}-\mathbf{n}_1, \mathbf{n}} \left[ \hat{U}^{(N,\text{int})}(t) \right]_{\bar{\mathbf{n}}+\mathbf{n}, \mathbf{n}-\mathbf{n}_2} \right\rangle_0 e^{-i\mathbf{X} \cdot (\bar{\mathbf{n}}+\mathbf{n})} \rho_{\bar{\mathbf{n}}+\mathbf{n}-\mathbf{n}_1, \bar{\mathbf{n}}+\mathbf{n}-\mathbf{n}_2}^{(\text{L})}. \end{aligned} \quad (\text{B5})$$

In the first equality, we have expressed Eq. (B2) in the Fock basis. In the second equality, we have introduced the notation  $\langle \bullet \rangle_0 = \text{tr} [\bullet \rho^{(\text{M})}(0)]$  and deployed Eq. (B4). In the third equality, we have shifted the dummy index  $\mathbf{n}$  by  $\bar{\mathbf{n}}$ .

Next, we carry out a Taylor series of the matter-system expectation value as a function of photon number around the mean-photon number of the system  $\bar{\mathbf{n}}$ , guided by the intuition that the photon-number dependence of the photonic creation and annihilation operators depends only weakly on the photon number in the high-occupation regime. In doing so, we obtain

$$\begin{aligned} M_{\mathbf{X}}(t) &= \sum_{r=0}^{\infty} \sum_{\iota_1 + \dots + \iota_D = r} \left\{ \partial_{\bar{n}_1}^{\iota_1} \dots \partial_{\bar{n}_D}^{\iota_D} \left\langle \left[ \hat{U}^{(N,\text{int})\dagger}(t) \right]_{\bar{\mathbf{n}}-\mathbf{n}_1, \bar{\mathbf{n}}} \left[ \hat{U}^{(N,\text{int})}(t) \right]_{\bar{\mathbf{n}}, \bar{\mathbf{n}}-\mathbf{n}_2} \right\rangle_0 \right\} \frac{n_1^{\iota_1} \dots n_D^{\iota_D}}{\iota_1! \dots \iota_D!} \\ &\quad \times e^{-i\mathbf{X} \cdot (\bar{\mathbf{n}}+\mathbf{n})} \rho_{\bar{\mathbf{n}}+\mathbf{n}-\mathbf{n}_1, \bar{\mathbf{n}}+\mathbf{n}-\mathbf{n}_2}^{(\text{L})}, \end{aligned} \quad (\text{B6})$$

where  $r$  denotes the Taylor expansion order. The subscript of the second summation ( $\iota_1 + \dots + \iota_{N_D} = r$ ) means that we have to sum over all combinations  $\iota_1, \dots, \iota_{N_D}$  whose index sum equals  $r$ . The derivatives with respect to the mean photon numbers  $\bar{n}_k$  are denoted by  $\partial_{\bar{n}_k}^i$ , where  $i$  denotes the order of the derivation.

We continue to carry out Fourier transformations from the photon-numbers  $\mathbf{n}$  to their conjugated phase  $\boldsymbol{\varphi}$ , which are explicitly defined by

$$\begin{aligned} \left[ \hat{U}^{(N,\text{int})}(t) \right]_{\bar{\mathbf{n}}, \bar{\mathbf{n}}-\mathbf{n}_1} &= \frac{1}{(2\pi)^D} \int_{-\pi}^{\pi} d\boldsymbol{\varphi} \hat{U}_{\bar{\mathbf{n}}, \boldsymbol{\varphi}}^{(N)\dagger}(t) e^{-i\boldsymbol{\varphi} \cdot \mathbf{n}_1}, \\ \rho_{\mathbf{n}_1, \mathbf{n}_2}^{(\text{L})} &= \frac{1}{(2\pi)^D} \iint_{-\pi}^{\pi} d\boldsymbol{\varphi}_1 d\boldsymbol{\varphi}_2 \rho_{\boldsymbol{\varphi}_1, \boldsymbol{\varphi}_2}^{(\text{L})} e^{-i(\boldsymbol{\varphi}_1 \cdot \mathbf{n}_1 - \boldsymbol{\varphi}_2 \cdot \mathbf{n}_2)}. \end{aligned}$$

Inserting these Fourier transformations, the moment-generating function reads

$$\begin{aligned} M_{\mathbf{X}}(t) &= \sum_{r=0}^{\infty} \sum_{\iota_1 + \dots + \iota_{N_D} = r} \frac{1}{(2\pi)^{3D}} \iiint \boldsymbol{\varphi}_1 \boldsymbol{\varphi}_2 \boldsymbol{\varphi}_3 \boldsymbol{\varphi}_4 \sum_{\mathbf{n}, \mathbf{n}_1, \mathbf{n}_2} \left\{ \partial_{\bar{n}_1}^{\iota_1} \dots \partial_{\bar{n}_D}^{\iota_D} \left\langle \hat{U}_{\bar{\mathbf{n}}, \boldsymbol{\varphi}_1}^{(N)\dagger}(t) \hat{U}_{\bar{\mathbf{n}}, \boldsymbol{\varphi}_2}^{(N)}(t) \right\rangle_0 \right\} \frac{n_1^{\iota_1} \dots n_D^{\iota_D}}{\iota_1! \dots \iota_D!} \\ &\quad \times \rho_{\boldsymbol{\varphi}_3, \boldsymbol{\varphi}_4}^{(\text{L})} e^{i\mathbf{n} \cdot (\boldsymbol{\varphi}_4 - \boldsymbol{\chi} + \boldsymbol{\varphi}_3) + i\mathbf{n}_1 \cdot (\boldsymbol{\varphi}_3 - \boldsymbol{\varphi}_1) - i\mathbf{n}_2 \cdot (\boldsymbol{\varphi}_4 - \boldsymbol{\varphi}_2) + i\bar{\mathbf{n}} \cdot (\boldsymbol{\varphi}_4 - \boldsymbol{\chi} + \boldsymbol{\varphi}_3)}. \end{aligned} \quad (\text{B7})$$

The ongoing strategy is to deploy the identity

$$\frac{1}{2\pi} \sum_{-\infty}^{\infty} e^{-i\varphi n} = \delta(\varphi) \quad (\text{B8})$$

to identify delta functions  $\delta(\varphi)$  in Eq. (B7), which can then be used to evaluate some of the phase integrals. However, the photon numbers  $n_k^{\ell_k}$  in Eq. (B7) prevent us from identifying the delta functions so far. For this reason, we express the photon numbers using derivatives with respect to the counting fields in the following way

$$\begin{aligned} M_{\mathbf{x}}(t) &= \sum_{r=0}^{\infty} \sum_{\ell_1+\dots+\ell_D=r} \frac{1}{(2\pi)^{3D}} \iiint \varphi_1 \varphi_2 \varphi_3 \varphi_4 \sum_{\mathbf{n}, \mathbf{n}_1, \mathbf{n}_2} \left\{ \partial_{\bar{n}_1}^{\ell_1} \dots \partial_{\bar{n}_D}^{\ell_D} \left\langle \hat{U}_{\bar{\mathbf{n}}, \varphi_1}^{(N)\dagger}(t) \hat{U}_{\bar{\mathbf{n}}, \varphi_2}^{(N)}(t) \right\rangle_0 \right\} \\ &\quad \times \rho_{\varphi_3, \varphi_4}^{(L)} e^{i\mathbf{n} \cdot (\varphi_4 + \varphi_3) + i\mathbf{n}_1 \cdot (\varphi_3 - \varphi_1) - i\mathbf{n}_2 \cdot (\varphi_4 - \varphi_2) + i\bar{\mathbf{n}} \cdot (\varphi_4 - \mathbf{x} + \varphi_3)} \frac{\partial_{-i\chi_1}^{\ell_1} \dots \partial_{-i\chi_D}^{\ell_D}}{\ell_1! \dots \ell_D!} e^{-i\mathbf{n} \cdot \mathbf{x}} \\ &= \sum_{r=0}^{\infty} \sum_{\ell_1+\dots+\ell_D=r} \frac{1}{(2\pi)^{3D}} e^{-i\bar{\mathbf{n}} \cdot \mathbf{x}} \frac{\partial_{-i\chi_1}^{\ell_1} \dots \partial_{-i\chi_D}^{\ell_D}}{\ell_1! \dots \ell_D!} \iiint \varphi_1 \varphi_2 \varphi_3 \varphi_4 \sum_{\mathbf{n}, \mathbf{n}_1, \mathbf{n}_2} \left\{ \partial_{\bar{n}_1}^{\ell_1} \dots \partial_{\bar{n}_D}^{\ell_D} \left\langle \hat{U}_{\bar{\mathbf{n}}, \varphi_1}^{(N)\dagger}(t) \hat{U}_{\bar{\mathbf{n}}, \varphi_2}^{(N)}(t) \right\rangle_0 \right\} \\ &\quad \times \rho_{\varphi_3, \varphi_4}^{(L)} e^{i\mathbf{n} \cdot (\varphi_4 - \mathbf{x} + \varphi_3) + i\mathbf{n}_1 \cdot (\varphi_3 - \varphi_1) - i\mathbf{n}_2 \cdot (\varphi_4 - \varphi_2) + i\bar{\mathbf{n}} \cdot (\varphi_4 + \varphi_3)}. \end{aligned} \quad (\text{B9})$$

In this form, we can now use the identity in Eq. (B8) to simplify the above expression. By evaluating the delta functions, we can cancel three of the four integrals over the phase  $\varphi_\alpha$ , such that we obtain

$$M_{\mathbf{x}}(t) = \sum_{r=0}^{\infty} \sum_{\ell_1+\dots+\ell_D=r} e^{-i\bar{\mathbf{n}} \cdot \mathbf{x}} \frac{\partial_{-i\chi_1}^{\ell_1} \dots \partial_{-i\chi_D}^{\ell_D}}{\ell_1! \dots \ell_D!} \int d\varphi \left\{ \partial_{\bar{n}_1}^{\ell_1} \dots \partial_{\bar{n}_D}^{\ell_D} \left\langle \hat{U}_{\bar{\mathbf{n}}, \varphi - \frac{\mathbf{x}}{2}}^{(N)\dagger}(t) \hat{U}_{\bar{\mathbf{n}}, \varphi + \frac{\mathbf{x}}{2}}^{(N)}(t) \right\rangle_0 \right\} \rho_{\varphi + \frac{\mathbf{x}}{2}, \varphi - \frac{\mathbf{x}}{2}}^{(L)} e^{i\bar{\mathbf{n}} \cdot \mathbf{x}}. \quad (\text{B10})$$

We emphasize that this is still an exact expression for the moment-generating function.

## 2. Semiclassical approximation

While exact, the expression in Eq. (B10) is impossible to evaluate. At this point, we recall the objective of this work to establish a theoretical framework that is capable to predict the measurement statistics of spectroscopic experiments using only semiclassical methods. Motivated by this aim, we carry out a semiclassical approximation in Eq. (B10). This semiclassical approach has a two-fold effect:

- (i) we replace the quantum optical time-evolution operators in Eq. (B10) by their semiclassical counterparts, i.e.,

$$\hat{U}_{\bar{\mathbf{n}}, \varphi}^{(N)} \rightarrow \hat{\mathcal{U}}_{\bar{\mathbf{n}}, \varphi}^{(N)}, \quad (\text{B11})$$

which is defined in Eq. (9). We note that this replacement is exact, when representing the Hamiltonian in Eq. (3) in the Sambe space as shown in Ref. [50]. The Sambe space is closely related to the Fock space, but with the common photonic operators replaced by  $\hat{a}_k^\dagger \hat{a}_k \rightarrow \sum_{n_k} n_k |n_k\rangle \langle n_k|$  and  $\hat{a}_k \rightarrow \sum_{n_k} \sqrt{n_k} |n_k\rangle \langle n_k + 1|$ , such that this approximation is well motivated in the large photon-number regime.

(ii) The second approximation concerns the integral over the phase variables in Eq. (B10). As we work in the semiclassical limit, we assume that the phase of the photonic field should be uniquely defined. Consequently, it is reasonable to assume that the photonic state  $\rho_{\varphi + \frac{\mathbf{x}}{2}, \varphi - \frac{\mathbf{x}}{2}}^{(L)}$  is strongly peaked around a specific mean phase  $\bar{\varphi}$ , at which we evaluate the integral.

When applying the semiclassical approximation, the moment-generating function in the semiclassical approximation becomes

$$M_{\mathbf{x}}(t) = \sum_{r=0}^{\infty} \sum_{\ell_1+\dots+\ell_D=r} e^{-i\bar{\mathbf{n}} \cdot \mathbf{x}} \frac{\partial_{-i\chi_1}^{\ell_1} \dots \partial_{-i\chi_D}^{\ell_D}}{\ell_1! \dots \ell_D!} \left\{ \partial_{\bar{n}_1}^{\ell_1} \dots \partial_{\bar{n}_D}^{\ell_D} \left\langle \hat{\mathcal{U}}_{\bar{\mathbf{n}}, \bar{\varphi} - \frac{\mathbf{x}}{2}}^{(N)\dagger}(t) \hat{\mathcal{U}}_{\bar{\mathbf{n}}, \bar{\varphi} + \frac{\mathbf{x}}{2}}^{(N)}(t) \right\rangle_0 \right\} e^{i\bar{\mathbf{n}} \cdot \mathbf{x}} \int d\varphi \rho_{\varphi + \frac{\mathbf{x}}{2}, \varphi - \frac{\mathbf{x}}{2}}^{(L)},$$

(B12)

in which we can identify

$$M_{\chi}(t=0) = \int d\varphi \rho_{\bar{\varphi}+\frac{\chi}{2}, \bar{\varphi}-\frac{\chi}{2}}^{(L)}. \quad (\text{B13})$$

Noteworthy, this relation becomes exact when the initial state is the pure Gaussian state given in Eq. (6). The photonic probability distribution in this case has been studied in details in Ref. [51].

To make progress, we use the defining relation between cumulant and moment-generating functions,

$$M_{\chi}(0) = \exp[K_{\chi}(0)]. \quad (\text{B14})$$

Moreover, we introduce the dynamical cumulant-generating function describing the action of the ensemble of  $N$  atoms on the photonic fields

$$\begin{aligned} \mathcal{K}_{\chi}^{(N)}(t) &\equiv \log \left\langle \hat{\mathcal{U}}_{\bar{n}, \bar{\varphi}-\frac{\chi}{2}}^{(N)\dagger}(t) \hat{\mathcal{U}}_{\bar{n}, \bar{\varphi}+\frac{\chi}{2}}^{(N)}(t) \right\rangle_0 \\ &= \log \left\langle \hat{\mathcal{U}}_{\bar{n}, \bar{\varphi}-\frac{\chi}{2}}^{\dagger}(t) \hat{\mathcal{U}}_{\bar{n}, \bar{\varphi}+\frac{\chi}{2}}(t) \right\rangle_0^N \\ &= N \log \left\langle \hat{\mathcal{U}}_{\bar{n}, \bar{\varphi}-\frac{\chi}{2}}^{\dagger}(t) \hat{\mathcal{U}}_{\bar{n}, \bar{\varphi}+\frac{\chi}{2}}(t) \right\rangle_0 \\ &= N \mathcal{K}_{\chi}(t). \end{aligned} \quad (\text{B15})$$

In the second line, we have assumed that the atoms are independent of each other, such that the expectation value of the ensemble is just the  $N$ -th power of the expectation value for an individual atom. In the last equality, we introduced  $G_{\chi}(t)$ , which describes the impact of a single atom on the photonic modes.

In the following, we assume that these  $N$  atoms are confined in a volume with area  $\mathcal{A}$  and infinitesimal length  $dz$ , i.e.,  $N = \rho_A \mathcal{A} dz$ . Using these definitions, the moment-generating function in Eq. (B12) becomes

$$M_{\chi}(t) = \sum_{r=0}^{\infty} \sum_{\iota_1+\dots+\iota_D} e^{-i\bar{n}\cdot\chi} \frac{\partial_{-i\chi_1}^{\iota_1} \dots \partial_{-i\chi_D}^{\iota_D}}{\iota_1! \dots \iota_D!} \left\{ \partial_{\bar{n}_1}^{\iota_1} \dots \partial_{\bar{n}_D}^{\iota_D} \exp[\rho_A \mathcal{A} dz \mathcal{K}_{\chi}(t)] \right\} e^{K_{\chi}(0)+i\bar{n}\cdot\chi}. \quad (\text{B16})$$

The following scaling analysis will show how this expression can be simplified.

To this end, we first have to specify in which fashion we approach the semiclassical limit. As one can see from Eq. (8), the bare light-matter interaction parameters  $g_{j,k}$  and mean photon numbers  $\bar{n}_k$  appear only as the products  $\Omega_{j,k} = g_{j,k} \sqrt{\bar{n}_k}$  (i.e., the Rabi frequencies) in the semiclassical Hamiltonian. Thus, the dynamical moment-generating function  $\mathcal{K}_{\chi}(t)$  is only a function of the Rabi frequencies. To reach the semiclassical limit in an unambiguous fashion, we thus require that

$$\begin{aligned} \bar{n}_k &\rightarrow \infty, \\ g_{j,k} &\rightarrow 0, \\ \text{s.t. } g_{j,k} \sqrt{\bar{n}_k} &= \Omega_{j,k} = \text{const.} \end{aligned} \quad (\text{B17})$$

Physically, the condition can be met by increasing the quantization volume of a pulse in the directions transversal to the propagation.

First, we investigate the scaling properties of the factor

$$\partial_{\bar{n}_1}^{\iota_1} \dots \partial_{\bar{n}_D}^{\iota_D} \exp[\rho_A \mathcal{A} dz \mathcal{K}_{\chi}(t)] \equiv \partial_{\bar{n}_1}^{\iota_1} \dots \partial_{\bar{n}_D}^{\iota_D} g_{\chi}(t), \quad (\text{B18})$$

when the mean photon numbers approach infinity  $\bar{n}_k \rightarrow \infty$ . Using the scaling assumptions in Eq. (B17), we can thus conclude that

$$\begin{aligned} \partial_{\bar{n}_1}^{\iota_1} \dots \partial_{\bar{n}_D}^{\iota_D} g_{\chi}(t) &= \partial_{\Omega_1}^{\iota_1} \dots \partial_{\Omega_D}^{\iota_D} g_{\chi}(t) (\partial_{\bar{n}_1}^{\iota_1} \Omega_1) \dots (\partial_{\bar{n}_D}^{\iota_D} \Omega_D) \\ &\propto \frac{g^r}{\sqrt{\bar{n}}^r} \propto \frac{1}{\bar{n}^r}, \quad r = \iota_1 + \dots + \iota_D. \end{aligned} \quad (\text{B19})$$

In the first equality, we have used the chain rule of differentiation. In the second line, we utilized  $g$  and  $\bar{n}$  as measures for the  $g_{j,k}$  and the  $\bar{n}_k$ . Importantly, note that the derivatives of  $g_{\chi}$  with respect to  $\Omega_k$  are independent of the photon

number, i.e.,  $g_{\chi} \propto \bar{n}^0$  under the scaling assumptions in Eq. (B17), as  $g_{\chi}$  is only a function of the Rabi frequencies. Thus, the scaling properties are solely determined by the derivatives of the Rabi frequencies with respect to the mean-photon numbers, showing the terms vanish with  $\bar{n}^{-r}$  in the Taylor order  $r$ .

Consequently, in order for the terms of order  $r$  to remain in Eq. (B16), we require additional factors which must jointly scale with  $\bar{n}^r$ . These factors can be delivered by the factor  $K_{\chi}(0)$  in the exponential appearing in Eq. (B16). To this end, we make the reasonable assumption that

$$K_{\chi}(0) \propto \bar{n}, \quad (\text{B20})$$

which implies that all initial cumulants scale as  $\propto \bar{n}$ . This is definitely fulfilled for Gaussian states or states which are similar to Gaussian states such as coherent squeezed states. More precisely, we have to repeatedly bring down the factor  $K_{\chi}(0)$  from the exponent by deriving  $r$  times to produce the scaling  $\propto \bar{n}^r$ .

Taking all these scaling relations into account, we can express the moment-generating function in Eq. (B12) as

$$M_{\chi}(t) = M_{\text{aux},\chi}(t)M_{\chi}(0), \quad (\text{B21})$$

where

$$\begin{aligned} M_{\text{aux},\chi}(t) &= \left\{ 1 + \rho_A \mathcal{A} \tilde{K}_{\text{aux},\chi}(t) dz + \mathcal{O} \left[ (\rho_A \mathcal{A} dz)^2, \frac{1}{\bar{n}} \right] \right\} e^{\rho_A \mathcal{A} K_{\chi}(t) dz}, \\ \tilde{K}_{\text{aux},\chi}(t) &= \sum_{r=1}^{\infty} \sum_{\ell_1 + \dots + \ell_D = r} \left\{ \frac{\partial^{\ell_1}}{\partial \bar{n}_1} \dots \frac{\partial^{\ell_D}}{\partial \bar{n}_D} K_{\chi}(t) \right\} \{ [\partial_{-i\chi_1} K_{\chi}(0) - \bar{n}_1]^{\ell_1} \dots [\partial_{-i\chi_D} K_{\chi}(0) - \bar{n}_D]^{\ell_D} \} \end{aligned} \quad (\text{B22})$$

will be denoted as the auxiliary moment-generating function in the following. Within the auxiliary moment-generating function, we have ordered the terms according to their powers of  $dz$  and  $1/\bar{n}$ . The terms with  $1/\bar{n}^r$  with  $r \geq 1$  will vanish in the semiclassical limit  $\bar{n} \rightarrow \infty$ . The terms  $dz^r$  with  $r \geq 2$  will become irrelevant when construction the cumulant flow equations in the next subsection.

### 3. Cumulant flow equation

In the previous subsection, we have derived an expression for the moment-generating function describing the occupation of the laser pulse modes after they have interacted with an ensemble of  $N = \rho_A \mathcal{A} dz$  atoms for a time duration  $t$ . As we have seen in the derivation of the pulse Hamiltonian in Sec. A, the interaction of a pulse with each atom is described by the time-dependent light-matter interaction parameters  $g_{m,k}(t)$ . For the following considerations, we assume that the train of pulses has a total duration of  $t_M$ , which we identify as the time of the light-matter interaction  $t = t_M$  in Eq. (B21).

More precisely, we describe the propagation of a laser pulse (train) through the cloud of atoms as a sequential interaction of the pulse with each layer of the atom cloud as sketch in Fig. 2(a). After each layer of interaction, the moment-generating function describing the probability distribution is slightly modified according to Eq. (B21). For brevity, we consider the interaction duration  $t = t_M$  as a fixed parameter and consider the moment and cumulant-generating functions as a function of position  $z$ , i.e.,  $K_{\chi}(z) = \log M_{\chi}(z)$  from now on.

We can thus interpret Eq. (B21) as the moment-generating function after interaction with the  $N$  atoms in the volume limited by  $z$  and  $z+dz$ . Taking the logarithm on both sides, we thus can formally write

$$K_{\bar{n}}(z + dz) = \log [M_{\text{aux},\chi}] + K_{\bar{n}}(z), \quad (\text{B23})$$

where  $M_{\chi}(0)$  in Eq. (B21) corresponds to  $K_{\bar{n}}(z)$  and denotes the cumulant-generating function before the interaction with the next atom layer. To derive an effective equation of motion, we expand  $\log [M_{\text{aux},\chi}]$  up to the first order in  $dz$ . In doing so, we finally obtain

$$\frac{d}{dz} K_{\bar{n}}(z) = \rho_A \mathcal{A} \left[ K_{\chi}(z) + \tilde{K}_{\text{aux},\chi}(z) \right], \quad (\text{B24})$$

which is equivalent to the equation of motion in Eq. (19). We note that  $\tilde{K}_{\text{aux}}$  defined in Eq. (B22) and  $K_{\text{aux}}$  in Eq. (20) differ only in the start of the Taylor expansion.

## Appendix C: Spectroscopic observables

### 1. Rotated measurement frame

Here we provide detailed derivations regarding the representation of the flow equation in a frame, which rotates along with the polarization direction of the electromagnetic field, as explained in Sec. III E. To this end, we consider the dynamics in terms of the variables

$$A_{\alpha} = \sqrt{n_{\alpha}} \quad (\text{C1})$$

for  $\alpha = 1, 2$ , where  $n_{\alpha}$  is the photon numbers of the occupations operators  $\hat{a}_{\alpha}^{\dagger} \hat{a}_{\alpha}$ . The observables  $A_1$  and  $A_2$  are proportional to the electromagnetic fields in  $x$  and

y directions. Besides for a notational reason, we have introduced the variables  $A_\alpha$  as they have more convenient transformation properties under rotations than the  $n_\alpha$ . Next, we distribute these variables in their mean and fluctuations parts, i.e.,  $A_\alpha = \bar{A}_\alpha + dA_\alpha$ . The same separation is also applied to  $n_\alpha = \bar{n}_\alpha + dn_\alpha$ .

First, we consider the mean values of the  $A_\alpha$ . We transform them into a rotated measurement frame defined by the rotation angle of the electric field polarization  $\bar{\theta} = \bar{\theta}(z)$ , such that

$$\begin{pmatrix} \bar{A}_{\text{rot},1} \\ \bar{A}_{\text{rot},2} \end{pmatrix} = e^{i\bar{\theta}\hat{\sigma}_y} \begin{pmatrix} \bar{A}_1 \\ \bar{A}_2 \end{pmatrix}. \quad (\text{C2})$$

Clearly, the condition in Eq. (39) is equivalent to the relation

$$\bar{A}_{\text{rot},1} = \bar{A}_{\text{rot},2} \quad (\text{C3})$$

for all positions, meaning that the electric field in the rotating frame encloses always an angle  $\pi/4$  with both measurement axes.

Using Eq. (C2), we find that the time evolution in the rotated frame is given by

$$\frac{d}{dz} \begin{pmatrix} \bar{A}_{\text{rot},1} \\ \bar{A}_{\text{rot},2} \end{pmatrix} = i \frac{d\bar{\theta}}{dz} \hat{\sigma}_y \begin{pmatrix} \bar{A}_{\text{rot},1} \\ \bar{A}_{\text{rot},2} \end{pmatrix} + \begin{pmatrix} \dot{\bar{A}}_{\text{rot},1} \\ \dot{\bar{A}}_{\text{rot},2} \end{pmatrix}, \quad (\text{C4})$$

where  $\dot{\bar{A}}_{\text{rot},\alpha}$  denotes the position derivative in the fixed measurement frame. Using now Eqs. (C1), (C3) and  $\bar{n}_+ = \bar{n}_1 + \bar{n}_2$ , we find

$$\begin{aligned} \frac{d\bar{\theta}}{dz} &= \frac{\dot{\bar{A}}_{\text{rot},2} - \dot{\bar{A}}_{\text{rot},1}}{\bar{A}_{\text{rot},2} + \bar{A}_{\text{rot},1}}, \\ \dot{\bar{n}}_+ &= 2\bar{A}_{\text{rot},2}\dot{\bar{A}}_{\text{rot},2} + 2\bar{A}_{\text{rot},1}\dot{\bar{A}}_{\text{rot},1}, \end{aligned} \quad (\text{C5})$$

which is equivalent to Eq. (40).

Next, we consider the covariance matrix  $\Sigma^2$ , which can be expressed in terms of the fluctuations  $dn_\alpha$ . In the rotated measurement basis, its differential fulfills

$$dn_{\text{rot},\alpha} = 2\bar{A}_{\text{rot},\alpha} dA_{\text{rot},\alpha}, \quad (\text{C6})$$

where the amplitude fluctuations are related to fluctuations in the fixed measurement basis by

$$\begin{pmatrix} dA_{\text{rot},1} \\ dA_{\text{rot},2} \end{pmatrix} = e^{i\theta_z \hat{\sigma}_y} \begin{pmatrix} dA_1 \\ dA_2 \end{pmatrix}. \quad (\text{C7})$$

Consequently, the amplitude fluctuations fulfill the same differential equations as their corresponding mean values, i.e.,

$$\frac{d}{dz} \begin{pmatrix} dA_{\text{rot},1} \\ dA_{\text{rot},2} \end{pmatrix} = i \frac{d\bar{\theta}}{dz} \hat{\sigma}_y \begin{pmatrix} dA_{\text{rot},1} \\ dA_{\text{rot},2} \end{pmatrix} + \begin{pmatrix} d\dot{A}_{\text{rot},1} \\ d\dot{A}_{\text{rot},2} \end{pmatrix}. \quad (\text{C8})$$

Using now Eqs. (C4) and (C8), we can construct the flow equation in the rotated measurement frame for  $\Sigma^2$ . For instance, we find

$$\begin{aligned} \frac{d}{dz} [\Sigma_{\text{rot}}^2]_{1,1} &= \frac{d}{dz} \langle dn_{\text{rot},1} dn_{\text{rot},1} \rangle \\ &= \left\langle \left( \frac{d}{dz} dn_{\text{rot},1} \right) dn_{\text{rot},1} \right\rangle \\ &+ \left\langle dn_{\text{rot},1} \left( \frac{d}{dz} dn_{\text{rot},1} \right) \right\rangle \\ &= \left\langle \dot{\bar{A}}_{\text{rot},1} \bar{A}_{\text{rot},1} dA_{\text{rot},1} dA_{\text{rot},1} \right\rangle \\ &+ \left\langle \bar{A}_{\text{rot},1} \dot{\bar{A}}_{\text{rot},1} dA_{\text{rot},1} dA_{\text{rot},1} \right\rangle \\ &+ \left\langle \bar{A}_{\text{rot},1} \bar{A}_{\text{rot},1} d\dot{A}_{\text{rot},1} dA_{\text{rot},1} \right\rangle \\ &+ \left\langle \bar{A}_{\text{rot},1} \bar{A}_{\text{rot},1} dA_{\text{rot},1} d\dot{A}_{\text{rot},1} \right\rangle \\ &+ \frac{d\bar{\theta}}{dz} \langle \bar{A}_{\text{rot},2} \bar{A}_{\text{rot},1} dA_{\text{rot},1} dA_{\text{rot},1} \rangle \\ &+ \frac{d\bar{\theta}}{dz} \langle \bar{A}_{\text{rot},1} \bar{A}_{\text{rot},2} dA_{\text{rot},1} dA_{\text{rot},1} \rangle \\ &+ \frac{d\bar{\theta}}{dz} \langle \bar{A}_{\text{rot},1} \bar{A}_{\text{rot},1} dA_{\text{rot},2} dA_{\text{rot},1} \rangle \\ &+ \frac{d\bar{\theta}}{dz} \langle \bar{A}_{\text{rot},1} \bar{A}_{\text{rot},1} dA_{\text{rot},1} dA_{\text{rot},2} \rangle. \end{aligned} \quad (\text{C9})$$

The first four terms represent the derivative of  $\Sigma^2$  in the fixed measurement basis. The second four terms can be simplified. Taking the fifth term as example, we find

$$\begin{aligned} &\langle \bar{A}_{\text{rot},2} \bar{A}_{\text{rot},1} dA_{\text{rot},1} dA_{\text{rot},1} \rangle \\ &= \langle \bar{A}_{\text{rot},1} \bar{A}_{\text{rot},1} dA_{\text{rot},1} dA_{\text{rot},1} \rangle \\ &= \langle dn_{\text{rot},1} dn_{\text{rot},1} \rangle = [\Sigma_{\text{rot}}^2]_{1,1}, \end{aligned} \quad (\text{C10})$$

where we have used Eq. (C3). Putting now everything together, we finally obtain

$$\begin{aligned} \frac{d}{dz} \Sigma_{\text{rot}}^2 &= \dot{\Sigma}_{\text{rot}}^2 \\ &+ \frac{d\bar{\theta}}{dz} \left[ \begin{pmatrix} 1 & 1 \\ -1 & -1 \end{pmatrix} \Sigma_{\text{rot}}^2 + \Sigma_{\text{rot}}^2 \begin{pmatrix} 1 & -1 \\ 1 & -1 \end{pmatrix} \right], \end{aligned} \quad (\text{C11})$$

where  $\dot{\Sigma}_{\text{rot}}^2$  denotes the derivative of the correlation matrix in the instantaneous fixed measurement basis. This expression is equivalent to Eq. (42).

Finally, we explain how to transform the measurement statistic found in the rotated basis back into the fixed laboratory basis. Using that the mean amplitudes in the fixed measurement basis fulfill

$$\begin{pmatrix} \bar{A}_1 \\ \bar{A}_2 \end{pmatrix} = \sqrt{\frac{\bar{n}_+}{2}} e^{i\bar{\theta}\hat{\sigma}_y} \begin{pmatrix} 1 \\ 1 \end{pmatrix}, \quad (\text{C12})$$

it is straightforward to show that the mean photon numbers in the fixed measurement basis are given by Eq. (43). To find the relation between  $\Sigma_{\text{rot}}^2$  and  $\Sigma^2$  we use that the differential of  $n_\alpha$  is given by  $dn_\alpha = 2\bar{A}_\alpha dA_\alpha$  for  $\alpha = 1, 2$ . Using the inverse relation of Eq. (C7), we can thus find, for example,

$$\begin{aligned} [\Sigma^2]_{1,1} &= \langle dn_x dn_x \rangle \\ &+ \cos(\bar{\theta}) \cos(\bar{\theta}) \bar{A}_x \bar{A}_x \langle dA_{\text{rot},1} dA_{\text{rot},1} \rangle \\ &+ \sin(\bar{\theta}) \cos(\bar{\theta}) \bar{A}_x \bar{A}_x \langle dA_{\text{rot},1} dA_{\text{rot},2} \rangle \\ &- \cos(\bar{\theta}) \sin(\bar{\theta}) \bar{A}_x \bar{A}_x \langle dA_{\text{rot},2} dA_{\text{rot},1} \rangle \\ &+ \sin(\bar{\theta}) \sin(\bar{\theta}) \bar{A}_x \bar{A}_x \langle dA_{\text{rot},2} dA_{\text{rot},2} \rangle, \end{aligned} \quad (\text{C13})$$

and similarly for the other entries of  $\Sigma^2$ . Using Eq. (C12), we can carry out the inverse transformation from the rotated frame to the fixed laboratory by calculating

$$\Sigma_{\alpha,\beta}^2 = \frac{2\bar{A}_\alpha \bar{A}_\beta}{\bar{n}_+} \left( e^{i\bar{\theta}\hat{\sigma}_y} \Sigma_{\text{rot}}^2 e^{-i\bar{\theta}\hat{\sigma}_y} \right)_{\alpha,\beta}. \quad (\text{C14})$$

This is equivalent to the expression in Eq. (44).

## 2. Phase measurement

Here, we provide background information regarding the statistics of phase measurements in Sec. III C. Using the beamsplitter relation of the photonic operators in Eq. (30), we find

$$\begin{aligned} \hat{a}_1^\dagger \hat{a}_1 + \hat{a}_2^\dagger \hat{a}_2 &= \hat{a}_0^\dagger \hat{a}_0 + \hat{a}_{\text{LO}}^\dagger \hat{a}_{\text{LO}}, \\ \hat{a}_1^\dagger \hat{a}_1 - \hat{a}_2^\dagger \hat{a}_2 &= i \left( \hat{a}_0^\dagger \hat{a}_{\text{LO}} - \hat{a}_{\text{LO}}^\dagger \hat{a}_0 \right), \end{aligned} \quad (\text{C15})$$

which tells us that (i) the total number of photons is preserved in the beamsplitter transformation, (ii) the measured photon number difference contains information about the phase relation of  $\hat{a}_0$  and  $\hat{a}_{\text{LO}}$ .

Assuming that the mean photon number  $\bar{n}_{\text{LO}}$  and the mean phase  $\bar{\varphi}_{\text{LO}}$  are known, we can define the following estimators for the total photon number  $n_0$  and the phase  $\varphi_0$  of the photonic mode  $\hat{a}_0$  via

$$\begin{aligned} n_0 &= n_1 + n_2 - \bar{n}_{\text{LO}}, \\ \sin(\varphi_0 - \bar{\varphi}_{\text{LO}}) &= \frac{n_1 - n_2}{2\sqrt{n_0 \bar{n}_{\text{LO}}}}, \end{aligned} \quad (\text{C16})$$

from which we trivially see that the average photon number and phase are predicted by Eq. (32).

In the considerations of Sec. III D, we have assumed that  $\bar{n}_0 = \bar{n}_{\text{LO}}$ , as this configuration is directly related to the case of the polarization measurement. For completeness, we sketch here how to calculate the measurement statistics if one employs a local oscillator with an arbitrary amplitude. In particular, the task is, given our

knowledge of  $\langle dn_\alpha dn_\beta \rangle$  in the  $\bar{n}_0 = \bar{n}_{\text{LO}}$  configuration, to calculate  $\langle dn_{\text{mod},\alpha} dn_{\text{mod},\beta} \rangle$  for a modified local oscillator.

To this end, we consider a similar approach as in Appendix C 1 by considering the electric field amplitudes

$$\begin{aligned} A_1 &= \frac{1}{\sqrt{2}} (A_{\text{LO}} + iA_0), \\ A_2 &= \frac{1}{\sqrt{2}} (A_{\text{LO}} - iA_0), \end{aligned} \quad (\text{C17})$$

where  $A_1$ ,  $A_2$ ,  $A_{\text{LO}}$ , and  $A_0$  are the electric fields related to the operators  $\hat{a}_1$ ,  $\hat{a}_2$ ,  $\hat{a}_{\text{LO}}$ , and  $\hat{a}_0$ . We note that these random variables are complex valued, and can be distributed into a mean-field part and a fluctuations part according to  $A_\alpha = \bar{A}_\alpha + dA_\alpha$ . When modifying the local oscillators by replacing  $A_{\text{LO}} \rightarrow A_{\text{mod,LO}}$ , the corresponding measured fields simply become

$$\begin{aligned} A_{\text{mod},1} &= \frac{1}{\sqrt{2}} (A_{\text{mod,LO}} + iA_0), \\ A_{\text{mod},2} &= \frac{1}{\sqrt{2}} (A_{\text{mod,LO}} - iA_0). \end{aligned} \quad (\text{C18})$$

for which we can determine the statistical properties of  $n_{\text{mod},\alpha} = A_{\text{mod},\alpha}^* A_{\text{mod},\alpha}$ .

We assume that many of the electric field fluctuations correlations vanish, except for

$$\begin{aligned} \langle dA_\alpha^* dA_\beta \rangle &= \langle dA_\beta dA_\alpha^* \rangle \neq 0, \\ \langle dA_{\text{mod},\alpha}^* dA_{\text{mod},\beta} \rangle &= \langle dA_{\text{mod},\alpha} dA_{\text{mod},\beta}^* \rangle \neq 0 \end{aligned} \quad (\text{C19})$$

for  $\alpha = 1, 2$ , as the electric fields before passing the beamsplitter can be considered to be uncorrelated and correlations like  $\langle dA_\alpha^* dA_\beta^* \rangle$  vanish because of a random phase relation.

Resolving Eq. (C17) for  $A_0$  and inserting into Eq. (C18), we find

$$A_{\text{mod},1} = \frac{1}{\sqrt{2}} A_{\text{mod,LO}} + \frac{1}{2} (A_1 - A_2), \quad (\text{C20})$$

$$A_{\text{mod},2} = \frac{1}{\sqrt{2}} A_{\text{mod,LO}} - \frac{1}{2} (A_1 - A_2), \quad (\text{C21})$$

from which we can calculate the modified entries of the covariance matrix of the photon-number measurement via

$$\begin{aligned} [\Sigma_{\text{mod}}]_{\alpha,\beta} &= \langle dn_{\text{mod},\alpha} dn_{\text{mod},\beta} \rangle \\ &= A_{\text{mod},\alpha}^* A_{\text{mod},\beta} \langle dA_{\text{mod},\alpha} dA_{\text{mod},\beta}^* \rangle \\ &+ A_{\text{mod},\alpha} A_{\text{mod},\beta}^* \langle dA_{\text{mod},\alpha}^* dA_{\text{mod},\beta} \rangle \end{aligned} \quad (\text{C22})$$

By evaluating these terms, one can express  $[\Sigma_{\text{mod}}]_{\alpha,\beta}$  in terms of the  $[\Sigma]_{\alpha,\beta}$  of the balanced  $\bar{n}_0 = \bar{n}_{\text{LO}}$  measurement configuration.

### Appendix D: Fisher information for Gaussian distributions

In this Appendix, we evaluate the leading-order contributions for the Fisher information under the assumption of a Gaussian probability distribution, which is parameterized by

$$p_{X,n} = \frac{1}{(2\pi)^{\frac{D}{2}} \sqrt{\det \Sigma^2}} e^{-\frac{1}{2}(\mathbf{n} - \bar{\mathbf{n}}) \Sigma^{-2} (\mathbf{n} - \bar{\mathbf{n}})^T}, \quad (\text{D1})$$

where  $X$  is the parameter which is to be estimated. To simplify the following calculation, we thereby assume that the entries of  $\mathbf{n}$  are continuous variables. The influence of the parameter  $X$  on the probability distribution enters via the dependence of the mean photon numbers and the covariance matrix, i.e.,  $\bar{\mathbf{n}} = \bar{\mathbf{n}}_X$  and  $\Sigma^2 = \Sigma_X^2$ .

The Fisher score of the probability distribution regarding the parameter  $X$  is defined by

$$\begin{aligned} g(X, \mathbf{n}) &\equiv -\partial_X \ln p_{X,n} \\ &= \frac{1}{2} (\partial_X \bar{\mathbf{n}}) \Sigma^{-2} (\mathbf{n} - \bar{\mathbf{n}})^T + \frac{1}{2} (\mathbf{n} - \bar{\mathbf{n}}) \Sigma^{-2} (\partial_X \bar{\mathbf{n}})^T \\ &\quad + (\mathbf{n} - \bar{\mathbf{n}}) \Sigma^{-2} (\partial_X \Sigma^2) \Sigma^{-2} (\mathbf{n} - \bar{\mathbf{n}})^T \\ &\quad + \frac{1}{2} \text{tr} [\partial_X \ln \Sigma^2]. \end{aligned} \quad (\text{D2})$$

Using the Fisher score, we can now evaluate the Fisher information

$$\begin{aligned} I_{\theta=0} &= \int d\mathbf{n} p_{\mathbf{n}}^{(0)} g(X, \mathbf{n})^2 \\ &= \int d\mathbf{n} \mathcal{N}_0 e^{-\frac{1}{2} \mathbf{n} \Sigma^{-2} \mathbf{n}^T} \left[ (\partial_X \bar{\mathbf{n}}) \Sigma^{-2} \mathbf{n}^T \right. \\ &\quad \left. + \mathbf{n} \Sigma^{-2} (\partial_X \Sigma^2) \Sigma^{-2} \mathbf{n}^T \right. \\ &\quad \left. + \frac{1}{2} \text{tr} (\partial_X \ln \Sigma^2) \right]^2 \\ &= (\partial_X \bar{\mathbf{n}}) \Sigma^{-2} (\partial_X \bar{\mathbf{n}})^T \\ &\quad + \text{tr} (\Sigma^{-2} \partial_X \Sigma^2)^2 + 2 \text{tr} (\Sigma^{-2} \partial_X \Sigma^2 \Sigma^{-2} \partial_X \Sigma^2) \\ &\quad + \text{tr} (\Sigma^{-2} \partial_X \Sigma^2) \text{tr} (\partial_X \ln \Sigma^2) \\ &\quad + \frac{1}{4} \text{tr} (\partial_X \ln \Sigma^2)^2, \end{aligned} \quad (\text{D3})$$

where  $\mathcal{N}_0$  is the normalization of the Gauss distribution in Eq. (D1). To further simplify this, we assume the scaling relation  $\bar{\mathbf{n}} \propto z$  and  $\Sigma^2 \propto z$ , where  $z$  is the propagation distance of the laser pulse within the atom cloud. Making a simple scaling analysis of the Fisher information, we find that only the first term scales with  $\propto z$ , while the other terms scale only with  $\propto z^0$ . For this reason, the Fisher information is approximately given by Eq. (45) for a Gaussian probability distribution.

### Appendix E: Truncated polynomial approach

To analytically evaluate the low-order cumulants, we take advantage of the truncated polynomial approach of Ref. [50]. The starting point is the characteristic polynomial of the Liouvillian, which can be formally expanded as

$$\mathcal{P}_{\chi}(z) = \sum_{j=0}^N a_j(\chi) z^j, \quad (\text{E1})$$

where the expansion coefficients  $a_j(\chi)$  depend on the counting field. When intending to evaluate a  $l$ -th order cumulant, it is sufficient to consider the truncated polynomial

$$\mathcal{P}_{\chi}^{(l)}(z) = \sum_{j=0}^l a_j(\chi) z^j, \quad (\text{E2})$$

as the derivatives of the dominating root of the full polynomial  $\lambda_{0;\chi}$  and of the truncated polynomial  $\lambda_{0;\chi}^{(l)}$  are equal, e.g.,

$$\frac{d^l}{d(-i\chi_{\alpha})^l} \lambda_{0;\chi=0} = \frac{d^l}{d(-i\chi_{\alpha})^l} \lambda_{0;\chi=0}^{(l)}. \quad (\text{E3})$$

The same relations hold also true for mixed derivatives.

As we intent to calculate the first two cumulants, we use the dominant eigenvalue of the corresponding truncating polynomial, which reads

$$\lambda_{0;\chi}^{(2)} = \frac{1}{2a_2} \left( -a_1 + \sqrt{a_1^2 - 4a_0a_2} \right),$$

where we have suppressed the dependence of the expansion coefficients on the counting fields. For brevity, we define the following short-hand notation for the derivatives of the polynomial coefficient

$$\begin{aligned} a_j^{(\alpha)} &= \left. \frac{d}{d\chi_{\alpha}} a_j \right|_{\chi=0}, \\ a_j^{(\alpha\beta)} &= \left. \frac{d}{d\chi_{\alpha}} \frac{d}{d\chi_{\beta}} a_j \right|_{\chi=0}. \end{aligned} \quad (\text{E4})$$

After some tedious but straightforward calculations, we find that the derivatives of the dominating eigenvalue with respect to the counting fields can be expressed as

$$\begin{aligned} \lambda_{0;\chi=0}^{(2)(\alpha)} &= -\frac{a_0^{(\alpha)}}{a_1} \\ \lambda_{0;\chi=0}^{(2)(\alpha\beta)} &= -\frac{a_0^{(\alpha\beta)}}{a_1} - \frac{a_0^{(\alpha)} a_2^{(\beta)} + a_0^{(\beta)} a_2^{(\alpha)}}{a_2 a_1} \\ &\quad + \frac{a_0^{(\alpha)} a_1^{(\beta)} + a_0^{(\beta)} a_1^{(\alpha)}}{a_1^2} - \frac{2a_2 a_0^{(\alpha)} a_0^{(\beta)}}{a_1^3}, \end{aligned} \quad (\text{E5})$$

which can be used to directly evaluate the cumulants of first and second orders by just determining the expansion coefficients of the characteristic polynomial.

## Appendix F: Analytical calculations for the two-level system

### 1. Coefficients of the flow equations

In this Appendix, we calculate the coefficients of the flow equation in Eq. (22) and Eq. (24) for the two-level system Liouvillian in Eq. (56). To this end, we use the truncated polynomial approach introduced in Appendix E. The coefficients of the characteristic polynomial are given by

$$\begin{aligned} a_4 &= 1, \\ a_3 &= 2\gamma, \\ a_2 &= \frac{1}{2}\mathcal{A}_\chi + \epsilon_\Delta^2 + \frac{5}{4}\gamma^2, \\ a_1 &= \frac{\gamma}{2}[\mathcal{A}_\chi - \mathcal{C}_\chi] + \gamma\epsilon_\Delta^2 + \frac{\gamma^3}{4}, \\ a_0 &= \frac{1}{16}\mathcal{B}_\chi^2 + \frac{\gamma^2}{8}(\mathcal{A}_\chi - 2\mathcal{C}_\chi) - i\frac{\epsilon_\Delta\gamma}{4}\mathcal{B}_\chi, \end{aligned} \quad (\text{F1})$$

in which we have introduced

$$\begin{aligned} \mathcal{A}_\chi &= 2\Omega_1^2 + 2\Omega_2^2 + 4\Omega_1\Omega_2 \cos(\bar{\varphi}_1 - \bar{\varphi}_2) \cos\left(\frac{\chi_1}{2} - \frac{\chi_2}{2}\right), \\ \mathcal{B}_\chi &= -4\Omega_1\Omega_2 \sin(\bar{\varphi}_1 - \bar{\varphi}_2) \sin\left(\frac{\chi_1}{2} - \frac{\chi_2}{2}\right), \\ \mathcal{C}_\chi &= \Omega_1^2 e^{i\chi_1} + \Omega_2^2 e^{i\chi_2} + 2\Omega_1\Omega_2 e^{i\frac{\chi_1+\chi_2}{2}} \cos(\bar{\varphi}_1 - \bar{\varphi}_2). \end{aligned} \quad (\text{F2})$$

To evaluate the cumulants using Eq. (E5), we calculate the first and second derivatives of the expansion coefficients in Eq. (F1). A straightforward calculation gives

$$\begin{aligned} a_0 &= 0, \\ a_0^{(1)} &= -i\frac{\gamma^2}{4}[\Omega_1^2 + \Omega_1\Omega_2 \cos(\tilde{\varphi})] + i\frac{\epsilon_\Delta\gamma}{4}2\Omega_1\Omega_2 \sin(\tilde{\varphi}), \\ a_0^{(2)} &= -i\frac{\gamma^2}{4}[\Omega_2^2 + \Omega_1\Omega_2 \cos(\tilde{\varphi})] - i\frac{\epsilon_\Delta\gamma}{4}2\Omega_1\Omega_2 \sin(\tilde{\varphi}), \\ a_0^{(11)} &= \frac{1}{16}[2\Omega_1\Omega_2 \sin(\tilde{\varphi})]^2, \\ &\quad + \frac{\gamma^2}{8}[-\Omega_1\Omega_2 \cos(\tilde{\varphi}) + 2\Omega_1^2 + \Omega_1\Omega_2 \cos(\tilde{\varphi})], \\ a_0^{(22)} &= \frac{1}{16}[2\Omega_1\Omega_2 \sin(\tilde{\varphi})]^2, \\ &\quad + \frac{\gamma^2}{8}[-\Omega_1\Omega_2 \cos(\tilde{\varphi}) + 2\Omega_2^2 + \Omega_1\Omega_2 \cos(\tilde{\varphi})], \\ a_0^{(12)} &= -\frac{1}{16}[2\Omega_1\Omega_2 \sin(\tilde{\varphi})]^2, \\ &\quad + \frac{\gamma^2}{8}[\Omega_1\Omega_2 \cos(\tilde{\varphi}) + \Omega_1\Omega_2 \cos(\tilde{\varphi})], \end{aligned}$$

$$a_0^{(21)} = a_0^{(12)},$$

$$\begin{aligned} a_1 &= \frac{\gamma}{2}[\Omega_1^2 + \Omega_2^2 + 2\Omega_1\Omega_2 \cos(\tilde{\varphi})] + \gamma\epsilon_\Delta^2 + \frac{\gamma^3}{4}, \\ a_1^{(1)} &= -i\frac{\gamma}{2}[\Omega_1^2 + \Omega_1\Omega_2 \cos(\tilde{\varphi})], \\ a_1^{(2)} &= -i\frac{\gamma}{2}[\Omega_2^2 + \Omega_1\Omega_2 \cos(\tilde{\varphi})], \\ a_2 &= \Omega_1^2 + \Omega_2^2 + 2\Omega_1\Omega_2 \cos(\tilde{\varphi}) + \epsilon_\Delta^2 + \frac{5}{4}\gamma^2, \\ a_2^{(1)} &= 0, \\ a_2^{(2)} &= 0, \end{aligned} \quad (\text{F3})$$

where we have defined  $\tilde{\varphi} = \bar{\varphi}_1 - \bar{\varphi}_2$ . Consequently, the coefficients of the flow equations in Eq. (22) and Eq. (24) are given by

$$\begin{aligned} [\mathbf{I}\bar{\mathbf{n}}]_{k_\alpha} &= -i\rho_A \mathcal{A} t_M \frac{a_0^{(\alpha)}}{a_1}, \\ [\mathbf{D}\bar{\mathbf{n}}]_{k_\alpha, k_\beta} &= \rho_A \mathcal{A} t_M \\ &\quad \times \left( \frac{a_0^{(\alpha\beta)}}{a_1} - \frac{a_0^{(\alpha)} a_1^{(\beta)}}{a_1^2} + \frac{2a_2 a_0^{(\alpha)} a_0^{(\beta)}}{a_1^3} \right), \end{aligned} \quad (\text{F4})$$

where we recall that  $\rho_A$  denotes the atom density and  $\mathcal{A}$  is the effective laser cross section.

### 2. Cumulant aptitudes

In a similar fashion we can also evaluate the cumulant aptitudes introduced in Eq. (66). To this end, we first express the characteristic polynomial in the rotated measurement basis, in which  $\Omega_1 = \Omega_2 = \frac{\Omega}{\sqrt{2}}$  with  $\Omega$  being the Rabi frequency experienced by the atoms. In doing so, the first three expansion coefficients become

$$\begin{aligned} a_2 &= \Omega^2 + \frac{1}{4}\epsilon_\Delta^2 + \frac{5}{4}\gamma^2, \\ a_1 &= \frac{\gamma}{2}[2\Omega^2 - \Omega^2 e^{i\chi_+} \cos(\chi_-)] + \frac{\gamma}{4}\epsilon_\Delta^2 + \frac{\gamma^3}{4}, \\ a_0 &= \frac{1}{4}[\Omega^2 \sin(\chi_-)]^2 + \frac{\gamma^2}{4}[\Omega^2 - \Omega^2 e^{i\chi_+} \cos(\chi_-)] \\ &\quad + i\frac{\epsilon_\Delta\gamma}{4}\Omega^2 \sin(\chi_-), \end{aligned} \quad (\text{F5})$$

where we have used the symmetric and anti-symmetric representation of the counting fields  $\chi_+ = \frac{1}{2}(\chi_1 + \chi_2)$  and  $\chi_- = \frac{1}{2}(\chi_1 - \chi_2)$ . Calculating the derivatives with respect to the counting fields  $\chi_+$  and  $\chi_-$ , we obtain

$$\begin{aligned} a_0^{(+)} &= -i\frac{\gamma^2}{4}\Omega^2, \\ a_0^{(-)} &= i\frac{\epsilon_\Delta\gamma}{2}\Omega^2, \end{aligned}$$

$$\begin{aligned}
a_0^{(++)} &= \frac{\gamma^2}{4}\Omega^2, \\
a_0^{(--)} &= \frac{1}{2}\Omega^4 + \frac{1}{4}\gamma^2\Omega^2, \\
a_0^{(+-)} &= 0, \\
a_0^{(-+)} &= 0, \\
a_1 &= \frac{\gamma}{2}\Omega^2 + \gamma\epsilon_\Delta^2 + \frac{\gamma^3}{4}, \\
a_1^{(+)} &= -i\frac{\gamma}{2}\Omega^2, \\
a_1^{(-)} &= 0, \\
a_2 &= \Omega^2 + \epsilon_\Delta^2 + \frac{5}{4}\gamma^2.
\end{aligned} \tag{F6}$$

Using now Eq. (E5), we can readily obtain closed-form expressions for the cumulant aptitudes

$$\begin{aligned}
\kappa_+^{(\delta)} &= -\frac{\gamma\Omega^2}{4\epsilon_\Delta^2 + 2\Omega^2 + \gamma^2}, \\
\kappa_-^{(\delta)} &= \frac{2\epsilon_\Delta\Omega^2}{4\epsilon_\Delta^2 + 2\Omega^2 + \gamma^2}, \\
\kappa_{++}^{(\delta)} &= \frac{a_0^{(++)}}{a_1} - \frac{2a_0^{(+)}a_1^{(+)}}{a_1^2} + \frac{2a_2a_0^{(+)}a_0^{(+)}}{a_1^3} \\
&= \frac{\gamma\Omega^2}{(4\epsilon_\Delta^2 + 2\Omega^2 + \gamma^2)} + \frac{\Omega^4\gamma(8\epsilon_\Delta^2 - 6\gamma^2)}{(4\epsilon_\Delta^2 + 2\Omega^2 + \gamma^2)^3}, \\
\kappa_{--}^{(\delta)} &= \frac{a_0^{(--)}}{a_1} + \frac{2a_2a_0^{(-)}a_0^{(-)}}{a_1^3} \\
&= \frac{2\Omega^4 + \gamma^2\Omega^2}{\gamma(4\epsilon_\Delta^2 + 2\Omega^2 + \gamma^2)} - \frac{8\epsilon_\Delta^2\Omega^4(4\Omega^2 + 4\epsilon_\Delta^2 + 5\gamma^2)}{\gamma(4\epsilon_\Delta^2 + 2\Omega^2 + \gamma^2)^3},
\end{aligned} \tag{F7}$$

which are the same as in Eq. (67).

### Appendix G: Weak coupling regime

In this Appendix, we explain the appearance of the diverging fluctuations in the weak dissipation regime which we have shortly discussed in Sec. IV G for the two-level system. To show that this is a generic effect, we consider the quantum master equation

$$\frac{d}{dt}\rho = -i\left[\hat{\mathcal{H}}_{\varphi+\frac{\chi}{2}}\rho - \rho\hat{\mathcal{H}}_{\varphi-\frac{\chi}{2}}\right] + \sum_j \gamma_j D_j[S_j]\rho, \tag{G1}$$

without further specifying the Hamiltonian  $\hat{\mathcal{H}}_\varphi$  or the dissipators  $D[S_j]$ , which are a function of some system operators  $\hat{S}_j$ .

Expanding in the eigenstate basis of  $\hat{\mathcal{H}}_\varphi$ , the master

equation approximately becomes

$$\begin{aligned}
\frac{d}{dt}\rho_{\mu_1,\mu_2} &\approx \left(i\epsilon_{\mu_2,\varphi-\frac{\chi}{2}} - i\epsilon_{\mu_1,\varphi+\frac{\chi}{2}} - \gamma_{\mu_1\mu_2,\mu_1\mu_2}\right)\rho_{\mu_1,\mu_2} \\
&+ \sum_{\mu_3} \gamma_{\mu_1\mu_2,\mu_3\mu_4}\rho_{\mu_3,\mu_4},
\end{aligned} \tag{G2}$$

where  $\epsilon_{\mu,\varphi}$  denote the energies of the eigenstates  $|u_{\mu,\varphi}\rangle$ . We note that the relation  $\langle u_{\mu_1,\varphi} | u_{\mu_2,\varphi-\frac{\chi}{2}} \rangle \approx \delta_{\mu_1,\mu_2}$  is only approximately fulfilled for small  $\chi$ . Yet, in the approximated master equation in Eq. (G2) we rely on the findings in Ref. [51] that the cumulants are dominated by the energies  $\epsilon_{\mu,\varphi}$  and not by the counting-field dependence of the eigenstates.

We use the following ansatz to solve Eq. (G2),

$$\rho_{\mu_1,\mu_2}(t) = \tilde{\rho}_{\mu_1,\mu_2} e^{\lambda_\chi t}, \tag{G3}$$

where the time independent  $\tilde{\rho}_{\mu_1,\mu_2}$  is a function of the counting field, and  $\lambda_\chi$  is the cumulant-generating function in the long-time limit as explained in Eq. (55). Inserting into Eq. (G3) and resolving for  $\rho_{\mu_1,\mu_2}^{(0)}$  we find

$$\tilde{\rho}_{\mu_1,\mu_2} = \frac{\sum_{(\mu_3,\mu_4) \neq (\mu_1,\mu_2)} \gamma_{\mu_1\mu_2,\mu_3\mu_4} \tilde{\rho}_{\mu_3,\mu_4}}{i\epsilon_{\mu_2,\varphi-\frac{\chi}{2}} - i\epsilon_{\mu_1,\varphi+\frac{\chi}{2}} - \gamma_{\mu_1\mu_2,\mu_1\mu_2} - \lambda_\chi}. \tag{G4}$$

From this relation we learn that the coherence elements  $\tilde{\rho}_{\mu_1,\mu_2}$  with  $\mu_1 \neq \mu_2$  are strongly suppressed in comparison to the diagonal terms with  $\mu_1 = \mu_2$ , as we consider the weak dissipation regime characterized by  $\epsilon_{\mu_2,\varphi-\frac{\chi}{2}} - \epsilon_{\mu_1,\varphi+\frac{\chi}{2}} \gg \gamma_{\mu_1\mu_2,\mu_1\mu_2}$ .

For this reason, we can restrict the differential equation in Eq. (G2) to the diagonal elements, which can be written in a vector form as

$$\frac{d}{dt}\mathbf{p}_\chi(t) = [\mathbf{K}_\chi + \mathbf{\Gamma}]\mathbf{p}_\chi(t). \tag{G5}$$

Thereby,  $\mathbf{p}_\chi = (p_{\chi,1}, \dots, p_{\chi,D})$  is the vector of diagonal elements, which are subject to the normalization condition  $\sum_\mu p_{\chi=0,\mu} = 1$ , where  $p_{\chi=0,\mu}$  is just the probability to be in eigenstate  $\mu$  in the stationary state. As we will see, the following considerations are independent of the normalization condition for  $\chi \neq 0$ . Moreover, we have defined the matrices

$$\begin{aligned}
[\mathbf{K}_\chi]_{\mu,\mu} &= i\left(\epsilon_{\mu,\varphi-\frac{\chi}{2}} - \epsilon_{\mu,\varphi+\frac{\chi}{2}}\right), \\
[\mathbf{\Gamma}]_{\mu_1,\mu_2} &= \gamma_{\mu_1\mu_1,\mu_2\mu_2}.
\end{aligned} \tag{G6}$$

Equation (G5) describes quantum jumps between the eigenstates of the closed Hamiltonian system. Depending on each eigenstate, the measurement properties are determined by the terms  $[\mathbf{K}_\chi]_{\mu,\mu}$ , which can be interpreted as the cumulant-generating function under the condition, that the system is in eigenstate  $\mu$ . The first derivative of  $[\mathbf{K}_\chi]_{\mu,\mu}$  with respect to the counting fields predicts the

mean-photon number change (i.e., photon flux) of the photonic laser pulses, conditioned on the eigenstate  $\mu$ . It is easy to show that the second derivatives of  $[\mathbf{K}_\chi]_{\mu,\mu}$  with respect to the counting field at  $\chi = 0$  vanishes. Thus, the photon number variance remains constant as long as the system stays in a specific eigenstate. The increase of the variance can thus only occur when the system jumps between different eigenstates, each featuring a different mean photon flux. The rates of these quantum jumps are given by the matrix elements of  $\mathbf{\Gamma}$ .

The ansatz in Eq. (G3) can now be written as

$$\mathbf{p}_\chi(t) = e^{\lambda_\chi t} \tilde{\mathbf{p}}_\chi, \quad (\text{G7})$$

which leads to the eigenvalue equation

$$\lambda_\chi \tilde{\mathbf{p}}_\chi = [\mathbf{K}_\chi + \mathbf{\Gamma}] \tilde{\mathbf{p}}_\chi, \quad (\text{G8})$$

containing the information about all cumulants in the long-time limit.

To simplify the notation in the following, we consider only a single counting field  $\chi$ , whose cumulants shall be determined. The following considerations are a simplified version of the derivations in Refs. [59, 92]. Deriving Eq. (G8) with respect to  $\chi$  and using the probability normalization condition, we find

$$\lambda'_0 \tilde{\mathbf{p}}_0 = \mathbf{K}'_0 \tilde{\mathbf{p}}_0 + \mathbf{\Gamma} \tilde{\mathbf{p}}'_0, \quad (\text{G9})$$

where the prime denotes the derivative with respect to  $\chi$  evaluated at  $\chi = 0$ . Summing over the states  $\mu$ , we find

an expression for the first cumulant aptitude

$$\kappa_1^{(\delta)} = -i\lambda'_0 = \sum_\mu \epsilon'_{\mu,\varphi} \tilde{p}_{0,\mu}. \quad (\text{G10})$$

In doing so, we took advantage of  $\sum_\mu [\mathbf{\Gamma}]_{\mu,\mu_1} = 0$  for all  $\mu_1$ .

In a similar fashion, we obtain the second cumulant aptitude. To this end, we derive Eq. (G8) two times and obtain

$$\lambda''_0 \tilde{\mathbf{p}}_0 + \lambda'_0 \tilde{\mathbf{p}}'_0 = \mathbf{K}''_0 \tilde{\mathbf{p}}_0 + \mathbf{\Gamma} \tilde{\mathbf{p}}''_0. \quad (\text{G11})$$

We can neglect the second term on the right-hand side, as it will vanish once we sum over the eigenstates. Moreover, from Eq. (G9) we find that

$$\tilde{\mathbf{p}}'_0 = \mathbf{\Gamma}^+ [\lambda'_0 - \mathbf{K}'_0] \tilde{\mathbf{p}}_0 = -\mathbf{K}'_0 \tilde{\mathbf{p}}_0, \quad (\text{G12})$$

in which  $\mathbf{\Gamma}^+$  denotes the pseudoinverse of  $\mathbf{\Gamma}$ . Inserting this expression for  $\tilde{\mathbf{p}}'_0$  into Eq. (G12) and summing over the eigenstates, we finally obtain an expression for the second cumulant aptitude

$$\kappa_2^{(\delta)} = -\lambda''_0 = \sum_{\mu_1 \mu_2} [\mathbf{\Gamma}^+]_{\mu_1 \mu_2} \epsilon'_{\mu_1, \varphi} \epsilon'_{\mu_2, \varphi} \tilde{p}_{0, \mu}, \quad (\text{G13})$$

which is a function of the energy derivatives  $\epsilon'_{\mu, \varphi}$ , i.e., the fluxes conditioned on the eigenstate. As this expression involves the pseudoinverse of the rate matrix  $\mathbf{\Gamma}$ , it will diverge for a vanishing dissipation.

- 
- [1] J. H. Baraban, P. B. Changala, G. C. Mellau, J. F. Stanton, A. J. Merer, and R. W. Field, Spectroscopic characterization of isomerization transition states, *Science* **350**, 1338 (2015).
  - [2] J. E. Colley, N. J. Dynak, J. R. C. Blais, and M. A. Duncan, Photodissociation spectroscopy and photofragment imaging to probe fe+(benzene)1,2 dissociation energies, *J. Phys. Chem. A* **127**, 2795 (2023).
  - [3] W. Domcke and D. R. Yarkony, Role of conical intersections in molecular spectroscopy and photoinduced chemical dynamics, *Annual Review of Physical Chemistry* **63**, 325 (2012).
  - [4] Z. Zhang, S. Zhao, and D. Lei, Quantum statistical theory for an exciton-polariton condensate: Fluctuations and coherence, *Phys. Rev. B* **106**, L220306 (2022).
  - [5] M. Reitz, A. Koner, and J. Yuen-Zhou, Nonlinear semiclassical spectroscopy of ultrafast molecular polariton dynamics, *Phys. Rev. Lett.* **134**, 193803 (2025).
  - [6] G. Ferioli, A. Glicenstein, I. Ferrier-Barbut, and A. Browaeys, A non-equilibrium superradiant phase transition in free space, *Nature Physics* **19**, 1345 (2023).
  - [7] S. Agarwal, E. Chaparro, D. Barberena, A. P. n. Orioli, G. Ferioli, S. Pancaldi, I. Ferrier-Barbut, A. Browaeys, and A. Rey, Directional superradiance in a driven ultracold atomic gas in free space, *PRX Quantum* **5**, 040335 (2024).
  - [8] D. Goncalves, L. Bombieri, G. Ferioli, S. Pancaldi, I. Ferrier-Barbut, A. Browaeys, E. Shahmoon, and D. Chang, Driven-dissipative phase separation in free-space atomic ensembles, *PRX Quantum* **6**, 020303 (2025).
  - [9] C. L. Degen, F. Reinhard, and P. Cappellaro, Quantum sensing, *Rev. Mod. Phys.* **89**, 035002 (2017).
  - [10] L. Pezzè, A. Smerzi, M. K. Oberthaler, R. Schmied, and P. Treutlein, Quantum metrology with nonclassical states of atomic ensembles, *Rev. Mod. Phys.* **90**, 035005 (2018).
  - [11] J. Ye and P. Zoller, Essay: Quantum sensing with atomic, molecular, and optical platforms for fundamental physics, *Phys. Rev. Lett.* **132**, 190001 (2024).
  - [12] P. W. Graham, J. M. Hogan, M. A. Kasevich, and S. Rajendran, Resonant mode for gravitational wave detectors based on atom interferometry, *Phys. Rev. D* **94**, 104022 (2016).
  - [13] J. M. Hogan and M. A. Kasevich, Atom-interferometric gravitational-wave detection using heterodyne laser links, *Phys. Rev. A* **94**, 033632 (2016).
  - [14] C. D. Panda, M. J. Tao, M. Ceja, J. Khoury, G. M. Tino, and H. Müller, Measuring gravitational attraction with a lattice atom interferometer, *Nature* **631**, 515 (2024).
  - [15] J. e. a. Wenxuan, Squeezing the quantum noise of a gravitational-wave detector below the standard quantum limit, *Science* **385**, 1318 (2024).

- [16] T. Li, F. Li, X. Liu, V. V. Yakovlev, and G. S. Agarwal, Quantum-enhanced stimulated brillouin scattering spectroscopy and imaging, *Optica* **9**, 959 (2022).
- [17] K. E. Dorfman, S. Asban, B. Gu, and S. Mukamel, Hongou-mandel interferometry and spectroscopy using entangled photons, *Communications Physics* **4**, 49 (2021).
- [18] Z. Zhang, T. Peng, X. Nie, G. S. Agarwal, and M. O. Scully, Entangled photons enabled time-frequency-resolved coherent Raman spectroscopy and applications to electronic coherences at femtosecond scale, *Light: Science and Applications* **11**, 10.1038/s41377-022-00953-y (2022).
- [19] J. J. Fan, Z.-Y. Ou, and Z. Zhang, Entangled photons enabled ultrafast stimulated raman spectroscopy for molecular dynamics, *Light: Science and Applications* **13**, 163 (2024).
- [20] A. D. Ludlow, M. M. Boyd, J. Ye, E. Peik, and P. O. Schmidt, Optical atomic clocks, *Rev. Mod. Phys.* **87**, 637 (2015).
- [21] J. M. Robinson, M. Miklos, Y. M. Tso, C. J. Kennedy, T. Bothwell, D. Kedar, J. K. Thompson, and J. Ye, Direct comparison of two spin-squeezed optical clock ensembles at the 10-17 level, *Nature Physics* **20**, 208 (2024).
- [22] D. Budker and D. F. Jackson Kimball, eds., *Optical Magnetometry* (Cambridge University Press, 2013).
- [23] F. Wolgramm, A. Cerè, F. A. Beduini, A. Predojević, M. Koschorreck, and M. W. Mitchell, Squeezed-light optical magnetometry, *Phys. Rev. Lett.* **105**, 053601 (2010).
- [24] Y. Ma, Y. Chen, M. Yu, Y. Wang, S. Lu, J. Guo, G. Luo, L. Zhao, P. Yang, Q. Lin, and Z. Jiang, Ultrasensitive serf atomic magnetometer with a miniaturized hybrid vapor cell, *Microsystems and Nanoengineering* **10**, 121 (2024).
- [25] M. Xu, M. Jiang, Y. Wang, H. Su, Y. Huang, and X. Peng, Cooperative spin amplifier for enhanced quantum sensing, *Phys. Rev. Lett.* **133**, 133202 (2024).
- [26] Z. Ma, C. Han, Z. Tan, H. He, S. Shi, X. Kang, J. Wu, J. Huang, B. Lu, and C. Lee, Adaptive cold-atom magnetometry mitigating the trade-off between sensitivity and dynamic range, *Science Advances* **11**, eadt3938 (2025).
- [27] J. Wang, J. Lee, H. Loughlin, M. Hedges, and M. V. Romalis, Pulsed dual-axis alkali-metal–noble-gas comagnetometer, *Phys. Rev. A* **111**, 053103 (2025).
- [28] D. Budker, P. W. Graham, M. Ledbetter, S. Rajendran, and A. O. Sushkov, Proposal for a cosmic axion spin precession experiment (CASPER), *Phys. Rev. X* **4**, 021030 (2014).
- [29] D. Aybas, H. Bekker, J. W. Blanchard, D. Budker, G. P. Centers, N. L. Figueroa, A. V. Gramolin, D. F. Jackson Kimball, A. Wickenbrock, and A. O. Sushkov, Quantum sensitivity limits of nuclear magnetic resonance experiments searching for new fundamental physics, *Quantum Science and Technology* **6**, 034007 (2021).
- [30] I. M. Bloch, G. Ronen, R. Shaham, O. Katz, T. Volansky, and O. Katz, New constraints on axion-like dark matter using a Floquet quantum detector, *Science Advances* **8**, eabl8919 (2022).
- [31] R. Löw, H. Weimer, J. Nipper, J. B. Balewski, B. Butscher, H. P. Büchler, and T. Pfau, An experimental and theoretical guide to strongly interacting rydberg gases, *Journal of Physics B: Atomic, Molecular and Optical Physics* **45**, 113001 (2012).
- [32] C. Holloway, M. Simons, J. Gordon, A. Dienstfrey, D. Anderson, and G. Raithel, Electric field metrology for SI traceability: Systematic measurement uncertainties in electromagnetically induced transparency in atomic vapor, *Journal of Applied Physics* **121**, 10.1063/1.4984201 (2017).
- [33] K. C. Cox, D. H. Meyer, F. K. Fatemi, and P. D. Kunz, Quantum-limited atomic receiver in the electrically small regime, *Phys. Rev. Lett.* **121**, 110502 (2018).
- [34] D. H. Meyer, Z. A. Castillo, K. C. Cox, and P. D. Kunz, Assessment of Rydberg atoms for wideband electric field sensing, *Journal of Physics B: Atomic, Molecular and Optical Physics* **53**, 034001 (2020).
- [35] M. Jing, Y. Hu, J. Ma, H. Zhang, L. Zhang, L. Xiao, and S. Jia, Atomic superheterodyne receiver based on microwave-dressed Rydberg spectroscopy, *Nature Physics* **16**, 911 (2020).
- [36] D. H. Meyer, P. D. Kunz, and K. C. Cox, Waveguide-coupled Rydberg spectrum analyzer from 0 to 20 GHz, *Phys. Rev. Appl.* **15**, 014053 (2021).
- [37] C. L. Holloway, N. Prajapati, J. A. Sherman, A. Rüfenacht, A. B. Artusio-Glimpse, M. T. Simons, A. K. Robinson, D. S. La Mantia, and E. B. Norrgard, Electromagnetically induced transparency based rydberg-atom sensor for traceable voltage measurements, *AVS Quantum Science* **4**, 034401 (2022).
- [38] B. Liu, L.-H. Zhang, Z.-K. Liu, Z.-Y. Zhang, Z.-H. Zhu, W. Gao, G.-C. Guo, D.-S. Ding, and B.-S. Shi, Highly sensitive measurement of a megahertz rf electric field with a Rydberg-atom sensor, *Phys. Rev. Appl.* **18**, 014045 (2022).
- [39] S. Borówka, U. Pylypenko, M. Mazelanik, and M. Parniak, Continuous wideband microwave-to-optical converter based on room-temperature Rydberg atoms, *Nature Photonics* **18**, 32 (2024).
- [40] A. Kumar, A. Suleymanzade, M. Stone, L. Taneja, A. Anferov, D. I. Schuster, and J. Simon, Quantum-enabled millimetre wave to optical transduction using neutral atoms, *Nature* **615**, 614 (2023).
- [41] S. Ghosh, E. Graham, S. Getz, A. Giman, and R. Maruyama, Advancing Rydberg atom-based axion detection, *Proc. SPIE Int. Soc. Opt. Eng.* **12912**, 86 (2024).
- [42] S. Mukamel, *Principles of nonlinear optical spectroscopy* (OXFORD UNIVERSITY PRESS, 1995).
- [43] M. O. Scully and M. S. Zubairy, *Quantum optics* (Cambridge University Press, 1997).
- [44] K. Hammerer, A. S. Sørensen, and E. S. Polzik, Quantum interface between light and atomic ensembles, *Rev. Mod. Phys.* **82**, 1041 (2010).
- [45] H. M. Wiseman and G. J. Milburn, Quantum theory of field-quadrature measurements, *Phys. Rev. A* **47**, 642 (1993).
- [46] C. W. Gardiner and M. J. Collett, Input and output in damped quantum systems: Quantum stochastic differential equations and the master equation, *Phys. Rev. A* **31**, 3761 (1985).
- [47] C. W. Gardiner and P. Zoller, *Quantum Noise: A Handbook of Markovian and Non-Markovian Quantum Stochastic Methods with Applications to Quantum Optics* (Springer, Berlin, Heidelberg, 2004).
- [48] K. E. Dorfman and S. Mukamel, Multidimensional photon correlation spectroscopy of cavity polaritons, *Proceedings of the National Academy of Sciences* **115**, 1451 (2018).
- [49] G. Engelhardt, S. Choudhury, and W. V. Liu, Unified light-matter floquet theory and its application to quantum communication, *Phys. Rev. Res.* **6**, 013116 (2024).

- [50] G. Engelhardt, J. Luo, V. M. Bastidas, and G. Platero, Photon-resolved Floquet theory. I. Full counting statistics of the driving field in Floquet systems, *Phys. Rev. A* **110**, 063707 (2024).
- [51] G. Engelhardt, J. Luo, V. M. Bastidas, and G. Platero, Photon-resolved Floquet theory. II. Open quantum systems, *Phys. Rev. A* **110**, 063708 (2024).
- [52] C. Rao, Information and the accuracy attainable in the estimation of statistical parameters, *Bulletin of Calcutta Mathematical Society* **37**, 81 (1945).
- [53] H. Cramér, *Mathematical Methods of Statistics* (Princeton University Press, Princeton, 1946).
- [54] L. S. Levitov, H. Lee, and G. B. Lesovik, Electron counting statistics and coherent states of electric current, *Journal of Mathematical Physics* **37**, 4845 (1996).
- [55] G. Platero and R. Aguado, Photon-assisted transport in semiconductor nanostructures, *Physics Reports* **395**, 1 (2004).
- [56] K. Schönhammer, Full counting statistics for noninteracting fermions: Exact results and the Levitov-Lesovik formula, *Phys. Rev. B* **75**, 205329 (2007).
- [57] T. Brandes, Waiting times and noise in single particle transport, *Ann. Phys. (Berlin)* **17**, 477 (2008).
- [58] M. Esposito, U. Harbola, and S. Mukamel, Nonequilibrium fluctuations, fluctuation theorems, and counting statistics in quantum systems, *Rev. Mod. Phys.* **81**, 1665 (2009).
- [59] R. Hussein and S. Kohler, Quantum transport, master equations, and exchange fluctuations, *Phys. Rev. B* **89**, 205424 (2014).
- [60] C. Flindt, C. Fricke, F. Hohls, T. Novotný, K. Netočný, T. Brandes, and R. J. Haug, Universal oscillations in counting statistics, *Proceedings of the National Academy of Sciences* **106**, 10116 (2009).
- [61] M. Ridley, M. Galperin, E. Gull, and G. Cohen, Numerically exact full counting statistics of the energy current in the Kondo regime, *Phys. Rev. B* **100**, 165127 (2019).
- [62] F. A. Pollock, E. Gull, K. Modi, and G. Cohen, Reduced Dynamics of Full Counting Statistics, *SciPost Phys.* **13**, 027 (2022).
- [63] E. Kleinherbers, P. Stegmann, and J. König, Revealing attractive electron-electron interaction in a quantum dot by full counting statistics, *New Journal of Physics* **20**, 073023 (2018).
- [64] M. Benito, M. Niklas, and S. Kohler, Full-counting statistics of time-dependent conductors, *Phys. Rev. B* **94**, 195433 (2016).
- [65] G. Schaller, J. Cerrillo, G. Engelhardt, and P. Strasberg, Electronic Maxwell demon in the coherent strong-coupling regime, *Phys. Rev. B* **97**, 195104 (2018).
- [66] J. Xu, S. Wang, J. Wu, Y. Yan, J. Hu, G. Engelhardt, and J. Luo, Noise suppression of transport through double quantum dots by feedback control, *Phys. Rev. B* **107**, 125113 (2023).
- [67] G. T. Landi, M. J. Kewming, M. T. Mitchison, and P. P. Potts, Current fluctuations in open quantum systems: Bridging the gap between quantum continuous measurements and full counting statistics, *PRX Quantum* **5**, 020201 (2024).
- [68] C. Wang, J. Ren, and J. Cao, Unifying quantum heat transfer in a nonequilibrium spin-boson model with full counting statistics, *Phys. Rev. A* **95**, 023610 (2017).
- [69] J. Cerrillo, M. Buser, and T. Brandes, Nonequilibrium quantum transport coefficients and transient dynamics of full counting statistics in the strong-coupling and non-Markovian regimes, *Phys. Rev. B* **94**, 214308 (2016).
- [70] S. Restrepo, J. Cerrillo, P. Strasberg, and G. Schaller, From quantum heat engines to laser cooling: Floquet theory beyond the Born-Markov approximation, *New Journal of Physics* **20**, 053063 (2018).
- [71] A. Soret and M. Esposito, Thermodynamics of coherent energy exchanges between lasers and two-level systems, *Phys. Rev. A* **111**, 062205 (2025).
- [72] M. Tavis and F. W. Cummings, Approximate solutions for an  $n$ -molecule-radiation-field hamiltonian, *Phys. Rev.* **188**, 692 (1969).
- [73] J. H. Shirley, Solution of the Schrödinger equation with a Hamiltonian periodic in time, *Phys. Rev.* **138**, B979 (1965).
- [74] V. M. Bastidas, C. Emary, B. Regler, and T. Brandes, Nonequilibrium quantum phase transitions in the Dicke model, *Phys. Rev. Lett.* **108**, 043003 (2012).
- [75] J. Naji, R. Jafari, L. Zhou, and A. Langari, Engineering floquet dynamical quantum phase transitions, *Phys. Rev. B* **106**, 094314 (2022).
- [76] I. Esin, M. S. Rudner, and N. H. Lindner, Floquet metal-to-insulator phase transitions in semiconductor nanowires, *Science Advances* **6**, eaay4922 (2020).
- [77] L.-N. Luan, M.-Y. Zhang, and L. Wang, Floquet dynamical quantum phase transitions of the xy spin-chain under periodic quenching, *Physica A: Statistical Mechanics and its Applications* **604**, 127866 (2022).
- [78] N. H. Lindner, G. Refael, and V. Galitski, Floquet topological insulator in semiconductor quantum wells, *Nature Physics* **7**, 490 (2011).
- [79] Y. T. Katan and D. Podolsky, Modulated floquet topological insulators, *Phys. Rev. Lett.* **110**, 016802 (2013).
- [80] M. Benito, A. Gómez-León, V. M. Bastidas, T. Brandes, and G. Platero, Floquet engineering of long-range  $p$ -wave superconductivity, *Phys. Rev. B* **90**, 205127 (2014).
- [81] R. Roy and F. Harper, Floquet topological phases with symmetry in all dimensions, *Phys. Rev. B* **95**, 195128 (2017).
- [82] D. V. Else, B. Bauer, and C. Nayak, Floquet time crystals, *Phys. Rev. Lett.* **117**, 090402 (2016).
- [83] V. Khemani, A. Lazarides, R. Moessner, and S. L. Sondhi, Phase structure of driven quantum systems, *Phys. Rev. Lett.* **116**, 250401 (2016).
- [84] N. Y. Yao, A. C. Potter, I.-D. Potirniche, and A. Vishwanath, Discrete time crystals: Rigidity, criticality, and realizations, *Phys. Rev. Lett.* **118**, 030401 (2017).
- [85] P. J. D. Crowley, I. Martin, and A. Chandran, Topological classification of quasiperiodically driven quantum systems, *Phys. Rev. B* **99**, 064306 (2019).
- [86] D. M. Long, P. J. D. Crowley, and A. Chandran, Nonadiabatic topological energy pumps with quasiperiodic driving, *Phys. Rev. Lett.* **126**, 106805 (2021).
- [87] H. Sambe, Steady states and quasienergies of a quantum-mechanical system in an oscillating field, *Phys. Rev. A* **7**, 2203 (1973).
- [88] D. Xu and J. Cao, Non-canonical distribution and nonequilibrium transport beyond weak system-bath coupling regime: A polaron transformation approach, *Frontiers of Physics* **11**, 110308 (2016).
- [89] G. Engelhardt and J. Cao, Unusual dynamical properties of disordered polaritons in microcavities, *Phys. Rev. B* **105**, 064205 (2022).
- [90] G. Engelhardt, A. Bhoonah, and W. V. Liu, Detecting

- axion dark matter with rydberg atoms via induced electric dipole transitions, *Phys. Rev. Res.* **6**, 023017 (2024).
- [91] A. A. Clerk, M. H. Devoret, S. M. Girvin, F. Marquardt, and R. J. Schoelkopf, Introduction to quantum noise, measurement, and amplification, *Rev. Mod. Phys.* **82**, 1155 (2010).
- [92] C. Emary, D. Marcos, R. Aguado, and T. Brandes, Frequency-dependent counting statistics in interacting nanoscale conductors, *Phys. Rev. B* **76**, 161404 (2007).